

# Dimensioning of Integrated Starter-Generator Mild Hybrid System Using Real World Drive Cycles

# **Dimensioning of Integrated Starter-Generator Mild Hybrid System Using Real World Drive Cycles**

by

Nickolas Leahey

A thesis

presented to McMaster University

in partial fulfillment

of the requirements for the degree of

Masters of Applied Science

in Electrical and Computer Engineering

Hamilton, Ontario, Canada, 2018

© Nickolas Leahey 2018

## Descriptive Note

Masters of Applied Science (2018)                      McMaster University  
Electrical and Computer Engineering)                Hamilton, Ontario

Title: Dimensioning of Integrated Starter-Generator Mild Hybrid System Using  
Real World Drive Cycles

Author: Nickolas K. Leahey, B. Tech (McMaster University)

Supervisor: Dr. Jennifer Bauman, P. Eng

Number of Pages: 91

## **Acknowledgements**

I would like to express my thanks to my parents. They have always supported and encouraged me to accomplish whatever I wanted, and have dealt with my stubborn nature when others could not. I would like to thank my father for introducing me to automobiles at the young age of four, and computers and electronics soon after, you truly inspired me to get into engineering and I have not looked back since. Thank you to my mother for always being my emotional support, even in times when I would not admit to myself that I needed it. Thanks also to my brother James for constantly being there not only as a brother, but also as a friend, and for pushing me in the right direction when I was lost.

I will be forever grateful to my supervisor Dr. Bauman, who has given me not only the knowledge to succeed in my graduate studies, but advice and support to help me in the real world. Thank you for taking a risk and accepting me as your first graduate student. I was consistently amazed by your ability to guide and support me when I felt as if I was stuck on an impossible problem, and the trust you gave me throughout my studies. I do not think I would have been able to accomplish what I did in my graduate studies with anyone else, and you will forever have my thanks. Thank you also to Dr. Emadi and Dr. Bakr, members of my committee, for their confidence and suggestions.

## **Abstract**

Hybrid vehicles are an important technology for reducing oil use and transportation-related emissions. It is well-known that hybrid and electric vehicles are often designed and tested using standard cycles such as the Highway Fuel Economy Test (HWY), Urban Dynamometer Driving Schedule (UDDS), and the US06 Supplementary Federal Test Procedure (US06). However, this begs the questions: How does real world driving compare to these cycles? Can a vehicle be designed using real world driving data which saves fuel in the real world compared to a vehicle designed using standard cycles? This thesis investigates this issue using a set of 5000km of real world driving data by light-duty pickup trucks, with the goal to optimize the fuel savings of a mild hybrid truck. The challenge with using a model-based design approach on thousands of kilometers of real driving data is the long model run-time required to iterate through plant and control parameters. Thus, this work develops a novel script which reduces optimization time by 78%. The key is to run the full model of the non-hybrid truck one time on the full driving data set, and then use the resulting vehicle speed, engine efficiency, engine torque, and engine speed, as inputs to the faster script. The script is then used to quickly iterate through the driving data set many times to find optimal control and plant parameters. In this work, exhaustive search is used; however, evolutionary optimization algorithms could also be used and would benefit from the fast script iteration on real world driving cycles. Overall, the use of the real world driving set for design of the mild hybrid truck resulted in a 7.10% decrease in fuel consumption compared to the non-hybrid truck, while the use of standard driving cycles for design resulted in a 5.45% fuel consumption decrease compared to the non-hybrid truck.

## Table of Contents

Abstract .....	iv
Table of Contents .....	v
Table of Figures .....	vii
1 Introduction.....	1
1.1 Background and Motivations .....	1
1.2 Contributions.....	3
1.3 Outline of Thesis.....	4
2 Fundamentals of Hybrid Powertrains .....	7
2.1 Hybrid Electric Vehicle Classification and Architecture.....	7
2.1.1 Degree of Hybridization in Hybrid Electric Vehicles.....	7
2.1.2 Architecture of Hybrid Electric Vehicles.....	10
2.1.3 Modern Mild Hybrid Technologies .....	12
2.2 Design Processes of Hybrid Electric Vehicles.....	13
3 Proposed Real World Data Driven Design Process .....	23
3.1 Setup and Procedure .....	27
3.2 Optimization Problem.....	30
3.3 Sizing Algorithm for Mild Hybrid Optimization.....	32
4 Modelling and Validation .....	41
4.1 ICE vehicle model.....	41
4.1.1 Engine Model.....	44
4.1.2 Engine Control .....	48

4.1.3	Gearbox Control.....	49
4.1.4	Model Validation .....	52
4.2	Mild HEV vehicle model .....	58
4.2.1	Battery Model .....	59
4.2.2	Motor Model .....	61
4.2.3	Inverter Model .....	63
4.2.4	Motor Control .....	64
4.2.5	Comparison to Existing Designs.....	69
4.3	Algorithm Validation .....	70
5	Hybrid Powertrain Design Results.....	74
5.1	Component Performance .....	74
5.2	Standard Drive Cycle Algorithm Results.....	78
5.3	Real World Optimization results.....	83
6	Conclusion and Future Works .....	87
6.1	Summary of Contributions.....	87
6.2	Suggestions for Future Work .....	89
	References.....	91

## Table of Figures

Figure 1-1: Canadian gasoline price trend [1] .....	1
Figure 2-1: Hybridization breakdown [11] .....	9
Figure 2-2: Series Hybrid Electric Vehicle Architecture .....	10
Figure 2-3: Parallel Hybrid Electric Vehicle Architecture .....	11
Figure 2-4: Exhaustive search design space [5] .....	15
Figure 3-1: Overview of data driven design process .....	24
Figure 3-2: Trip distance histogram .....	26
Figure 3-3: Trip average speed histogram .....	26
Figure 3-4: Trip maximum speed histogram .....	27
Figure 3-5: Mild HEV ISG powertrain diagram .....	28
Figure 3-6: Exhaustive search grid .....	31
Figure 3-7: Logic flowchart for sizing of battery and electric motor .....	33
Figure 3-8: Motor torque supply controller sub process .....	37
Figure 3-9: Motor torque demand controller sub process .....	40
Figure 4-1: Vehicle model overview .....	42
Figure 4-2: Conventional ICE plant model .....	43
Figure 4-3: Zero fuel engine torque map .....	45
Figure 4-4: Created Engine fuel map for F-150 .....	47
Figure 4-5: Gearbox upshift map .....	51
Figure 4-6: Gearbox downshift map .....	52
Figure 4-7: HWY vehicle speed comparison .....	53

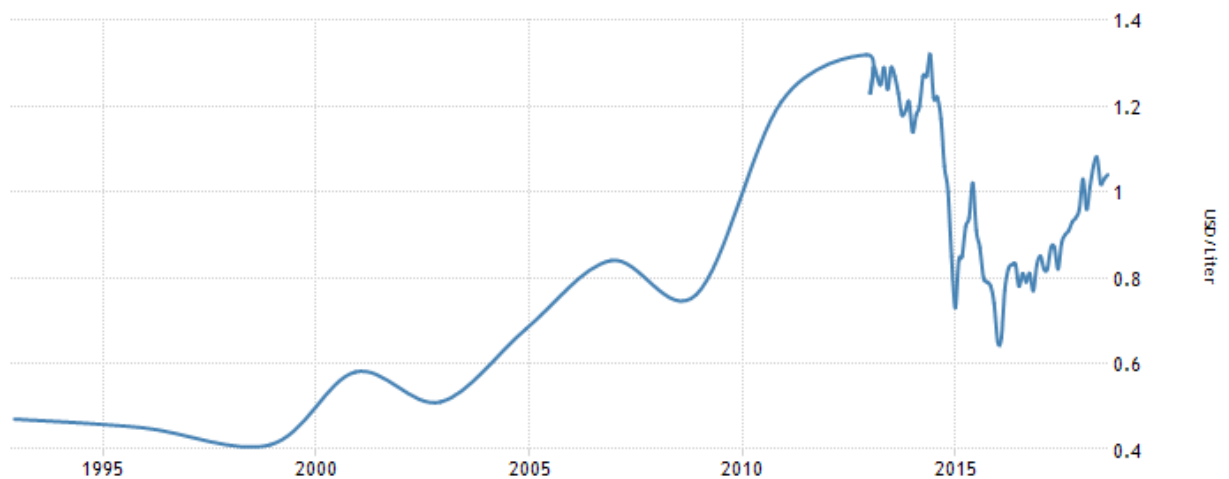
Figure 4-8: HWY engine speed comparison.....	54
Figure 4-9: HWY fuel rate comparison .....	54
Figure 4-10: UDDS vehicle speed comparison .....	55
Figure 4-11: UDDS engine speed comparison .....	56
Figure 4-12: UDDS fuel rate comparison.....	56
Figure 4-13: Mild hybrid plant model .....	58
Figure 4-14: OCV-R model of battery.....	59
Figure 4-15: SOC-OCV curve for Li-Ion cell [48].....	61
Figure 4-16: SOC-OCV curve for 12V lead-acid battery [49] .....	61
Figure 4-17: General Motors eAssist induction motor efficiency map [18].....	62
Figure 4-18: Toyota Prius inverter efficiency map [43] .....	63
Figure 4-19: Motor Controller .....	65
Figure 4-20: UDDS Li-Ion SOC validation.....	71
Figure 4-21: HWY Li-Ion SOC validation .....	72
Figure 4-22: US06 Li-Ion SOC validation.....	72
Figure 5-1: Simulated US06 motor torque.....	75
Figure 5-2: Simulated US06 engine torque .....	75
Figure 5-3: Simulated US06 li-ion battery current .....	77
Figure 5-4: Simulated US06 li-ion battery terminal voltage .....	77
Figure 5-5: US06 li-ion battery SOC .....	78
Figure 5-6: HWY fuel savings comparison .....	80
Figure 5-7: UDDS fuel savings comparison.....	81

Figure 5-8: US06 fuel savings comparison.....	82
Figure 5-9: SEW fuel savings comparison .....	83
Figure 5-10: Real world dataset fuel savings.....	84

# 1 Introduction

## 1.1 Background and Motivations

With an ever-expanding population of drivers on the road, gasoline and diesel have become precious resources. As part of the increased demand for gasoline, the average price of gasoline has risen significantly over the past 20 years. Figure 1-1 shows the past 25 years of gasoline prices in Canada, which demonstrates a clear upwards trend [1]. In addition, the large amount of fossil fuel emissions produced in the past few decades has led to increased emissions control. One example of the increased regulations surrounding vehicle emissions is the Clean Car Act [2].



**Figure 1-1: Canadian gasoline price trend [1]**

In order to reduce fuel use and emissions, fuel reduction technologies can be implemented. Although full hybrid electric vehicles (HEVs) can drastically reduce fuel consumption, they require a higher cost to the user, with a \$3800 increase from the Toyota Camry LE model from conventional to hybrid [3]. In addition, the modifications to the

powertrain require significant changes in the manufacturing process. In comparison, a mild hybrid option can be added for only \$500, and provide the vehicle with an overall 5% increase in fuel economy [4]. The components also integrate into the existing design of the vehicle, reducing the changes required in the manufacturing process. Due to the potential mass application of mild hybrid technology due to its relatively low cost, this thesis focuses on optimizing plant and control parameters of a mild hybrid powertrain.

When designing a mild hybrid vehicle there are a variety of approaches to optimize component sizing and control [5]. In particular, these approaches focus on the sizing of the battery in conjunction with the electric motor, and the controller used in the vehicle that determines when the battery accepts charge and when the battery provides charge. Although there are a variety of control strategies, a commonly used approach is a rule-based control algorithm. These algorithms are often used due to their simplicity and ability to run in real time [5].

Furthermore, most powertrain optimizations utilize standard drive cycles such as the New European Drive Cycle (NEDC) or Urban Dynamometer Driving Schedule (UDDS) [6], [7]. These drive cycles are often used for emissions and fuel economy certifications but are not representative of real world driving conditions. However, using real world driving data, significant improvements can be made when optimizing an electrified vehicle [8]. In this thesis, an approach to the mild hybridization of conventional internal combustion engine vehicles is proposed that uses real world driving data from similar vehicles to optimize the component sizing and control.

Currently, trucks are one of the bestselling passenger vehicles in North American, with the Ford F-150 being the bestselling vehicle of 2017 [9]. Light duty trucks often obtain poor engine efficiencies when compared to passenger vehicles because they are designed to operate at high loads (such as towing or moving heavy goods) yet are often driven without additional loads, meaning lower torque requests at the engine. As the energy consumption in trucks is high due to their large mass, full electrification would require a very large battery and is thus a potential longer-term solution. In the near- to mid-term however, mild hybridization is an excellent option to reduce light duty truck fuel cost due to its lower cost, and lower footprint.

## **1.2 Contributions**

This thesis presents a data-driven design process for the mild hybridization of an internal combustion engine vehicle. A data-driven approach through real world driving data is used, as the standard certification cycle used in government testing can vary greatly from an individual's driving habits, causing a discrepancy in the total fuel savings, which can lead to a less than optimal design [10]. The real world dataset used in this paper provides information on the driving habits of nine drivers for over 5000km of trips, with a large variety of city and highway driving styles, from the Greater Toronto Area.

The optimized plant/control pairing is found on standard drive cycles, and the real world dataset, and the fuel savings results are compared on the real world dataset. Specifically, a 2017 Ford F-150 is modelled in Simulink, and verified on standard drive cycles. The model is then modified to incorporate an integrated starter-generator system, removing the alternator and starter found in the vehicle. All final results are compared by

running the optimized plant/control on the real world driving data using the modified model.

The design process utilizes a nested plant/control approach to size the electric motor and battery, and the control of the system. An exhaustive search is used to optimize the component sizing, and the performance of a rule-based control strategy. In order to decrease the computation time to find an optimal plant/control pairing, the optimization algorithm is implemented via a MATLAB script, reducing the computation time by 78% when compared to running a vehicle model in Simulink using Accelerator mode.

The use of real world driving data demonstrates increased fuel savings when compared to a three cycle average (7.10% vs 5.45%), when run on real world driving data. The use of real world data allows for an accurate representation of fuel consumption for the average driver, and demonstrates a larger fuel savings when compared to modelling on standard drive cycles. The combination of a decreased computational time, optimized on real world driving data, allows for the further implementation of other plant/control optimizations in the future.

### **1.3 Outline of Thesis**

This thesis is organized into five chapters. Chapter 1 has given the motivation for the application of mild hybridization in internal combustion engine vehicles. Chapter 2 introduces hybrid electric vehicles and the design process for hybrid vehicles, including the optimization methods currently used in hybrid design. In addition, Chapter 2 demonstrates the current flaws in using standard drive cycles to design electrified drivetrains, and foreshadows the benefits of using real world data to design powertrains.

Chapter 3 discusses a proposed strategy for the optimization of the plant/control for the implementation of an integrated start-generator mild hybrid system. Specifically, the chapter discusses the algorithm used to optimize the plant/control of the mild hybrid system. The chapter further discusses the implementation of an exhaustive search optimization with a rule-based control for a nested plant/control design. Furthermore, the chapter discusses the specific optimization boundaries, and the optimization setup used in the mild hybridization of the vehicle. The results from the optimization algorithm are used in Chapter 5.

Chapter 4 discusses the modelling and validation of the internal combustion engine vehicle, as well as the modification of the vehicle model into a mild hybrid model. The chapter details the use of an integrated starter-generator, and the removal of the starter and alternator from the original vehicle model. The modified model is used to demonstrate the real world benefits in Chapter 5. Furthermore, the chapter compares the low-level performance of the optimization algorithm to the modified vehicle model.

Chapter 5 demonstrates the detailed results of implementing a mild hybrid system. This chapter also compares the optimal plant/control pairing found using standard drive cycles to that using real world data, on the real world dataset. Chapter 5 demonstrates the benefits of using the real world data to optimize the plant/control in comparison to standard drive cycles. In addition, the chapter demonstrates the decreases in computation time for the MATLAB script, in comparison to using a Simulink model in Accelerator Mode. Lastly, conclusions and recommendations for future work are presented in Chapter 6. The

recommendations for the project include different control strategies and the use of other vehicles in the near future.

## **2 Fundamentals of Hybrid Powertrains**

### **2.1 Hybrid Electric Vehicle Classification and Architecture**

The classification of hybrid electric vehicles (HEV) is key to determining the functionality and possible benefits that a hybrid vehicle can provide. Specifically, the degree of hybridization will heavily influence the cost of implementing the hybrid electric components, as well as the architecture determining the control strategy, and benefits the system can provide.

#### **2.1.1 Degree of Hybridization in Hybrid Electric Vehicles**

When comparing ICE vehicles to HEVs, the difference lies in the power sources, and power delivery in the drivetrain of the vehicle itself. The main difference lies in the introduction of a battery as a second energy source to the ICE, and the addition of a traction motor, usually in the form of an alternating current (AC) motor. The introduction of these components allows for increased control over engine operating points. In addition, it introduces engine start-stop functionality, and the ability to capture regenerative braking energy that would have otherwise been dissipated. The extent to which these functions are implemented determines the degree of hybridization in a hybrid electric vehicle, as shown in Figure 2-1.

Micro HEVs implement the most basic of functionality in comparison to a conventional ICE vehicle. In order for a vehicle to qualify to be considered a micro HEV, it must be able to assist in the basic start/stop functionality of the engine [11]. Many vehicles in the marketplace offer this functionality, which can be achieved through the

design of the starter motor and battery pack, adding little cost. However, the benefits to fuel economy are small, with estimates at 2% fuel savings over the year for a driver, with the only difference occurring during idle [12]. Although the use of electronics in a micro hybrid system is common, mechanical systems can also be implemented with similar functionality [13]. There are a variety of topologies available, but most make use of a clutch and flywheel to store energy [14].

In comparison, mild HEVs offer the increased functionality and fuel savings associated with regenerative braking. Mild hybridization usually includes the additional functionality of some limited torque assist, allowing the electric drivetrain to aid the engine in high torque applications such as steep inclines or sudden accelerations [11]. Mild HEVs will require additional components to be inserted into the powertrain of an ICE vehicle, with a more powerful motor and battery pack being required to aid the vehicle in propulsion. In particular, the design of the motor for propulsion is paramount in a mild hybrid design, as it must be designed to operate for a wide variety of operating conditions [15]. It is in the mild hybrid stage that the vehicle starts to show more significant fuel benefits.

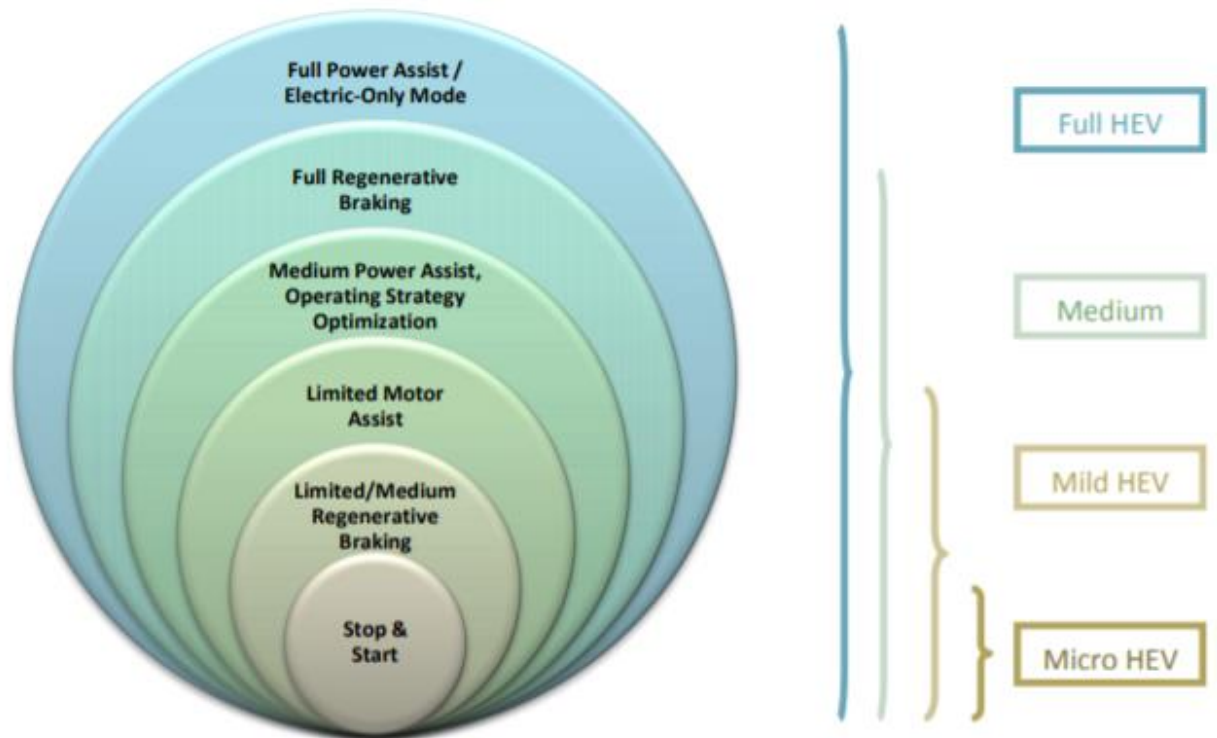


**Figure 2-1: Hybridization breakdown [11]**

Although mild hybridization starts to demonstrate fuel benefits when compared to standard ICE vehicles, medium hybridization and full hybridization demonstrate significant reduction in fuel consumption, but at an additional cost of larger batteries and motors. In order for an HEV to qualify as a medium hybrid, it must be able to achieve full regenerative braking [11], requiring the motor to be connected to the drive shaft in the powertrain, whereas the mild hybrid does not. In addition, the motor will be able to assist at a higher degree, and will usually require a complex operating strategy. The difference between full and medium hybridization is in the ability of the electric motor to drive the vehicle. For a HEV to be considered full, it must be able to perform full power assist, or an electric only mode. Full HEVs are the most common on the market with vehicles such as the Chevy Volt and Toyota Prius.

## 2.1.2 Architecture of Hybrid Electric Vehicles

Although there are a variety of possible architectures present in HEVs, all derive from two primary architectures, series and parallel. Figure 2-2 demonstrates a system level overview of the series HEV architecture. The basic functionality of the series HEV architecture relies on the electric motor to propel the vehicle during driving, with the engine acting solely as a power source to recharge or provide electrical power to the HEV, demonstrating that the series HEV is essentially a pure electric vehicle, with an ICE generator [16]. The benefits of a series architecture lie in the operation of the ICE itself. By allowing the engine to act as a generator, the engine can operate close to its optimal efficiency point [11]. However, the drawback of the series architecture is that the power from the engine must go through both the generator and motor to reach the wheels, and undergoes losses at each conversion.

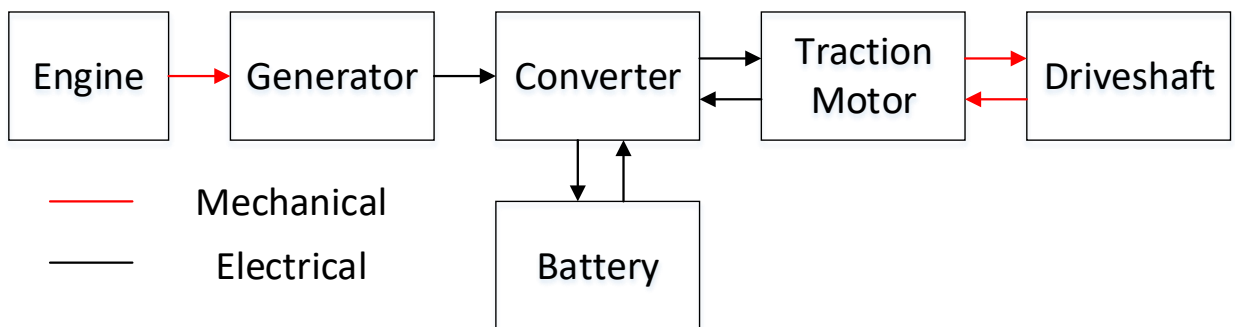


**Figure 2-2: Series Hybrid Electric Vehicle Architecture**

In contrast to the series hybrid architecture, a parallel HEV allows the engine to directly propel the vehicle. As shown in Figure 2-3, the parallel architecture joins both the electric motor and the ICE through a mechanical coupler. Although maximum power output can be significantly increased through a parallel HEV, the overall efficiency of the system

is significantly decreased due to efficiency losses through the mechanical coupler, and the engine operating at an overall lower efficiency when compared to a series HEV [16].

Although series hybrid vehicles tend to be higher efficiency, they are still essentially electric vehicles with an extended range. The electric vehicle base of the series architecture also means that it is only applicable to full hybridization. The degree of hybridization means that existing ICE vehicle designs cannot be easily adapted into a series HEV. Furthermore, simple variations of the parallel architecture exist that allow for easy implementation of mild hybrid technologies, which are easily implemented into an ICE vehicle's design.

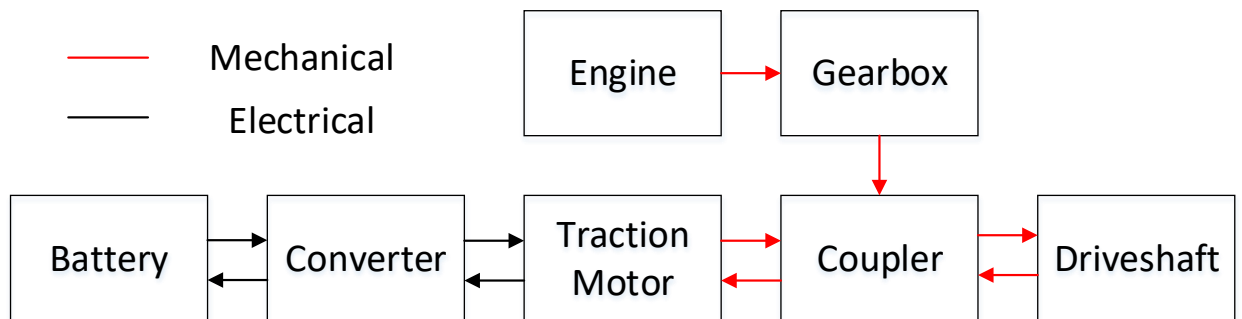


**Figure 2-3: Parallel Hybrid Electric Vehicle Architecture**

In addition to the base architecture associated with parallel and series HEVs, there also exist plug-in HEVs or PHEVs. PHEVs are a necessity when it comes to reaching full hybridization, as regenerative braking and engine regeneration cannot replace the energy used to propel the vehicle solely on electric. However, PHEVs require larger batteries, and thus are a much more expensive alternative than mild hybrids.

### **2.1.3 Modern Mild Hybrid Technologies**

This thesis focuses on mild hybrid powertrains because they are a cost-effective alternative to ICE vehicles, with the potential to be integrated into most popular vehicle designs. Since light duty trucks are popular vehicles, with the F-150 being the bestselling vehicle in the US in 2017 [9], and exhibit worse fuel consumption than most passenger vehicles, this thesis will focus hybridization of light duty trucks. Of interest in this paper are technologies demonstrated in three different light duty trucks produced by General Motors, Ford, and Fiat-Chrysler. Each of these vehicles takes a different approach to the hybridization of their products, as discussed below.

Currently, the 2019 Ford F-150 demonstrates a middle ground between a mild and micro hybrid. The vehicle is able to use an integrated starter/generator to perform simple start-stop operations, and comes with an inverter built into the vehicle. The inverter allows the entire vehicle to act as a generator for worksite applications [17].

General Motors has implemented mild hybrid technology into their vehicles since their eAssist technology premiered in the 2012 Buick Regal. General Motor's eAssist technology functions as a mild hybrid vehicle. Specifically, the 2017 Chevrolet Silverado replaces both the starter motor and alternator found in their ICE standard models with an integrated started/generator in the form of an induction motor [18]. The eAssist technology allows for start/stop functionality and regenerative braking, as well as vehicle launch assist, and transient power supplementing, which decreases the vehicle's fuel consumption at higher performance points. General Motors accomplishes this feat over an 115V DCDC bus, with a 15kW electric motor.

Finally, Fiat-Chrysler introduced a system similar to eAssist on their 2019 RAM pickup lineup. Unlike the eAssist technology, the technology found in the RAM runs on a 48V DCDC bus [19]. The RAM demonstrates similar functionality to that found in the Silverado, but also claims to improve efficiency by 15% [19]. Both systems use an integrated starter/generator that is attached via a belt to the ICE crankshaft.

## **2.2 Design Processes of Hybrid Electric Vehicles**

In order to find an accurate approach to the dimensioning of components in a mild HEV, a literature review was performed to determine basic powertrain control strategies and proper optimization methods. As shown in [20] vehicle electrification is highly dependent on the design and control of the electrical components in the powertrain. This is particularly important when examining HEV, where engine efficiencies play a large role in total energy consumption. This review details methods used in electrified vehicle optimization, from a cost-based approach to motor power demand. In addition, methods of using standard drive cycles as well as real world data are explored. Finally, control methods used in HEV optimization are examined in order to build the control strategy in the sizing algorithm, and mild HEV vehicle model.

The authors, *Emilia Silvas et al.* review a large variety of methods used to design an HEV from a system level perspective [5]. The paper demonstrates four classifications of the optimization strategies, based upon the coordination of the plant and controller design. The first method classification is the alternating method. In the alternating method, the plant for the vehicle is first optimally designed, and from the primary results, a controller is then optimally designed [21]. Subsequently, the plant is again optimized based

on the new controller, and the process is repeated as such until the coupled variables used in the optimization converge [21]. A special instance of the alternating method is the sequential method, where the plant is first designed, and the controller is then optimized only once [5]. In addition to the alternating method, the nested method allows for a large variety of algorithms when it comes to plant and controller design. In the nested method, the controller is optimized fully within each instance of the plant optimization, allowing for a variety of control strategies to be used [5]. Finally, the simultaneous method is highly dependent on convex optimization. The simultaneous method allows the plant to be optimized at the same time as the controller, in contrast to the nested method that requires the full controller optimization, as shown in [22], which demonstrates the use of convex optimization in electrified vehicles, and its elimination of control bias.

The nested optimization method is by far the most common, and allows a plethora of plant design and control strategies [23]. For the component sizing found in the plant, the nested method allows for complex methods such as SQP to as simple as exhaustive search. An example of the diversity of the nested optimization, with an exhaustive search algorithm is found in [24], which uses said optimization method to compare four hybrid topologies (conventional HEV, micro HEV, Parallel HEV, and a power split HEV). Exhaustive search or brute-force is an iterative optimization where one or more variables used for component sizing are iterated through until the optimal combination is found, and can be used for a variety of design applications such as the use of a power split strategy in the Toyota Prius [25]. The combination of variables is represented via a gridded design space, with each point representing the optimization variable pair, with a resulting cost function evaluation

[26]. Figure 2-4 demonstrates design space grid for an exhaustive search method, where the fuel consumption for the vehicle is optimized, by using the cost of the powertrain and the maximum power of the powertrain. The brute-force method is simple, and excels when a small number of optimization variables are used [5]. In [27], an exhaustive search was used to determine the battery size of an urban Microbus, using an offline energy management strategy, significantly reducing CO<sub>2</sub> emissions.

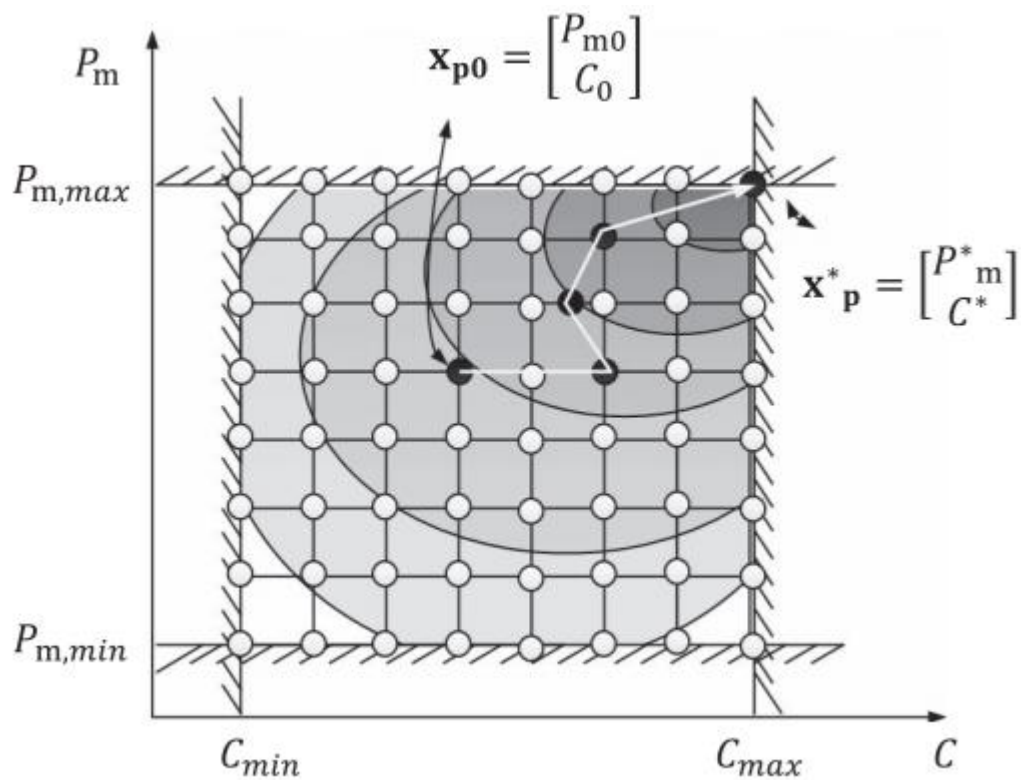


**Figure 2-4: Exhaustive search design space [5]**

In addition to the component sizing algorithms, nested optimization allows for the use of a variety of control algorithms. In particular, there are two categories, rule based and optimization based [28], [29]. Rule based controller design requires knowledge of

powertrain design, but are indeed very simple to implement and require very little computation time to evaluate. The main downside to rule based controllers is that there is no assurance that the optimal control can ever be found, thus the existence of optimization algorithms in the controller [5].

In [30], a dynamic optimization algorithm is used in place of a rule based control strategy to determine the optimal power management strategy for a parallel HEV truck. The resulting strategy allows for a parallel HEV where the engine operates only at its highest efficiency points. In addition, control optimization algorithms can also make use of ECMS and SQP, but gain the ability to use dynamic programming (DP). DP allows for the offline optimization of the controller, but can only truly be used as a benchmark for other control design performance [31], [32].

In a paper by *Meilan Zhou et al.*, the design process for the conversion of an ICE vehicle to a parallel HEV is detailed. The authors select a generic ICE vehicle model and simulate the vehicle using ADVISOR software, focusing on the fuel economy results derived from the vehicle simulation. The vehicle is simulated on the New European Driving Cycle (NEDC) driving cycle exclusively, but focuses on increasing the load on the vehicle through the means of increasing the cargo mass during simulation [7]. The authors use the Honda Insight energy management/ motor control strategy as their base [7]. In said strategy, the motor can assist the engine during start/stop functionality, and allows for battery charging from the engine at higher speeds. In addition, the vehicle can make use of the hybrid motor to perform regenerative braking. The strategy in its original form is

commonly placed in a mild hybrid architecture due to its limited ability to operate in electric only mode.

The authors first use the maximum rated values of the vehicle to determine the maximum power necessary for the engine. The total power that required is determined by applying scaling factors to the maximum ratings for the vehicle, and add a constant power draw for electrical accessories. The difference between the total rated power and the scaled power is determined to be the motor power [7]. Afterwards, the battery is sized by observing the total theoretical energy used by the motor.

*Thomas Szalai et al.* demonstrate a design approach that allows for the addition of an UC to an electric vehicle's powertrain [6]. The methods described in the paper use the power draw from standard drive cycles to attempt to optimize the sizing of the UC and the resizing of the battery through an iterative optimization, cycling through UC sizing. The authors state that the vehicle can be designed with two variables in mind, optimal weight savings from battery reduction, and range extension. The papers is useful for demonstrating a basic design process to hybridize a vehicle, but lacks in model complexity, similar to the paper by *Meilan Zhou et al.*.

Standard drive cycles are used in the certification of vehicle are often geared specifically towards city or highway driving styles. The Environmental Protection Agency (EPA) dictates vehicle testing procedures, and those pertaining to vehicle fuel economy, and certification. Previously, the EPA used a two-cycle approach to fuel economy certification. The two-cycle approach was using the city (FTP) and highway (HFET) cycles, where the final results of each cycle would be adjusted by 10% and 22%, regardless

of the vehicle [33]. However, in 2008 the EPA introduced the five-cycle approach to calculate fuel economy for each vehicle [34] in an attempt to better represent actual real world driving. This approach introduced scaling factors to account for fuel consumption changes due to temperature changes, accessory usage, and aggressive accelerations. The calculations for both the city and highway fuel economy are shown in (2-1)-(2-8), as well as the definitions found in Table 2-1 [35]. The main difference in the 5-cycle approach between city and highway fuel economy ratings are in the scaling factors that adjust for the acceleration and temperature differences in the vehicle.

$$CityFE = \frac{0.905}{StartFC + RunningFC} \quad (2-1)$$

Where:

$$StartFC = 0.33 \times \left( \frac{0.76 \times StartFuel_{75} + 0.24 \times StartFuel_{20}}{4.1} \right) \quad (2-2)$$

$$StartFuel_x = 3.6 \times \left[ \frac{1}{Bag1FE_x} - \frac{1}{Bag3FE_x} \right] \quad (2-3)$$

$$\begin{aligned} RunningFC = & 0.82 \times \left[ \frac{0.48}{Bag2FE_{75}} + \frac{0.41}{Bag3FE_{75}} + \frac{0.11}{US06CityFE} \right] \\ & + 0.18 \times \left[ \frac{0.5}{Bag2FE_{20}} + \frac{0.5}{Bag3FE_{20}} \right] \\ & + 0.133 \times 1.083 \\ & \times \left[ \frac{1}{SC03FE} - \left( \frac{0.61}{Bag3FE_{75}} + \frac{0.39}{Bag2FE_{75}} \right) \right] \end{aligned} \quad (2-4)$$

$$HigwayFE = \frac{0.905}{StartFC + RunningFC} \quad (2-5)$$

Where:

$$StartFC = 0.33 \times \left( \frac{0.76 \times StartFuel_{75} + 0.24 \times StartFuel_{20}}{60} \right) \quad (2-6)$$

$$StartFuel_x = 3.6 \times \left[ \frac{1}{Bag1FE_x} - \frac{1}{Bag3FE_x} \right] \quad (2-7)$$

$$RunningFC = 1.007 \times \left[ \frac{0.79}{US06HighwayFE} + \frac{0.21}{HFETFE} \right] + 0.133 \times 0.377 \times \left[ \frac{1}{SC03FE} - \left( \frac{0.61}{Bag3FE_{75}} + \frac{0.39}{Bag2FE_{75}} \right) \right] \quad (2-8)$$

**Table 2-1: 5-Cycle fuel economy calculation terms**

<b>Term</b>	<b>Description</b>
<i>US06CityFE</i>	Fuel economy over city portion of US06 test (mpg)
<i>US06HighwayFE</i>	Fuel economy over highway portion of US06 test (mpg)
<i>US06FE</i>	Fuel economy of US06 test (mpg)
<i>SC03FE</i>	Fuel economy of SC03 test (mpg)
<i>HFETFE</i>	Fuel economy of HFET test (mpg)
<i>BagYFE<sub>x</sub></i>	Bag Y fuel economy during FTP test at temperature X Fahrenheit (mpg)
<i>StartFuel<sub>x</sub></i>	Start fuel calculation at X Fahrenheit (1/mpg)
<i>StartFC</i>	Start fuel calculation (1/mpg)
<i>RunningFC</i>	Running fuel calculation (1/mpg)
<i>CityFE</i>	City fuel economy (mpg)
<i>HighwayFE</i>	Highway fuel economy (mpg)

In addition to the standard 5-cycle test, a modified calculation exists for hybrid vehicles [35]. The calculations are shown in (2-9)-(2-18). Similar to the difference between city and highway, the hybrid tests use different scaling factors to adjust for different driving conditions. However, the 5-cycle approach still assumes standard scaling factors that are not entirely applicable for the average driver. A study by David Greene et al. demonstrate the differences between individual driver fuel economy and the government fuel economy

rating, with fuel economy ratings becoming increasingly distant from user reported fuel economies [10].

$$CityFE = \frac{0.905}{StartFC + RunningFC} \quad (2-9)$$

Where:

$$StartFC = 0.33 \times \left( \frac{0.76 \times StartFuel_{75} + 0.24 \times StartFuel_{20}}{4.1} \right) \quad (2-10)$$

$$StartFuel_{75} = 3.6 \times \left[ \frac{1}{Bag1FE_{75}} - \frac{1}{Bag3FE_{75}} \right] + 3.9 \times \left[ \frac{1}{Bag2FE_{75}} - \frac{1}{Bag4FE_{75}} \right] \quad (2-11)$$

$$StartFuel_{20} = 3.6 \times \left[ \frac{1}{Bag1FE_{20}} - \frac{1}{Bag3FE_{20}} \right] \quad (2-12)$$

$$RunningFC = 0.82 \times \left[ \frac{0.48}{Bag2FE_{75}} + \frac{0.41}{Bag3FE_{75}} + \frac{0.11}{US06CityFE} \right] + 0.18 \times \left[ \frac{0.5}{Bag2FE_{20}} + \frac{0.5}{Bag3FE_{20}} \right] + 0.133 \times 1.083 \times \left[ \frac{1}{SC03FE} - \left( \frac{0.61}{Bag3FE_{75}} + \frac{0.39}{Bag2FE_{75}} \right) \right] \quad (2-13)$$

$$HigwayFE = \frac{0.905}{StartFC + RunningFC} \quad (2-14)$$

Where:

$$StartFC = 0.33 \times \left( \frac{0.76 \times StartFuel_{75} + 0.24 \times StartFuel_{20}}{60} \right) \quad (2-15)$$

$$\begin{aligned}
StartFuel_{75} &= 3.6 \times \left[ \frac{1}{Bag1FE_{75}} - \frac{1}{Bag3FE_{75}} \right] \\
&+ 3.9 \times \left[ \frac{1}{Bag2FE_{75}} - \frac{1}{Bag4FE_{75}} \right]
\end{aligned} \tag{2-16}$$

$$StartFuel_{20} = 3.6 \times \left[ \frac{1}{Bag1FE_{20}} - \frac{1}{Bag3FE_{20}} \right] \tag{2-17}$$

$$\begin{aligned}
RunningFC &= 1.007 \times \left[ \frac{0.79}{US06HighwayFE} + \frac{0.21}{HFETFE} \right] \\
&+ 0.133 \times 0.377 \\
&\times \left[ \frac{1}{SC03FE} - \left( \frac{0.61}{Bag3FE_{75}} + \frac{0.39}{Bag2FE_{75}} \right) \right]
\end{aligned} \tag{2-18}$$

In an attempt to bridge the gap between standard drive cycles and real-world results, some authors have used drive cycle equivalence and transformation. Using real world driving data, authors transform the speed profiles of standard drive cycles to represent more realistic driving habits [36]. The transformed drive cycles help mitigate the use of scaling factors found in the five-cycle approach. Furthermore, authors have attempted to utilize charge sustaining techniques for hybrid vehicles to reduce the final difference in SOC, reducing fuel economy variability, and providing an optimized design [37]. In addition, authors have proposed a method to synthesize drive cycles in an attempt to generate standard drive cycles that are more realistic than the current certification cycles [38].

Finally, *Mitra Pourabdollah et al.* demonstrate a complex approach to the optimization method itself when examining the design process of a hybrid powertrain, with the use of real world driving data. The real world driving data allows the authors to size a powertrain to the average driver, instead of emissions and fuel certification cycles [8]. The

paper makes use of non-linear efficiencies, allowing the optimization to find an extremely accurate approach to the design of the entire powertrain. However, the authors simplified the battery model significantly with their assumption of constant efficiencies, and open circuit voltage. In addition, utilizing simplified equations to represent power flow throughout the vehicle led to the exclusion of losses from inertial sources. Although this method is suitable to design a vehicle from the ground up at the system level, it uses convex optimization to size three of the powertrain components, with a very minimalistic control strategy. This decreases its usefulness when optimizing a mild hybrid configuration on an ICE vehicle, where the vehicle plant is already primarily designed.

### **3 Proposed Real World Data Driven Design Process**

This thesis proposes a design process to convert an ICE vehicle to a mild HEV using real world drive cycles. Specifically, the thesis focuses on the design process of converting a light-duty pickup truck (Ford F-150) to a mild hybrid electric vehicle. Light duty pickup trucks are designed to be operated at higher loads, which is not always the case, and thus lower efficiencies often occur at lower loads. The implementation of hybridization allows for trucks to utilize an electric motor during low speed operations, and reduce the low efficiency operation of their engines. However, full PHEV may not be realistic for trucks used in industry, as the energy required allowing the vehicle to drive in electric only mode would require a large amount of energy due to the large mass and loading scenarios, forcing the required battery to be very large. In contrast, a mild HEV is highly advantageous due to its small impact on vehicle cost, small form, and ability to integrate into existing manufacturing processes.

The utilization of real world driving data when designing a vehicle would ease the discrepancy between vehicle performance on standard cycles, and individual driver expectations. In order to utilize real world driving in the design of a mild hybrid powertrain, the proposed design process uses three main stages, as shown in Figure 3-1: the modelling of the vehicle in Simulink, the optimization of the mild hybrid component sizing and controller using a MATLAB script, and the use of Simulink to generate results for a modified mild hybrid model on real world driving data using Simulink and the results from the optimization algorithm. A vehicle model is created to allow for the ease of implementation of mild hybrid components after the optimization process. The

optimization algorithm utilizes an exhaustive search in a nested plant/controller design to determine the optimal component sizing, and rule based controller parameters. The rule-based controller is partially based up that shown in the Honda Insight [39]. Using a MATLAB script instead of the base vehicle model, the optimization algorithm computational time can reduced by 78% when compared to running on the vehicle model. Finally, the results from the optimization algorithm are run on real world driving cycles to determine the total benefits observed by the mild hybrid system.

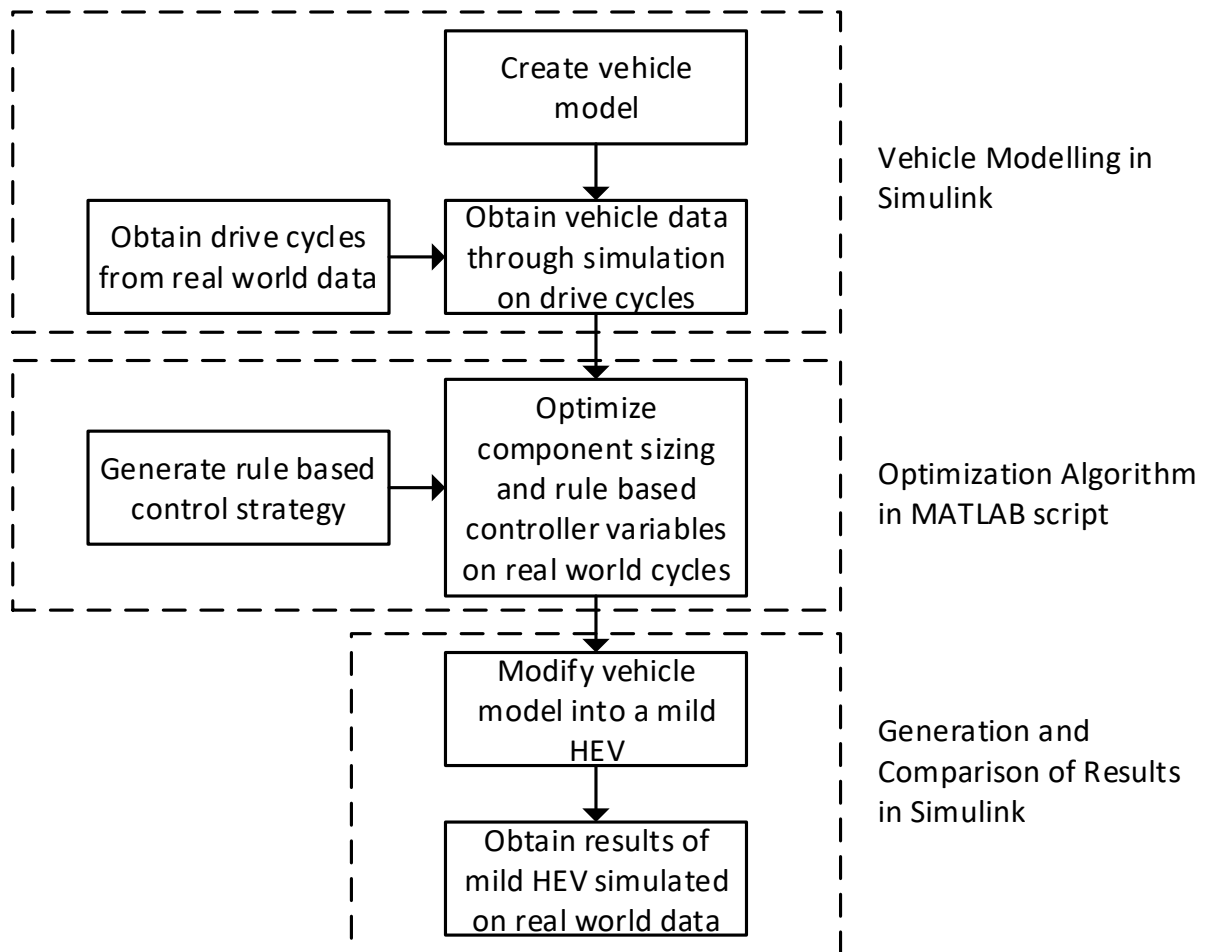


**Figure 3-1: Overview of data driven design process**

For the real world driving data, nine drivers of light-duty pick-up trucks were logged for several weeks in the Toronto area, covering a total of 5450km. The data from every driver were pooled together to determine the driving habits of the entire dataset. Figure 3-2 shows a histogram of the distance driven during the driver's trips. From the figure, it is clear that there were a large amount of short distance trips, indicating a fair amount of city style driving. In contrast, Figure 3-3 demonstrates the average speed during the trips. The average speed varies greatly between trips, but it can be shown that there are a large trips where the drivers demonstrates average speeds over 50km/h, mimicking highway driving styles. Finally, Figure 3-4 shows the maximum speed the vehicles achieved during each trip. The majority of trips had average speeds over 70km/h, but some trips went as low as 5km/h. Overall these three figures demonstrate a large variety of driving styles between each of the trips, representative of real world driving.

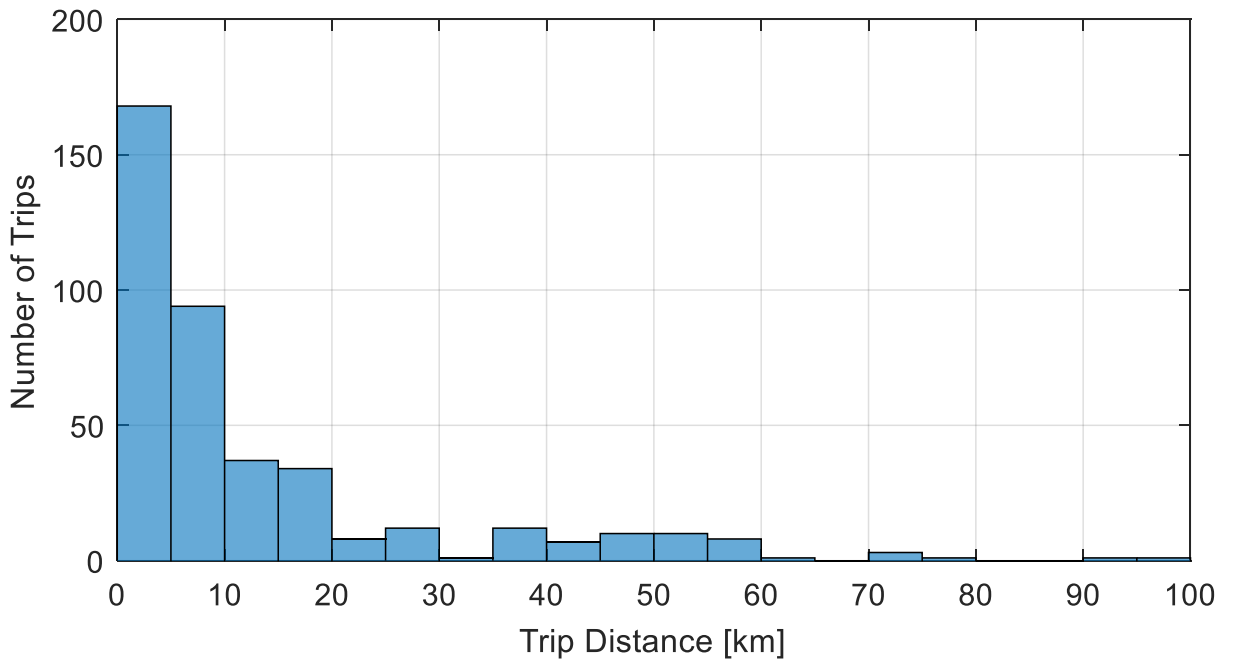


**Figure 3-2: Trip distance histogram**

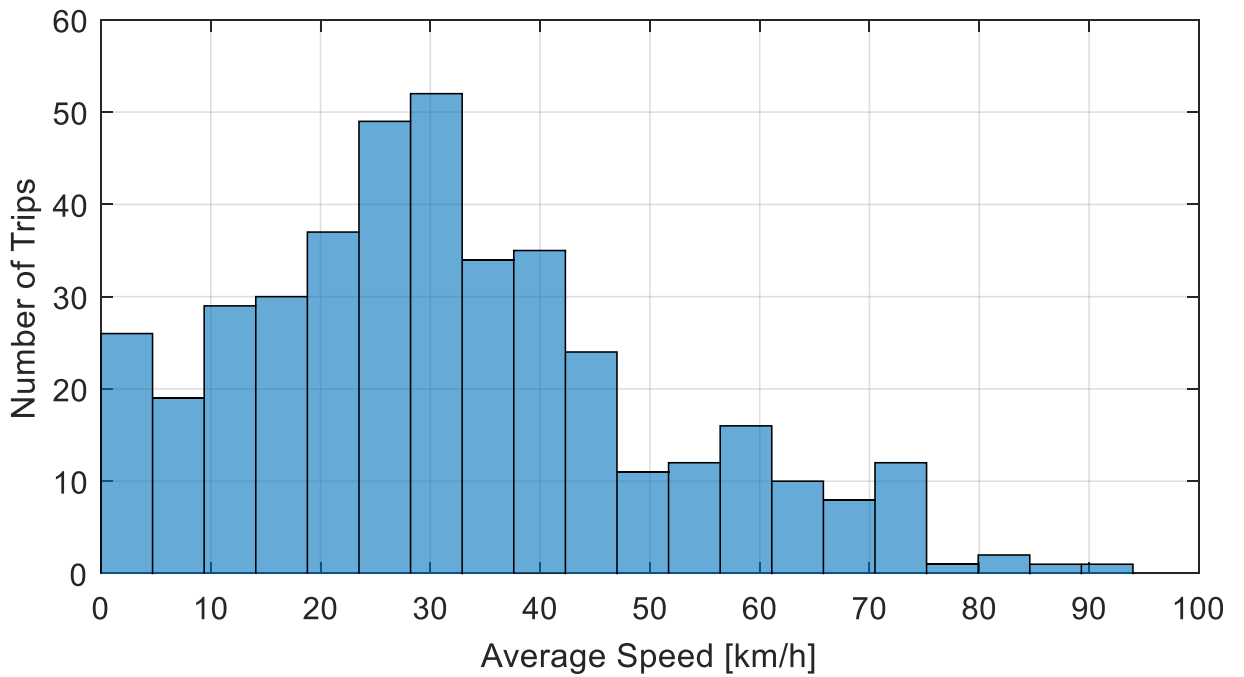


**Figure 3-3: Trip average speed histogram**

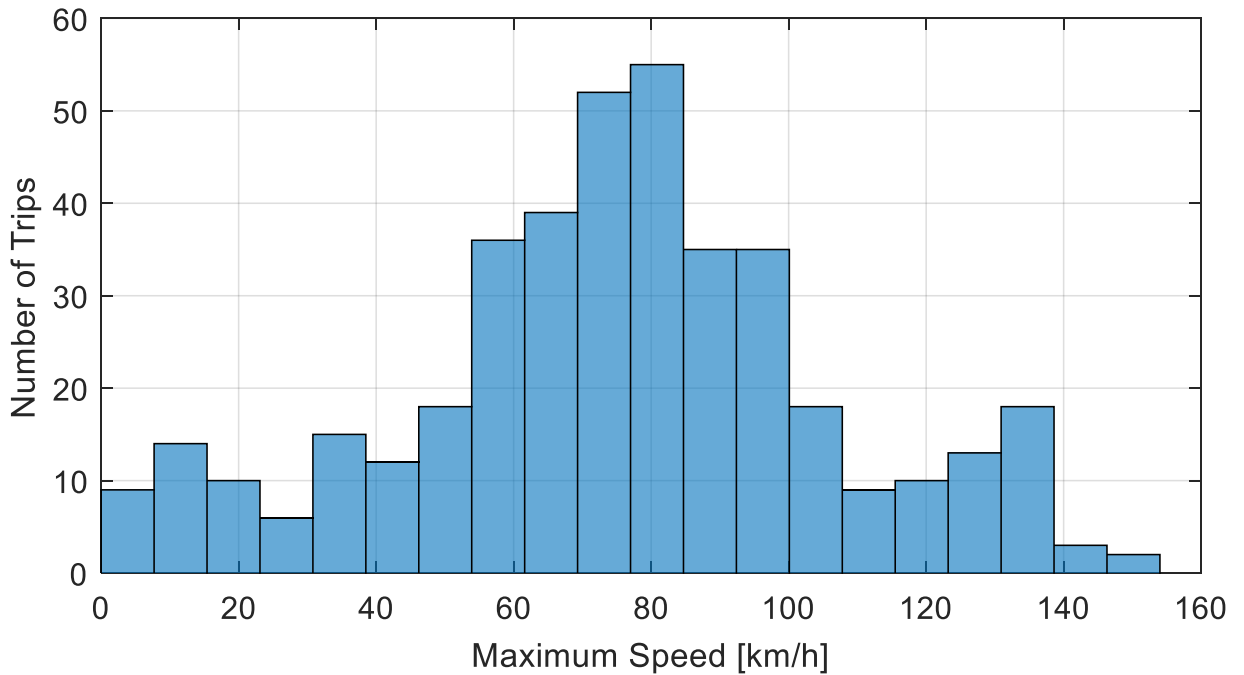


**Figure 3-4: Trip maximum speed histogram**

### 3.1 Setup and Procedure

The purpose of this thesis is to optimize the component sizing and control for the conversion of an ICE vehicle to a mild HEV on real-world drive cycles for a given cost of the main hybrid components, the battery and motor. This process will specifically look at mild hybridization through the implementation of a belt driven integrated started generator (ISG) in the form of an electric motor, along with a lithium ion (Li-Ion) battery pack. In this powertrain setup shown in Figure 3-5, the motor and its subsequent inverter and battery replace the starter and alternator attached to the engine.

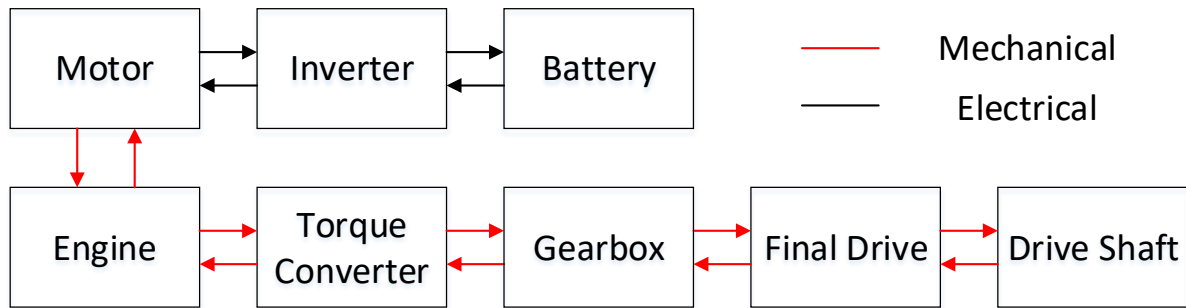


**Figure 3-5: Mild HEV ISG powertrain diagram**

The purpose of this algorithm is to determine the optimal sizing and control based on real-world light-duty truck drive cycles. By using this algorithm in the form of a MATLAB script, significant timesavings can be implemented when compared to using Simulink or other full model simulations. By using data taken from a single run of the ICE model created in Simulink, the MATLAB script does not have to perform calculation related to the losses from any components after the crankshaft of the engine, significantly reducing computational time. As discussed prior, the algorithm is part of a larger process to use real world data in a nested optimization algorithm. The algorithm utilizes an exhaustive search optimization process with a rule based control strategy to optimize the battery/motor combination as well as the control of the rule-based controller. The results from the algorithm's script will be used to run a final simulation on a modified mild HEV simulation the original vehicle, on real world driving data.

The setup of the data driven design process can be broken down into three main stages: model implementation, sizing optimization, and comparative testing. Model implementation deals with the creation and conversion of an ICE vehicle model to a mild HEV model. The sizing optimization deals with the implementation of the sizing algorithm

to determine battery/motor size, as well as control parameters for standard cycles and real world driving data. Finally, comparative testing demonstrates the performance of the optimized parameters on the vehicle model, and compares the use of standard drive cycle optimized parameters on the real world data.

Model implementation first starts with deciding the vehicle to model. The vehicle chosen is an F-150, which has run on various drive cycles with a large amount of second by second signal data such as engine speed and fuel rate, found in the Argonne Labs testing of the vehicle [40]. The vehicle is converted into a vehicle model using the Simulink software, and validated to demonstrate an accurate fit, as shown in Chapter 4.1.4. A second model is then generated by modifying the base vehicle model. The second model contains the key components pertaining to the mild HEV, such as the motor, inverter, battery, and DCDC converter. The starter and alternator components are removed from the vehicle model as well. In addition, a motor control strategy is added to mirror that used in the sizing algorithm, and the existing alternator and starter control strategies are implemented into the model. Once both models are complete, they can be easily modified to accommodate any ICE vehicle, with the largest alternation occurring in the gearbox and its controller.

Sizing optimization is used to determine the battery/ motor size on the vehicle, as well as the control parameters. The exact details for the sizing algorithm used for this optimization can be found in Section 3. However, the sizing optimization takes driver data from the ICE vehicle model run on a particular drive cycle, and uses this in the sizing algorithm. The algorithm then sets a fixed cost, and iterates through battery sizes and a

control variable to achieve brute force optimization of the mild HEV setup. The results are generated for both the real world data, and the standard drive cycles.

Finally, comparative testing is used to determine the validity of results, as well as comparing the sizing algorithm results from real world data and standard cycles, to a simulation on the real world data using the mild HEV model. In this scenario, the standard cycle sizing and control parameters from the algorithm are implemented into the mild HEV model and run on their respective cycles. Afterwards, these same parameters are simulated using the real world data, and the final results are compared to demonstrate the possible benefits of using the real world data to size the vehicle components.

### **3.2 Optimization Problem**

The goal of this optimization problem is to obtain the highest fuel savings through a nested optimization of the plant/control, as shown in. The control will use a rule-based control algorithm that is further discussed below. Specifically, the nested optimization will use an exhaustive search method to determine the optimal plant/control pairing. Figure 3-6 shows the gridded design space used in the exhaustive search. The grid demonstrates that the exhaustive search increments through the battery capacity (Cap) and the vehicle speed motor assist limit ( $v$ ), at a set evenly spaced steps size, as shown by the grid. The resulting fuel savings ( $f$ ) used to determine the optimal plant/control design, and is represented by (3-1)-(3-2). The limits and step sizes for the optimization runs found in the results section are detailed in Table 3-1.

$$Obj = \min(f(Cap, v)) \quad (3-1)$$

Where:

$$C_{limit} = C_{mot} + C_{bat}, v < 60km/h \quad (3-2)$$

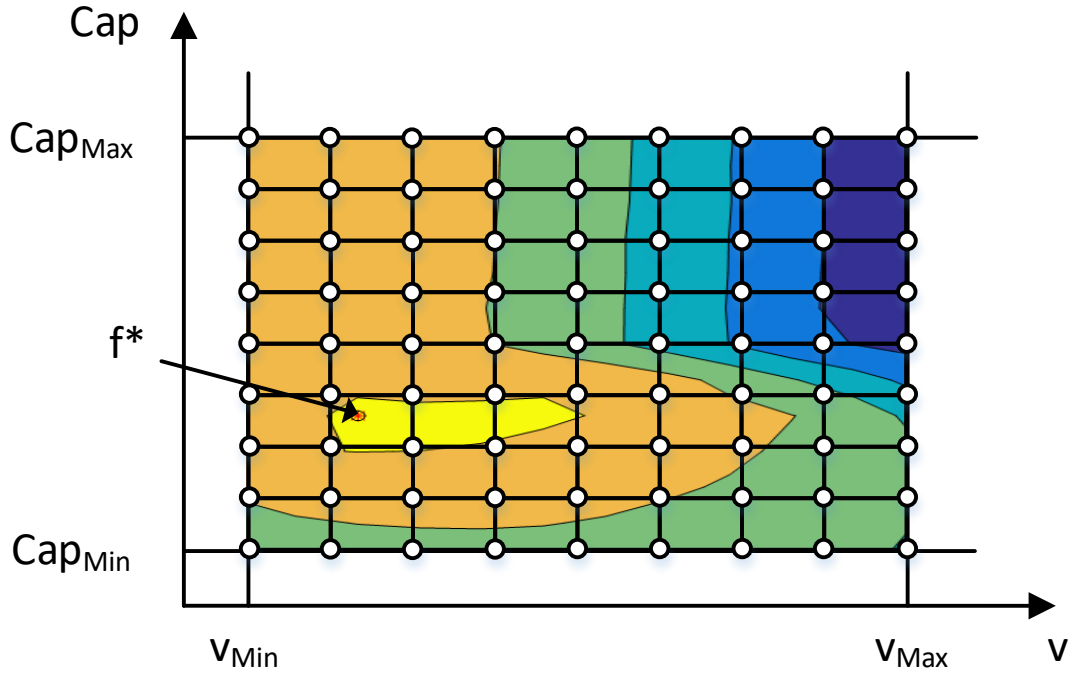


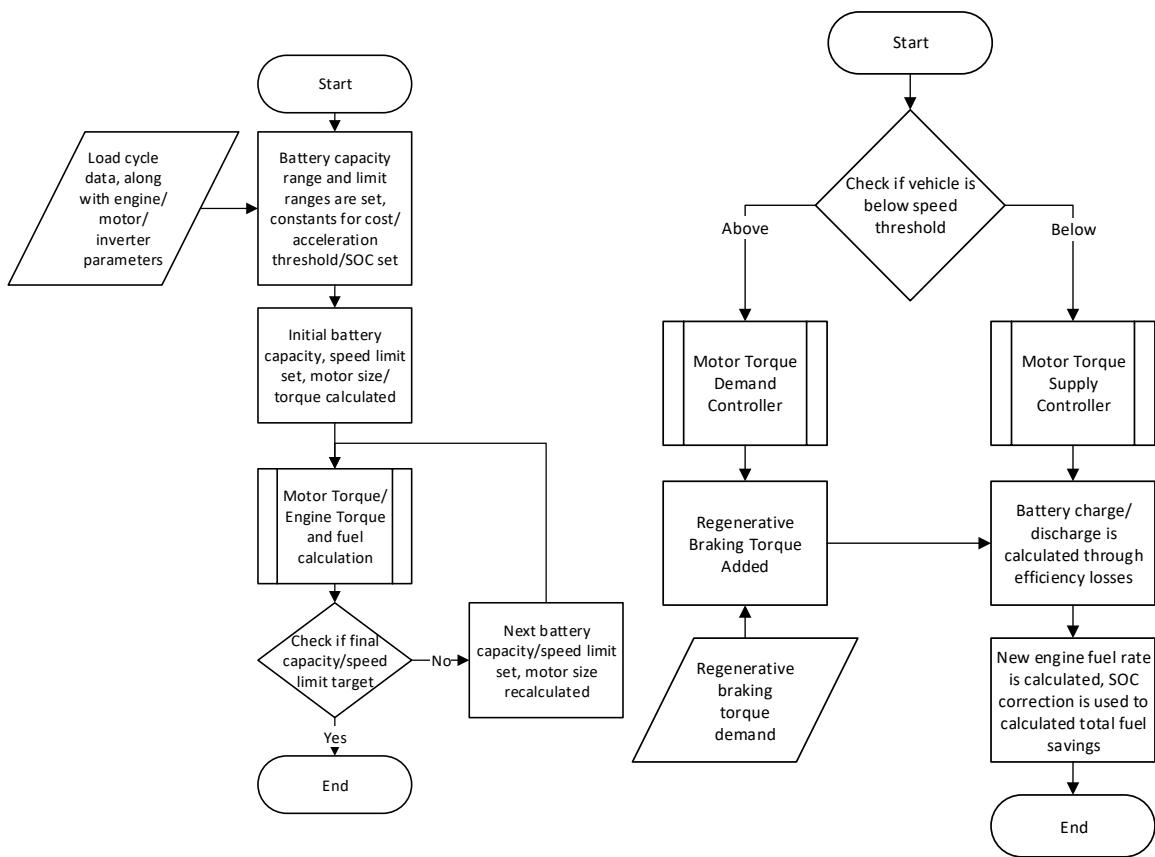
Figure 3-6: Exhaustive search grid

Table 3-1: Optimization problem parameters

Term	Description	Value
$Cap$	Battery capacity (kWh)	(Varies)
$Cap_{min}$	Minimum battery capacity (kWh)	0.3
$Cap_{max}$	Maximum battery capacity (kWh)	1.4
$Cap_{step}$	Battery capacity step size (kWh)	0.1
$v$	Motor assist vehicle speed limit (m/s)	(Varies)
$v_{min}$	Maximum motor assist vehicle speed limit (m/s)	5
$v_{max}$	Maximum motor assist vehicle speed limit (m/s)	17
$v_{step}$	Motor assist vehicle speed limit step size (m/s)	1
$f$	Fuel savings (kg)	(Varies)
$C_{bat}$	Cost of battery (\$)	(Varies)
$C_{mot}$	Cost of motor (\$)	(Varies)
$C_{limit}$	Cost limit (\$)	(Varies)

### **3.3 Sizing Algorithm for Mild Hybrid Optimization**

In order to properly dimension an ICE vehicle to convert it to a mild hybrid, selection of the motor and battery are a priority. The motor in a parallel HEV is only as good as its complimenting battery, as it will always draw power from the battery to assist in torque operations. A proposed algorithm is used to determine the size of the battery and motor. The proposed algorithm is based upon a rule based motor control strategy which allows for the induction motor to supply torque during the acceleration of the vehicle, as well as start/stop functionality. The motor supply controller is based upon the Honda Insight controller, which allows the motor to help during propulsion, only when at low speeds [39]. In addition, the motor can demand torque from the engine during low-no acceleration periods when efficiency is low, as well as assist during braking operations, allowing for regenerative braking. Figure 3-7 demonstrates a logic based flow chart for the algorithm as well as the basic process of the motor controller.



a) Overview of sizing algorithm

b) Motor torque/engine torque and fuel calculation sub process

**Figure 3-7: Logic flowchart for sizing of battery and electric motor**

To allow for an iterative brute force optimization method, various constraints were set to allow for the simplification of the optimization. In this algorithm, the cost of the system is restrained with the battery and motor sharing a set cost. Thus, as the battery size goes up, the motor size goes down, and vice versa. The algorithm iterates across a set of battery capacities, with battery capacity being the primary factor in battery cost, at approximately \$209/kWh [41]. Furthermore, induction motors for automotive applications are conservatively assumed to have a power based cost, at approximately \$10.8/kW [42].

In addition to the battery capacity as an iterative variable in the optimization process, the desired rated speed of the motor must be determined in order to properly size the motor. This rated speed can be achieved through the design of the motor itself, or through changing the pulley ratio between the motor and engine. After the rated speed and battery capacity are set, the maximum motor torque is calculated, as shown in equations (3-3) to (3-6), with all terms defined in Table 3-2.

$$C_{mot} = C_{total} - C_{bat} \quad (3-3)$$

$$C_{bat} = Cap_{bat} Rate_{bat} \quad (3-4)$$

$$P_{max} = \frac{C_{mot}}{Rate_{mot}} \quad (3-5)$$

$$T_{max} = \frac{9550 \cdot P_{max}}{RPM_{rated}} \quad (3-6)$$

**Table 3-2: Costing and motor sizing terms**

Term	Description	Value
$C_{mot} C_{bat} C_{total}$	Cost terms (motor, battery, total)	(Varies)
$Cap_{bat}$	Battery capacity (kWh)	
$Rate_{bat}$	Cost per kWh of battery pack	\$209/kWh
$Rate_{mot}$	Cost per kW of induction motor	\$10.8/kW
$P_{max}$	Maximum motor power (kW)	(Dependent on cost)
$RPM_{rated}$	Rated motor speed (RPM)	(Varies)
$T_{max}$	Max motor torque (Nm)	(Dependent on cost/rated speed)

After the motor and battery size are determined, the algorithm then determines the max motor torque curve, based upon the induction motor design found in General Motors e-Assist technology [18]. Furthermore, the motor efficiency map is assumed to match that

found within the e-Assist technology, and the torque and rotation speed axis are scaled accordingly. As the inverter needs to be paired between the motor and the battery, its efficiency is based upon the motor's rotational speed and torque output, and is assumed to be scaled to the motor based on the results found during low voltage operation of the 2004 Toyota Prius drivetrain [43].

In order to effectively determine operational points for the motor, several parameters need to be tracked during the duration of a drive cycle. These parameters are obtained through the simulation of the ICE vehicle model. Specifically, the vehicle's speed, acceleration, brake power, engine speed, engine torque, fuel rate, and engine efficiency are required. In addition, the efficiency, and fuel consumption of the engine across its breadth of torque and speed limits are required.

A control variable is used to modify the amount of time the motor is supplying or demanding torque to the engine. In the motor control strategy, vehicle speed is used to determine a cutoff at which the motor no longer aids the engine during propulsion, and switches to regenerate energy from the engine to the battery. The speed limit will be used in tandem with the battery state of charge to limit the operation of the motor during torque assist, altering fuel savings depending on the driven cycle. Similarly to the battery capacity, the algorithm will use the speed limit as an iterative variable in order to optimize the vehicle's performance. This algorithm assumes that the grade of the road during the drive cycle is zero, and does not take into account differences in elevation over the duration of the cycle. The algorithm uses the nested motor controller and determines motor operational points during the cycle. The algorithm then modifies the engine torque and speeds

according to the changes induced by the motor controller. The algorithm feeds the resulting calculated power from the motor is fed back into the new Li-Ion battery through the inverter, and the new SOC, fuel rate, and total fuel are calculated. Finally, the initial and ending SOC of the battery are compared and used with the average efficiency of the engine, motor, and inverter to determine the required additional fuel to compensate for the difference in SOC.

In order to determine the amount of torque that the motor can assist the engine during propulsion, several factors need to be considered, as shown in Figure 3-9. Primarily, the vehicle needs to be at a low speed. Using the motor to assist at low speeds prevents the engine from operating at low efficiency points, and allows the motor to deal with sudden accelerations. Next, the battery SOC must be at an acceptable level in order to power the motor during propulsion. If the SOC is drained too low, then the state of health (SOH) of the battery will decrease significantly, as such the motor provides no torque assistance. Finally, the motor sizing shown in Figure 3-7, and described above determined the maximum torque at any given rotational speed. The engine torque demand is compared to the maximum motor torque at the current rotational speed, and if the motor can supply the engine torque, it alone will propel the vehicle; otherwise, it will assist the engine to its maximum capacity. The sub process for torque supply is demonstrated in Figure 3-8.

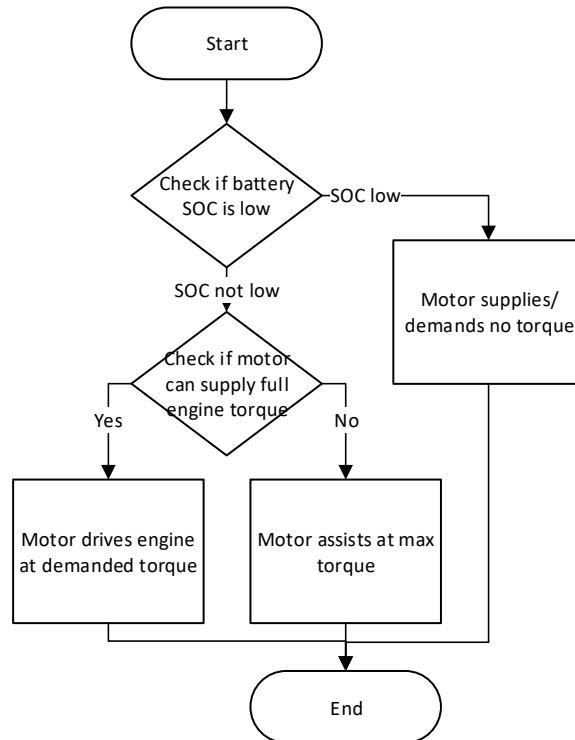


**Figure 3-8: Motor torque supply controller sub process**

In contrast to the torque supply controller sub process, the torque demand controller sub process as shown in Figure 3-9 acts to increase the load on the engine in order to regenerate energy. In addition to the controller, the vehicle can also regenerate power through regenerative braking. In a belt configuration, regenerative braking acts through the various gear ratios found in the transmission, and through the torque converter itself, but generates a torque that is opposite to that of the vehicle’s motion. The regenerative braking is a key factor in the torque demand sub process, as it limits the amount of torque that the motor can solely load onto the engine without burdening the rest of the drive train and the torque output of the vehicle itself. In order to determine the amount of regenerative braking, a simple speed-percentage brake power is used to dictate the maximum possible brake load the motor can supply. This load is further decreased by the physical torque limitation of the

motor's size, and no regenerative braking occurs if the SOC of the battery is at its maximum.

The first check in determining the motor torque demand is comparing the vehicle's speed. If the vehicle is at a standstill, the engine is assumed to have shutoff, setting the engine and motor torque and speed to zero. Otherwise, the engine efficiency at the current engine speed is compared to the peak possible efficiency at the given speed. If the engine efficiency is near its possible maximum, then the motor will provide no additional torque load. If the efficiency is below its highest value, the SOC of the Li-Ion battery is then examined to see if it is at its maximum. As discussed prior with torque assist, pushing the battery past its safe capacity results in a decreased SOH, as such the motor will demand no torque from the engine if the battery SOC is too high.

After the required checks have been made, the total torque required to push the engine to the maximum efficiency point is calculated. At this point both the engine torque difference and the regenerative braking torque are added, and compared to the maximum motor torque. If the torque demand is too high, the engine torque increase is lowered, while keeping the regenerative braking torque at its current value. Afterwards, the new theoretical engine efficiency from the increased torque is calculated, along with the motor, inverter, belt, and battery losses. If the losses from the mild hybrid components are higher than the gain from the efficiency increase, no torque is demanded from the motor. Otherwise, the motor will output the required torque increase.

In summary, the algorithm uses exhaustive search on a nested plant/control optimization method for a belt driven ISG mild HEV. The search iterates through a range

of battery sizes that directly affect the size of the motor through a fixed cost for the battery/motor combination. The search also iterates through a range of speed limit values for the controller. The speed limit value is used to determine the whether the electric motor with supply or demand torque from the engine. The optimized component sizing/control combination, is determined by the largest fuel savings, and is then simulated on the mild HEV model.

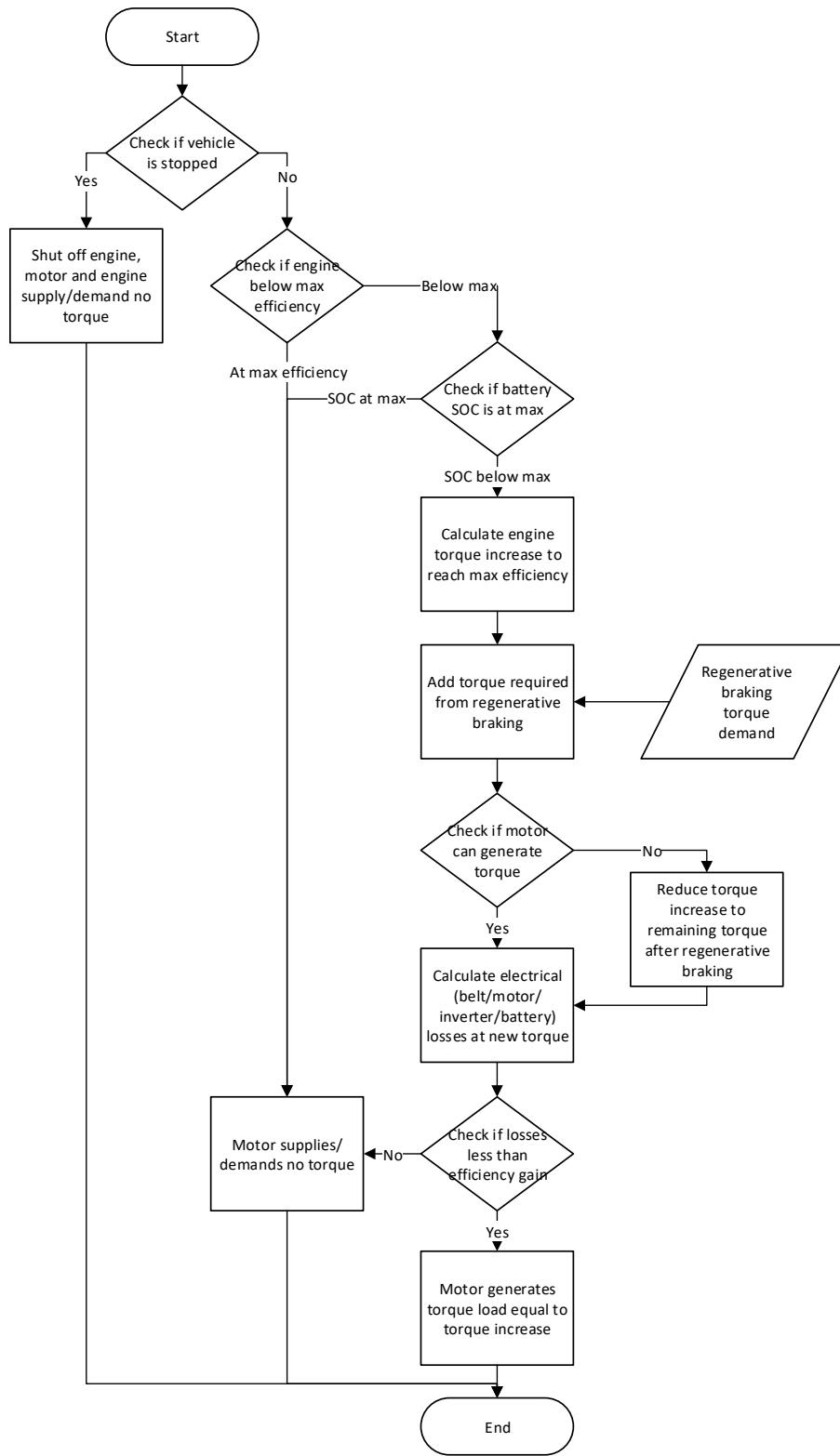


**Figure 3-9: Motor torque demand controller sub process**

## **4 Modelling and Validation**

In order to implement the design process described in Chapter 3, the following modeling, coding, and validation must occur:

- 1) Create a Simulink model of an ICE F-150 truck based on the available dynamometer data [40]. Validate the model to this dataset. (Section 4.1)
- 2) Modify the validated ICE F-150 Simulink model to be a mild hybrid with battery and motor/inverter components. Implement the control strategy described in Chapter 3. (Section 4.2)
- 3) Create a script to reflect the rule based control in the hybrid Simulink model, and the component implementation. The script runs in a fraction of the time as the actual hybrid Simulink model. This script will be used to iterate through all the plant and control parameters due to its fast run-time. (Section 4.3)

Once these steps are implemented, the optimization algorithm is used to determine the plant/control design of the mild hybrid on both real world and standard cycles. The plant/control pairings of both the real world and standard drive cycles are run on the real world driving data, and the resulting fuel savings are compared.

### **4.1 ICE vehicle model**

A vehicle model was developed in MATLAB/Simulink that consists of three core modules: the driver, the controller, and the plant, as shown in Figure 4-1. The driver model is essentially a proportional-integral (PI) control loop that controls the vehicle speed to approximately follow the reference cycle speed. The driver model generates a torque demand signal (positive for accelerations, negative for braking), which is the wheel torque

needed to follow the drive cycle. The torque demand is sent from the driver model to the controller model. In the controller model, a control strategy was developed to use various vehicle parameters and the driver torque demand to calculate commands for braking, gear shifting, engine torque, and alternator power. These signals are sent to the plant, which is the vehicle powertrain and chassis.

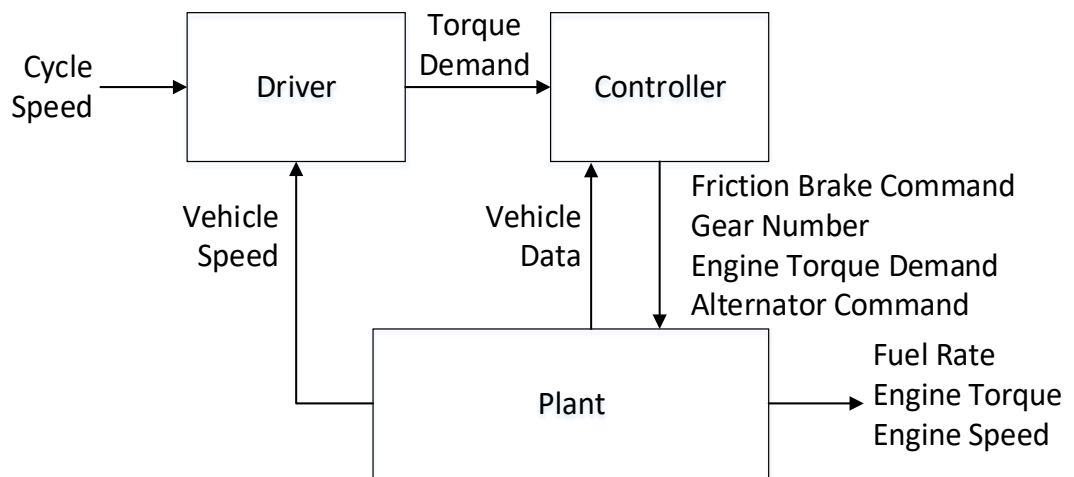


**Figure 4-1: Vehicle model overview**

The plant accepts the controller commands and calculates outputs such as fuel rate and vehicle speed. The plant is based on physical models of each component, where power flows through the drive train. As shown in Figure 4-2, both electrical and mechanical power are considered. Starting from the torque demand from the controller to the engine, torque output is recalculated after engine efficiency losses, so that the fuel rate can be calculated. The resulting torque value is sent through the mechanical accessories, alternator, torque converter, transmission, wheel, and chassis, with the appropriate losses being subtracted in each component. For example, in the wheel model, rolling losses are subtracted to get a net torque into the chassis, and in the chassis, aerodynamic losses are subtracted to get the net

force applied to accelerate or decelerate the chassis. The chassis block then calculates the vehicle speed. From the chassis/wheel block, the rotational speed flows back through the powertrain components. Equations (4-1) to (4-5) approximate the linear force required to reach the desired speed, along with the force input from the PI controller.

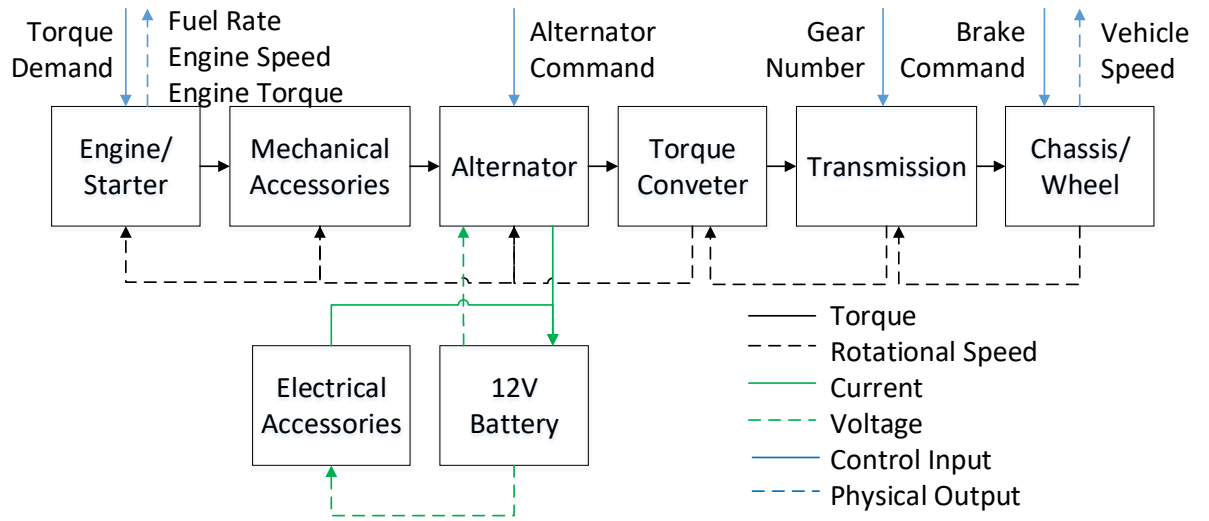


**Figure 4-2: Conventional ICE plant model**

Along with the mechanical power calculations, the electrical power from the battery and alternator are calculated for the electrical accessories and starter motor. The alternator generates current from the mechanical power supplied to it, and sends that current signal into the battery model. The electrical accessories and starter motor draw current from either the battery or alternator, depending on SOC of the 12 V lead-acid battery model. Table 4-1 shows the basic parameters of the 2017 F-150 engine and chassis, along with the terms in equations (4-1) to (4-5).

$$F_{aero} = \frac{1}{2} \rho_{air} A_{frontal} C_{drag} V^2 \quad (4-1)$$

$$F_{roll} = C_{roll}m_{veh}g \quad (4-2)$$

$$F_{accel} = m_{veh} \frac{dV}{dt} \quad (4-3)$$

$$F_{accel} = m_{veh}g \sin\left(\frac{\theta\pi}{180}\right) \quad (4-4)$$

$$P_{mech} = (F_{aero} + F_{roll} + F_{accel} + F_{incline} + \Delta F_{PI})V \quad (4-5)$$

**Table 4-1: Vehicle parameters and terms**

<b>Term</b>	<b>Description</b>	<b>Value</b>
$C_{drag}$	Aerodynamic Drag	0.38 <sup>1</sup>
$m_{veh}$	Vehicle Mass	1838 kg
$P_{max}$	Max Power	375hp @5,000RPM
$T_{max}$	Max Torque	470lb-ft @2,500RPM
$A_{frontal}$	Frontal area	3.34m <sup>2</sup>
$\rho_{air}$	Atmospheric density	1.2kg/m <sup>3</sup>
$C_{roll}$	Rolling resistance coefficient	0.007
$g$	Acceleration due to gravity	9.81m/s <sup>2</sup>
$F_{aero}$	Force due to aerodynamic losses (N)	
$F_{roll}$	Force due to rolling resistance losses (N)	
$F_{accel}$	Force required for acceleration (N)	
$F_{incline}$	Force due to road incline (N)	
$\theta$	Road inclination angle (degrees from horizontal)	

#### 4.1.1 Engine Model

The first step in replicating the ICE vehicle in a simplified model was to model the engine of the vehicle. The engine is modelled through two main calculations, the torque

---

<sup>1</sup> Assumed based on past generation F-150, and current generation competitors [19]

calculation, and the fuel rate calculation. The engine torque calculation is determined from the engine speed, engine on/off state, and the filtered torque demand from the engine controller. Equation (4-6) demonstrates the basic logic in choosing the outputted engine torque. The filtered engine torque is determined by feeding the demanded engine torque through a transfer function that represents the response time of the engine, in this case the engine response time is assumed at 0.3 seconds.

$$\tau_{eng} = \begin{cases} \tau_{filt\_dmd}, & X_{eng} > 0 \\ \tau_{zero\_fuel}, & otherwise \end{cases} \quad (4-6)$$

If the engine is currently off, the engine will then produce a zero fuel torque. The zero fuel torque is determined through a script and is based on the engine size. Shown in Figure 4-3 is the zero fuel torque map representative of the engine found in the F-150. The torque expressed in this map is representative to the resistance the powertrain will receive if the engine is propelled by a force other than combustion, such as the induction motor in the mild hybrid setup.

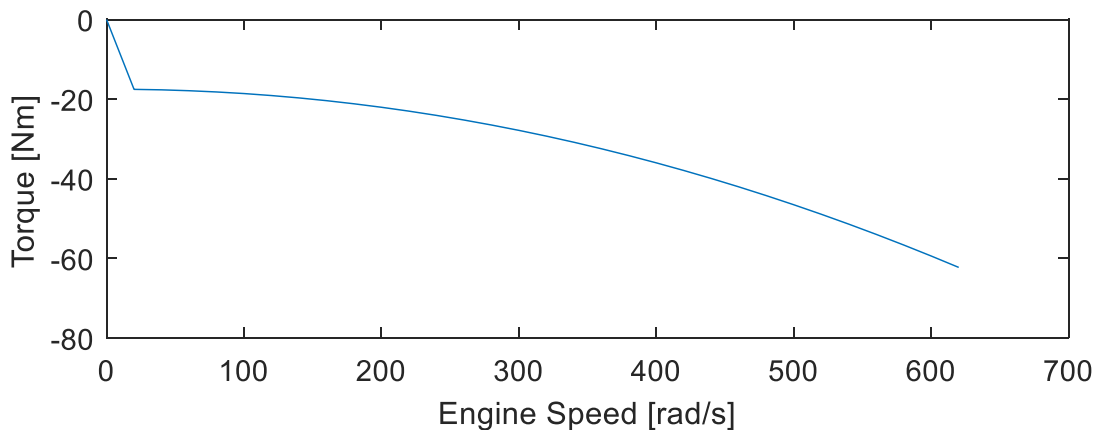


**Figure 4-3: Zero fuel engine torque map**

Next, the fuel map of the engine must be determined in order for the vehicle model to be properly valid. The first step in mapping the fuel rate of the vehicle is to collect data from various operating points of the engine. This is done by examining standard drive cycle such as NEDC, US06, UDDS, and HWY, and collecting fuel, engine speed, and engine torque at any given time. Once all of the data points have been collected into a single dataset, the points are then plotted against a standard fuel map of a similarly sized engine. The fuel map is then adjusted to fit the operating points found in the cycle. The fuel map will be adjusted after initial validation stages of the vehicle model to increase its accuracy. A fuel map demonstrating the mid-range speed of the engine commonly seen in the standard drive cycles is shown in Figure 4-4.

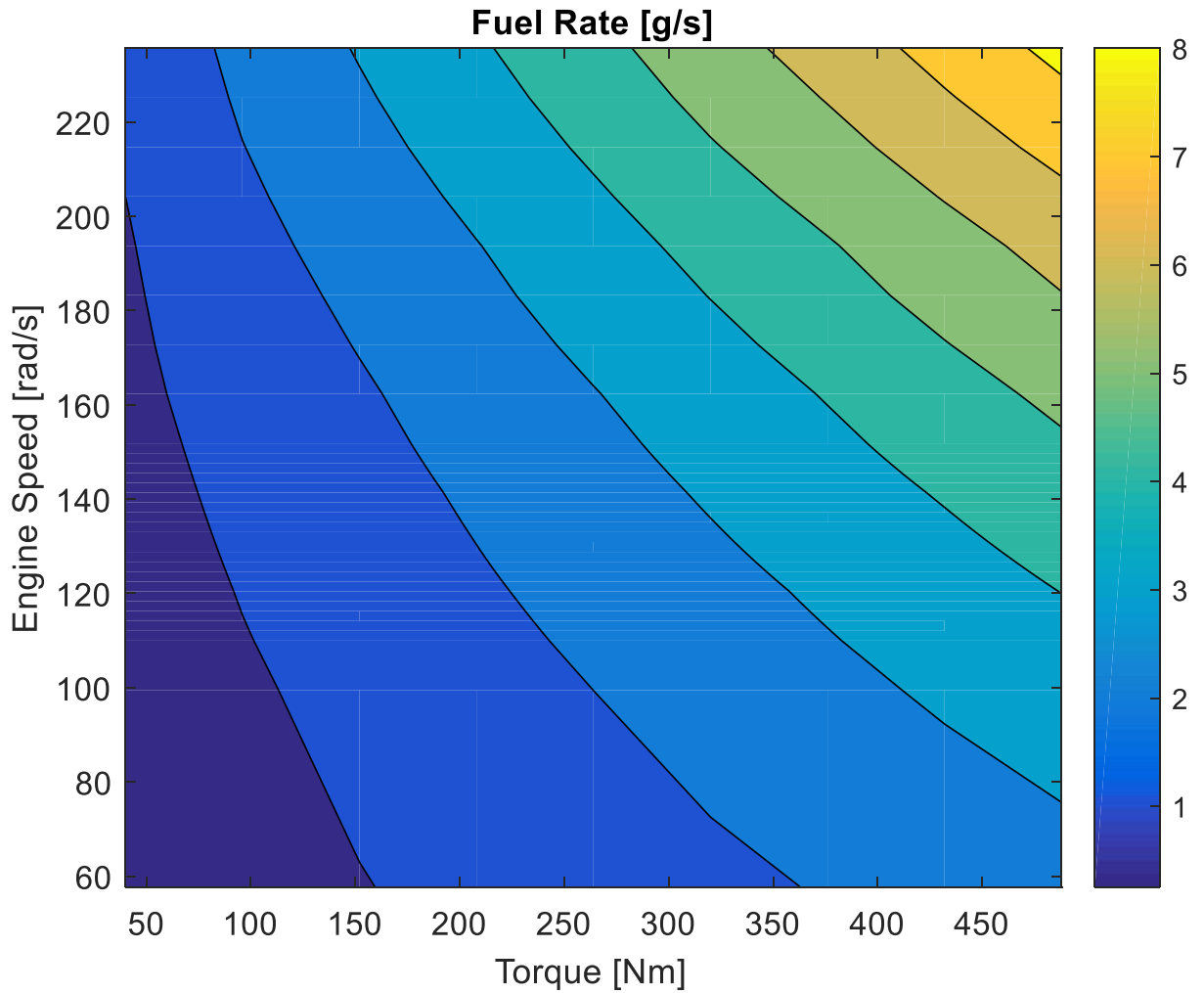


**Figure 4-4: Created Engine fuel map for F-150**

Once a proper fuel map is implemented, the engine can effectively calculate the fuel consumed at any given time. In order to calculate the fuel rate, the engine needs to determine the operating condition of the engine. The primary factor in determining the operating condition of the engine is if the engine is operating above the required starting speed, and igniting fuel. In this state, the engine is considered to be cranking, as shown in (4-7). If the engine is above cranking speed and the torque output is positive, the engine

will solely use the fuel map to determine its fuel rate. However, if the vehicle is cranking but the torque that the engine is producing is negative, the engine determines the fuel through a calculated value ( $\dot{m}_{fuel_{neg}}$ ). In the case of negative torque, the model uses linear extrapolation between the torque and the minimum torque index value of the fuel map, to give an approximate estimation of fuel consumption.

$$X_{crank} = \begin{cases} 1, & X_{eng} > 0, \omega_{eng} > \omega_{str} \\ 0, & otherwise \end{cases} \quad (4-7)$$

$$\dot{m}_{fuel} = \begin{cases} \dot{m}_{fuel_{lookup}}, & X_{crank} > 0, \tau_{eng} > 0 \\ \dot{m}_{fuel_{neg}}, & X_{crank} > 0, \tau_{eng} \leq 0 \\ 0, & X_{crank} = 0 \end{cases} \quad (4-8)$$

**Table 4-2: Engine model parameters**

Term	Description	Value
$\tau_{filt\_dmd}$	Filter engine torque demand (Nm)	
$\tau_{zero\_fuel}$	Zero fuel engine torque (Nm)	
$X_{eng}$	Engine on/off state	
$\tau_{eng}$	Engine torque (Nm)	
$X_{crank}$	Engine cranking state	
$\omega_{eng}$	Engine speed (rad/s)	
$\omega_{str}$	Starter speed (rad/s)	10.0
$\dot{m}_{fuel_{lookup}}$	Fuel rate lookup (kg/s)	
$\dot{m}_{fuel_{neg}}$	Negative torque fuel rate (kg/s)	
$\dot{m}_{fuel}$	Fuel rate (kg/s)	

#### 4.1.2 Engine Control

The engine controller determines the torque demand that is sent to the engine. The controller works by examining the previous time step's efficiency losses throughout the powertrain. The PI controller power demand is determined through the linear speed

demand, wheel size, and the PI torque request. Afterwards, the power losses from the mechanical accessories, torque converter, final drive, and gearbox are added to the PI power demand to determine the total power output that the engine will supply. In the mild hybrid model, the supplied or demanded torque from the induction motor are also included in the powertrain losses.

After the total power demand is determined, the engine's torque limit is determined by the vehicle's current speed. The engine's current rotational speed is used to determine the demanded torque request after compensating for losses. The torque demand is then limited by the torque limit, described in the engine modelling section.

### **4.1.3 Gearbox Control**

The largest influence of performance in an ICE outside of the basic engine size and parameters is the gearbox design. A large portion of the gearbox revolves around the selection of gear ratios. The gear ratios determine the amount of torque that the engine will output to the wheels of the vehicle. Displayed in Table 4-3: Gear ratio and specifications of 2017 F-150 drivetrain are the gear ratios found in the 2017 F-150 when paired with the 3.5L ecotech engine.

After the gear ratios are determined, a control strategy is implemented to determine when the vehicle should be in each individual gear. A common control strategy to determine the current gear of a vehicle is to use the pedal position and the current gear of the vehicle to determine the output speed the vehicle to determine its shift points. In the vehicle model, pedal position is not a direct signal as the driver model is based upon a PI

controller. As such, the tractive force output of the driver model is used to approximate a 0-100% throttle pedal position signal in the controller.

**Table 4-3: Gear ratio and specifications of 2017 F-150 drivetrain [44]**

<b>Gear</b>	<b>Ratio</b>
1 <sup>st</sup>	4.70
2 <sup>nd</sup>	2.99
3 <sup>rd</sup>	2.15
4 <sup>th</sup>	1.80
5 <sup>th</sup>	1.52
6 <sup>th</sup>	1.28
7 <sup>th</sup>	1.00
8 <sup>th</sup>	0.85
9 <sup>th</sup>	0.69
10 <sup>th</sup>	0.64
Final Drive	3.31 [45]

In order to properly determine a gearbox control strategy, the data from standard drive cycles was examined. Specifically, the pedal position, along with the gearbox shift points during the operation of the vehicle, were examined in order to reverse engineer a shifting strategy. Figure 4-5 demonstrates the approximate upshift gear points for the gearbox between the 10 gears. The map demonstrates the approximate speed to upshift to each gear, along with the required pedal position. The map spans from 10-100%, with the upshift targets stabilizing from 0-10%.

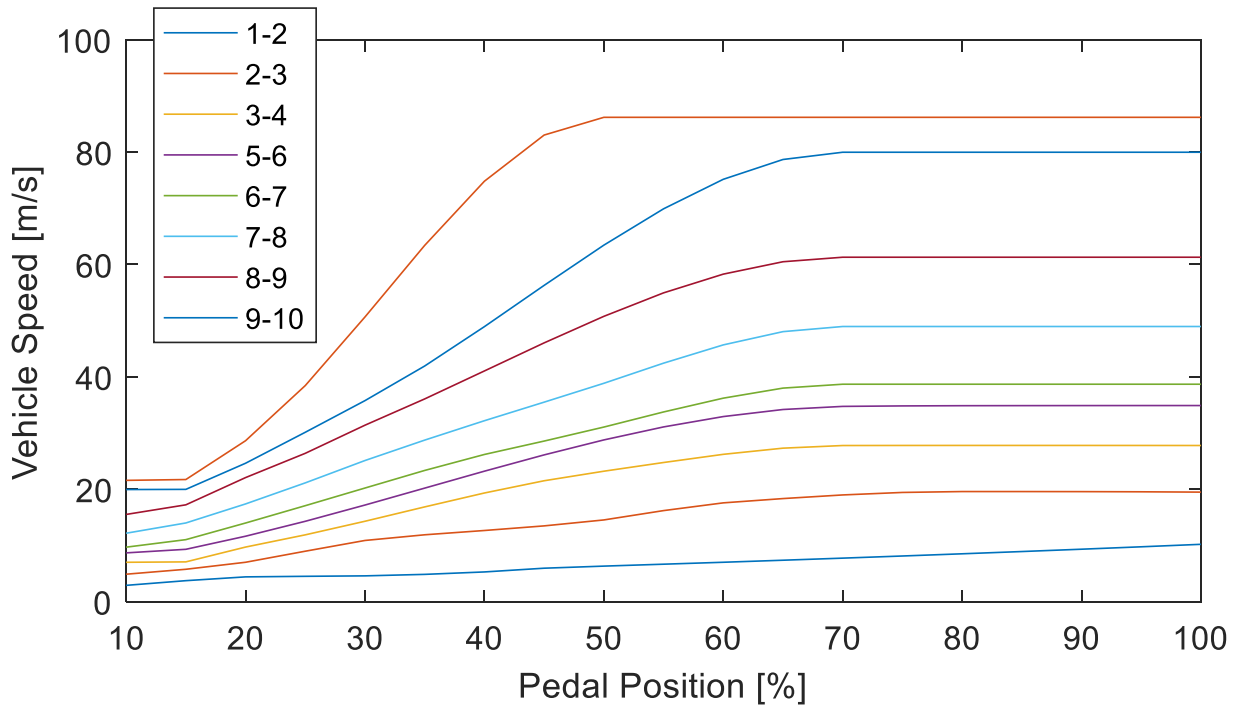


**Figure 4-5: Gearbox upshift map**

In addition to the upshift map, a downshift map was also created. In contrast to upshifting, this control strategy assumes that the pedal position to be 0% when decelerating. As such, the downshift map of the vehicle relies only on the current gear and speed of the vehicle, as shown in Figure 4-6.

In the vehicle model, the controller observes the current gear and determines if an upshift or downshift will occur based on vehicle acceleration. Afterwards, the vehicle controller will change gears, and hold the selected gear for the duration of the shifting time observed in the standard cycle data.

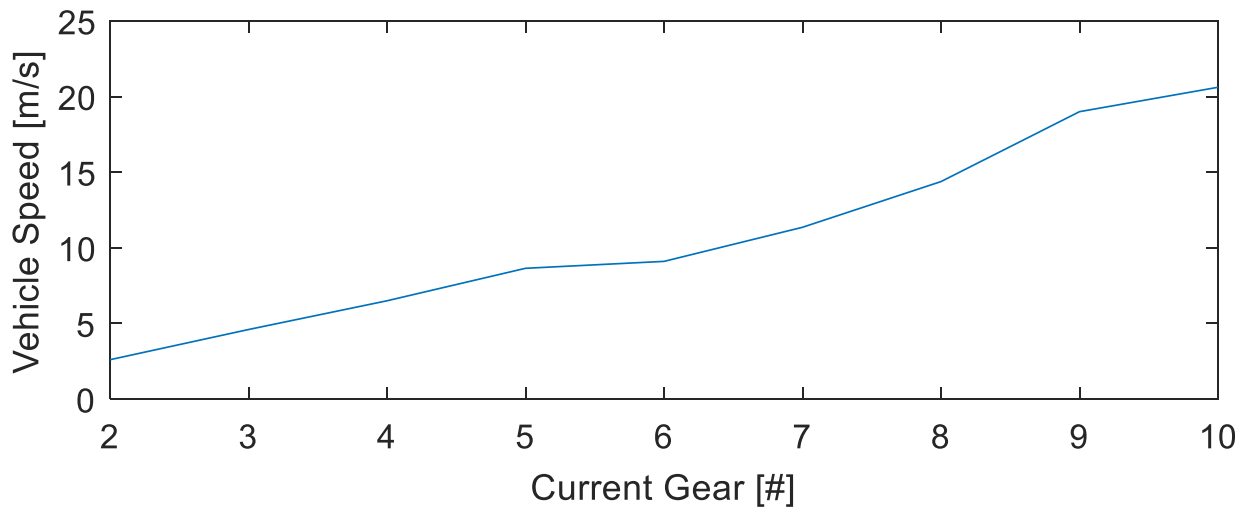


**Figure 4-6: Gearbox downshift map**

#### 4.1.4 Model Validation

In order to ensure that the vehicle model is accurate to the vehicle itself, it must be validated. The key aspect in validating the vehicle model is comparing the time-based data for key variables. In this study, the most important variables to ensuring a valid model are found in the gearbox control, fuel rate, and the speed of the vehicle itself. As such, engine speed is used to determine if the model is in a suitable gear, while fuel rate and vehicle speed are directly compared. The model is validate on the standard highway (HWY) and city (Urban Dynamometer Driving Schedule – UDDS) cycles. These two cycles were chosen due to their combined mixture of highway and city driving conditions.

Shown in Figure 4-7, is the vehicle speed comparison for the HWY cycle. As demonstrated, the model follows the vehicle extremely well, with the only error occurring at high acceleration points. Next, the engine speed is validated, as a representation of the current gear and torque converter. The engine speed is shown in Figure 4-8, and demonstrates a tight fit between the vehicle and model, with some accuracy lost during

large gear shifting periods. Finally, the fuel rate demonstrates a tight fit, with less noise shown in the model than the vehicle data, as demonstrated in Figure 4-9.

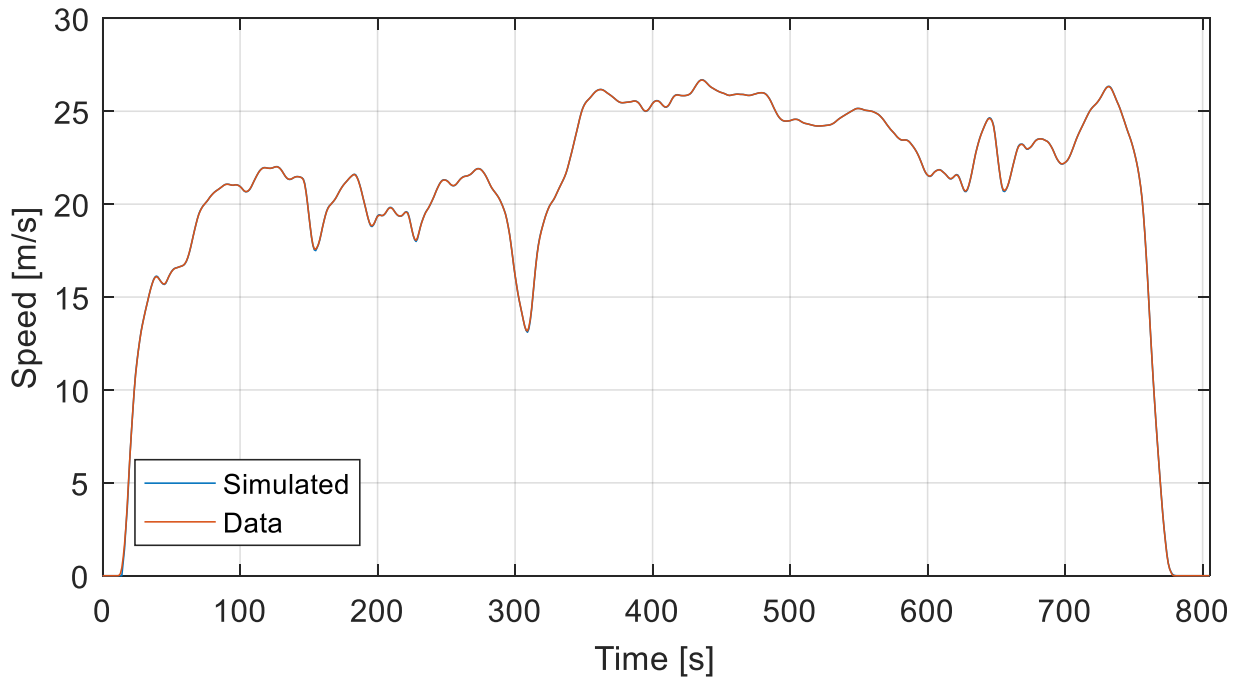


**Figure 4-7: HWY vehicle speed comparison**

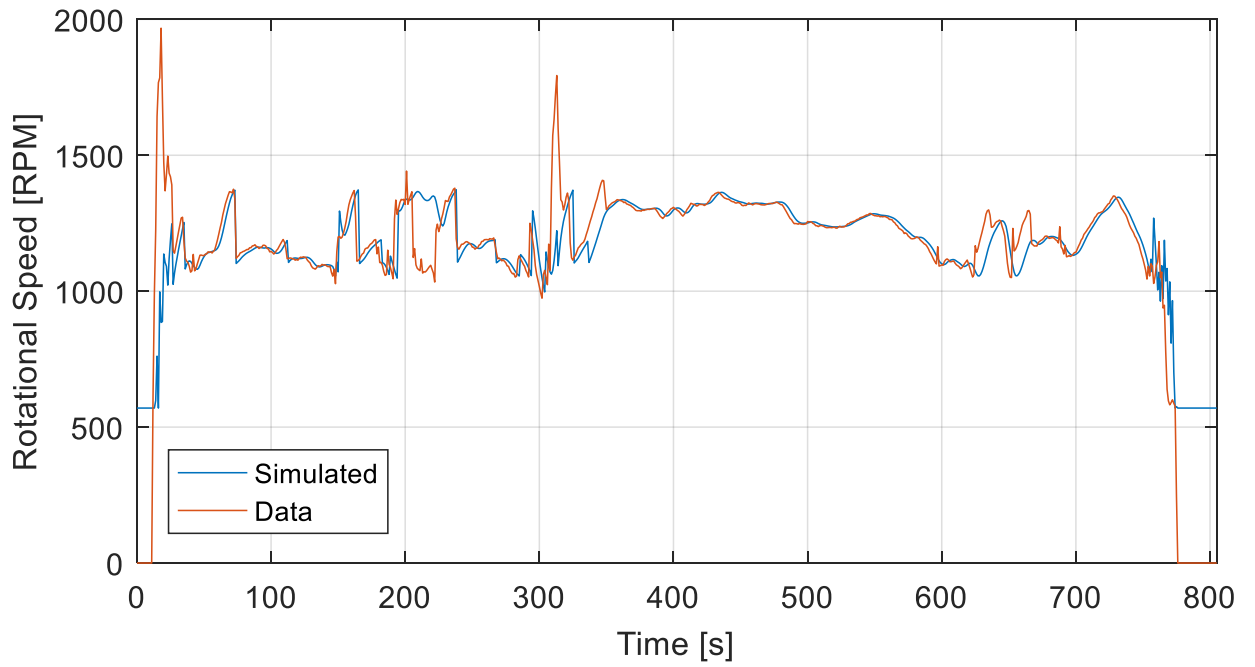


**Figure 4-8: HWY engine speed comparison**

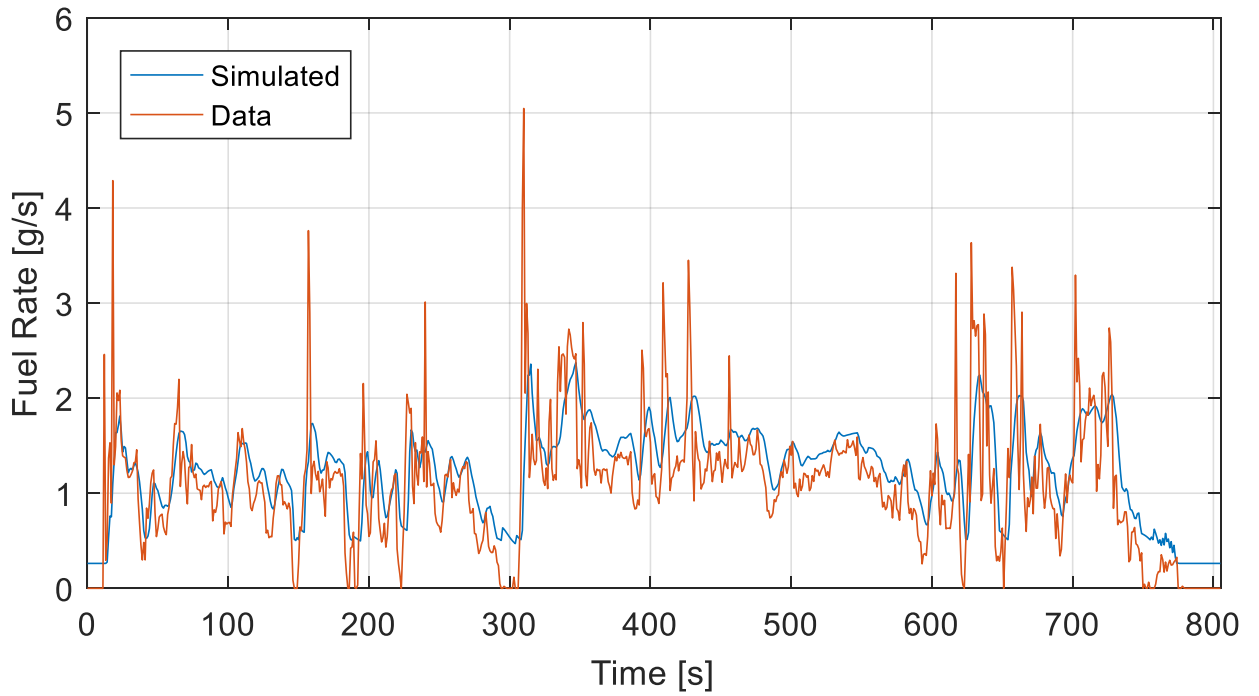


**Figure 4-9: HWY fuel rate comparison**

In contrast to the HWY cycle demonstrating the steady state performance, the UDDS cycle demonstrates the city like driving conditions, as shown by the vehicle speed comparison in Figure 4-10. Similar to the HWY cycle, during the UDDS cycle, the model follows the vehicle extremely well, with some error during acceleration. Next, the engine speed is compared, and the model is validated at higher acceleration points. The engine speed is shown in Figure 4-11, and demonstrates a tight fit between the vehicle and model; however, there are more discrepancies than shown in the HWY comparison, due to the sheer number of gear changes. Finally, the fuel rate comparison demonstrates similar results to the HWY cycle, with slightly less noise in the model, as shown in Figure 4-10.

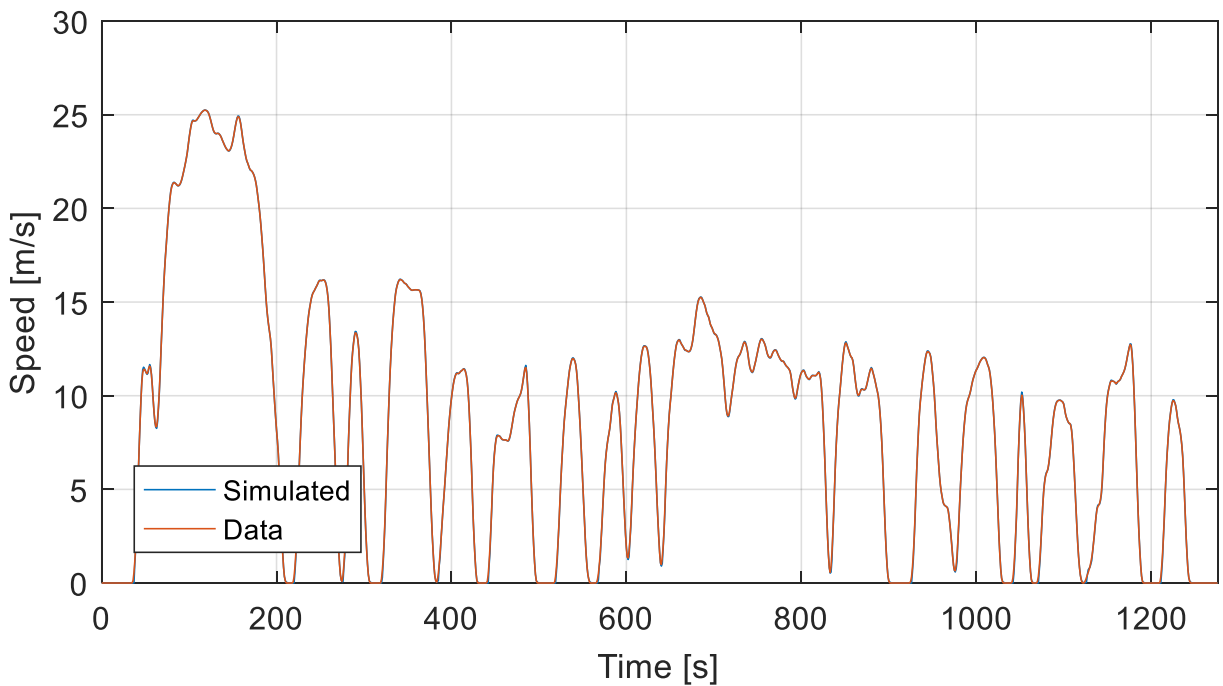


**Figure 4-10: UDDS vehicle speed comparison**

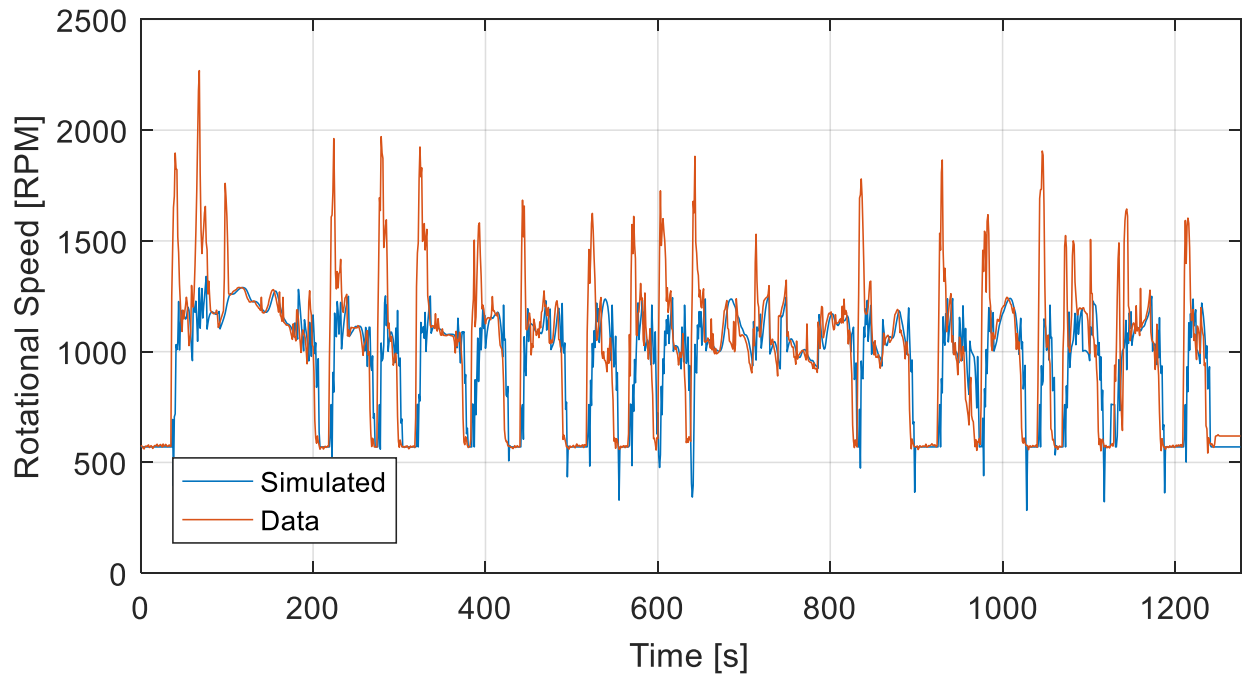


**Figure 4-11: UDDS engine speed comparison**

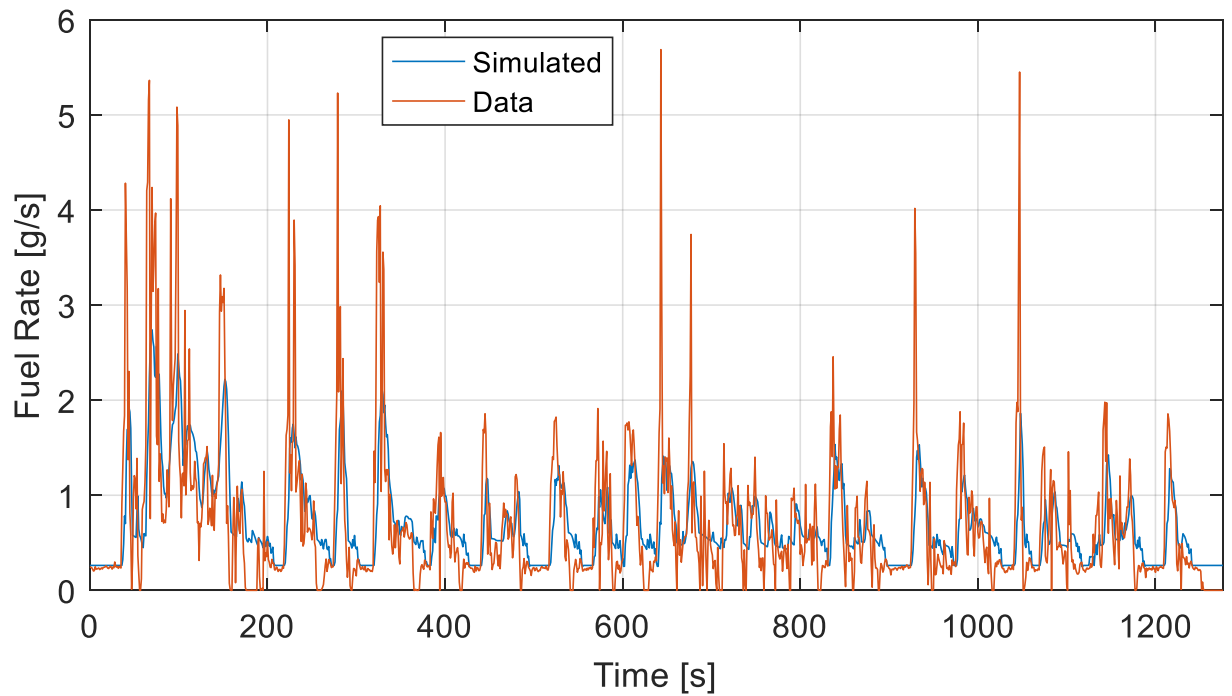


**Figure 4-12: UDDS fuel rate comparison**

As the total fuel savings will determine the sizing of the motor/battery, the overall fuel consumption of the model in comparison to the actual vehicle must be accurate. Table 4-4 demonstrates the fuel validation results between the two cycles. The UDDS cycle demonstrated that the model was within 3.77% of the vehicle, whereas the HWY cycle demonstrated a 5.87% difference. Both cycles demonstrated that the model sufficiently fits the vehicle in terms of total fuel consumption.

**Table 4-4: Fuel consumption model validation results**

Cycle	Vehicle Fuel Consumption (kg)	Simulated Fuel Consumption (kg)	Difference (%)
UDDS	0.919	0.885	-3.77
HWY	0.930	0.988	5.87

As an additional validation, the three time based variable's errors are compared using their mean absolute error (MAE). MAE compares the second by second error between the model and vehicle, and takes the average of the error across the cycle, as demonstrated in (4-9). Table 4-5 demonstrates the MAE for both the HWY and UDDS cycles. Both the UDDS and HWY cycles shown little error when comparing vehicle speeds, with UDDS having the largest MAE at 0.0329m/s. In addition, the UDDS cycle demonstrates some error in engine speed with an MAE of 155.51RPM, whereas the HWY cycle is far lower at 79.31RPM. Finally, both cycles demonstrate similar MAE with their fuel rate, at 0.3593g/s for UDDS and 0.3581g/s for HWY.

$$MAE = \frac{\sum_{i=1}^n |y - \hat{y}|}{n} \quad (4-9)$$

**Table 4-5: MAE model validation results**

Cycle	Engine Speed (RPM)	Fuel Rate (g/s)	Vehicle Speed (m/s)
UDDS	155.51	0.3593	0.0329
HWY	79.31	0.3581	0.0110

## 4.2 Mild HEV vehicle model

After the algorithm described in Chapter 3 has determined the dimensioning of the battery and motor combination, the model will be modified into a mild hybrid configuration. Primarily, the ISG is incorporated in the form of an induction motor, along with the Li-Ion battery and a DC-DC converter to connect the original lead-acid battery. Figure 4-13 demonstrates the new plant model for the mild hybrid configuration. Specifically to note, is that the ISG is connected through a belt driven system, where the losses are considered in the motor/inverter model. The rule based control strategy for the electric motor found in Chapter 3 is implemented into the mild HEV model.

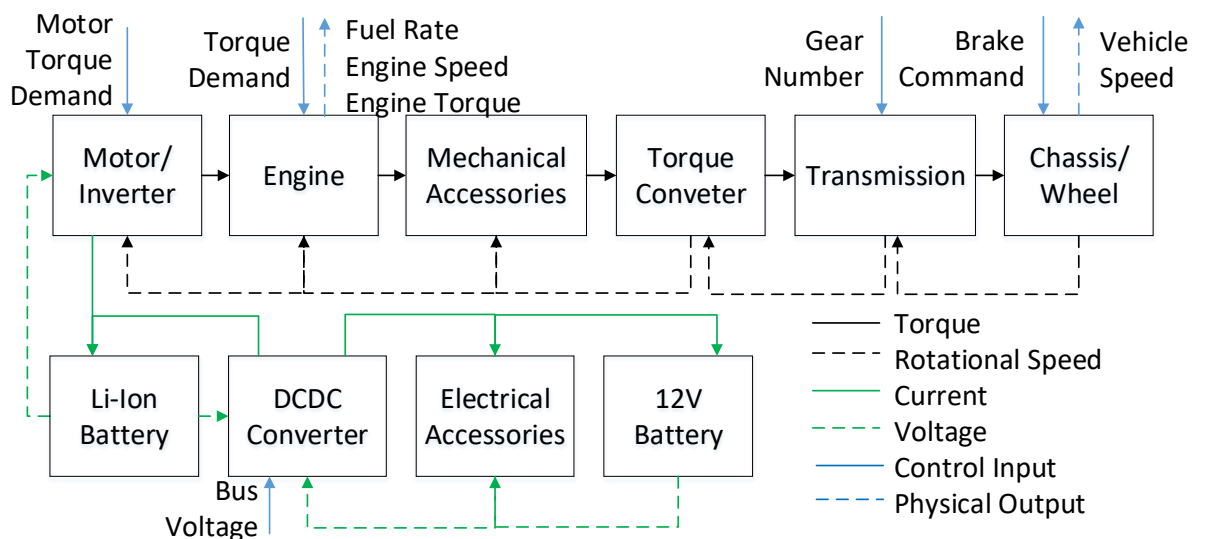


**Figure 4-13: Mild hybrid plant model**

### 4.2.1 Battery Model

In both the conventional ICE vehicle model and the mild hybrid model, the two batteries are modelled using the same basic approach. Each battery is represented using an open circuit voltage- resistor model (OCV-R). Figure 4-14 demonstrates the topology of the battery model, with the current output from the battery and the battery capacity determining the SOC, and then the SOC determining the OCV of the battery. The discharge/charging resistance is then calculated based on the SOC. Finally, the columbic efficiency of the battery is used to calculate voltage drop from the charge/discharge resistance, and the terminal voltage of the battery is determined. The mathematic process and model can be found in equations (4-10) to (4-14), with their terms defined in Table 4-1.

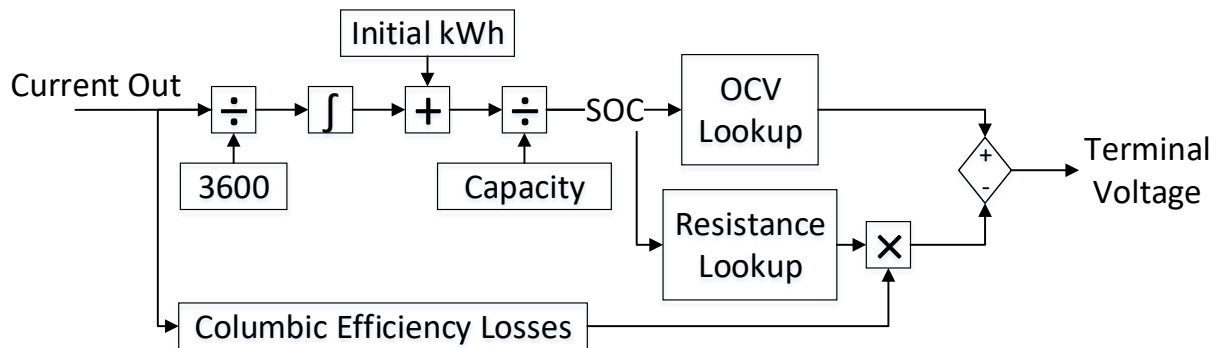


Figure 4-14: OCV-R model of battery

$$V_{terminal} = V_{ohm} + V_{oc} \quad (4-10)$$

$$V_{oc} = f(SOC) \quad (4-11)$$

$$V_{ohm} = I \cdot R_{ohm} \quad (4-12)$$

$$R_{ohm} = f(SOC) \quad (4-13)$$

$$SOC(t) = SOC(t_i) + \frac{1}{Cap_{Ahr} \cdot 3600} \int_{t_i}^t I(t) \eta_{bat} (SOC, sign(I(t))) dt \quad (4-14)$$

**Table 4-6: Battery terms**

<b>Term</b>	<b>Description</b>	<b>Value</b>
$V_{terminal}$	Terminal voltage (V)	
$V_{ohm}$	Voltage on ohmic resistor (V)	
$V_{oc}$	Open circuit voltage (V)	(Dependent on SOC)
$R_{ohm}$	Ohmic resistor (ohm)	(Dependent on SOC, charge/discharge)
$SOC(t)$	State of charge	(Dependent on current, capacity)
$SOC(t_i)$	Initial state of charge	
$I(t)$	Current output of battery	(Dependent on power electronics load)
$Cap_{Ahr}$	Battery capacity (Ah)	
$\eta_{bat}$	Coulombic efficiency of battery	0.95 (lead-acid) 0.99 (Li-Ion)

Both the lead-acid and Li-Ion batteries have high coulombic efficiency, with the lead acid battery assumed to be 95% efficient [46] whereas the Li-Ion battery is assumed to have a coulombic efficiency of 99% [47]. The Li-Ion battery model is based on Lithium Iron Phosphate cells, which have a nominal voltage of 3.2V, and its SOC-OCV curve can be found in Figure 4-15. The total selected nominal voltage for the Li-Ion battery is approximately 96V. As such, 30 cells are combined in series to reach the desired nominal voltage, and the total number of cells in parallel will be decided upon the completion of the optimization result. In addition, the lead-acid battery has a nominal voltage of 12V and its SOC-OCV curve can be found in Figure 4-16.

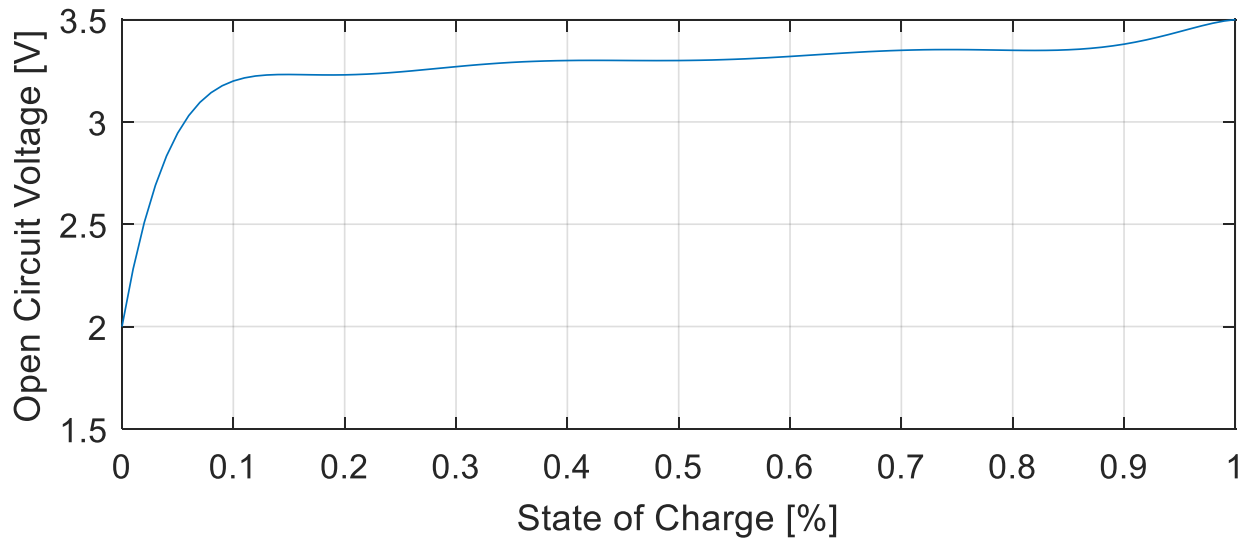


**Figure 4-15: SOC-OCV curve for Li-Ion cell [48]**

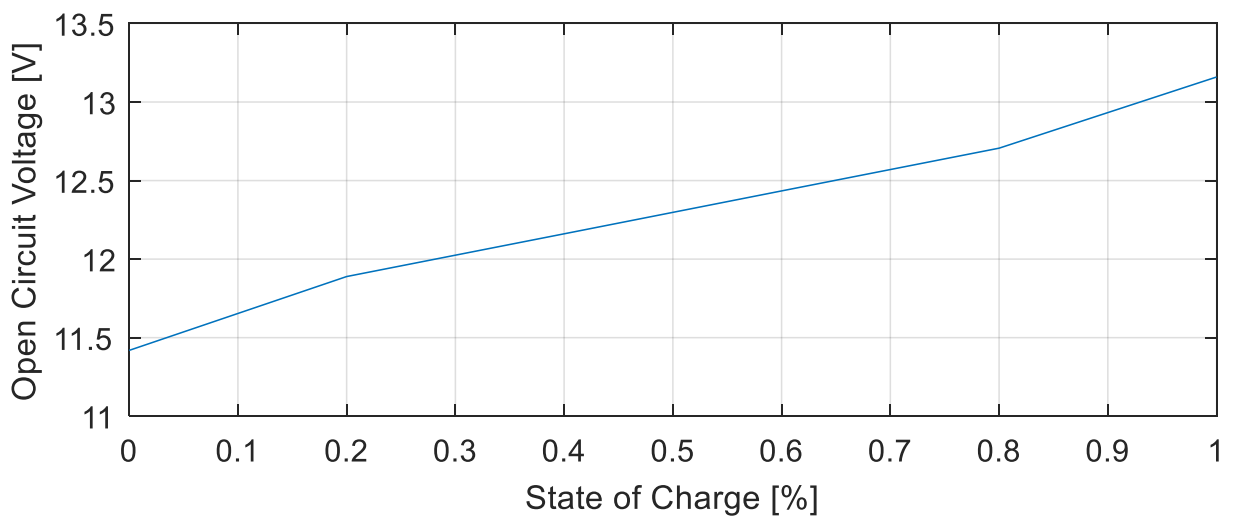


**Figure 4-16: SOC-OCV curve for 12V lead-acid battery [49]**

#### 4.2.2 Motor Model

The motor model works on a simple premise, an input torque signal is sent through the motor controller, which is fed into a transfer function that filters the motor's mechanical torque output based on the time response, which is assumed to be 0.05 seconds. After the torque is filtered, its output is sent through the belt to engine model, simulating the power

transfer to the crankshaft. In order to determine the electrical power draw from the motor, an efficiency lookup table is used. Shown in Figure 4-17 is the efficiency map found in the current generation of General Motors eAssist technology.

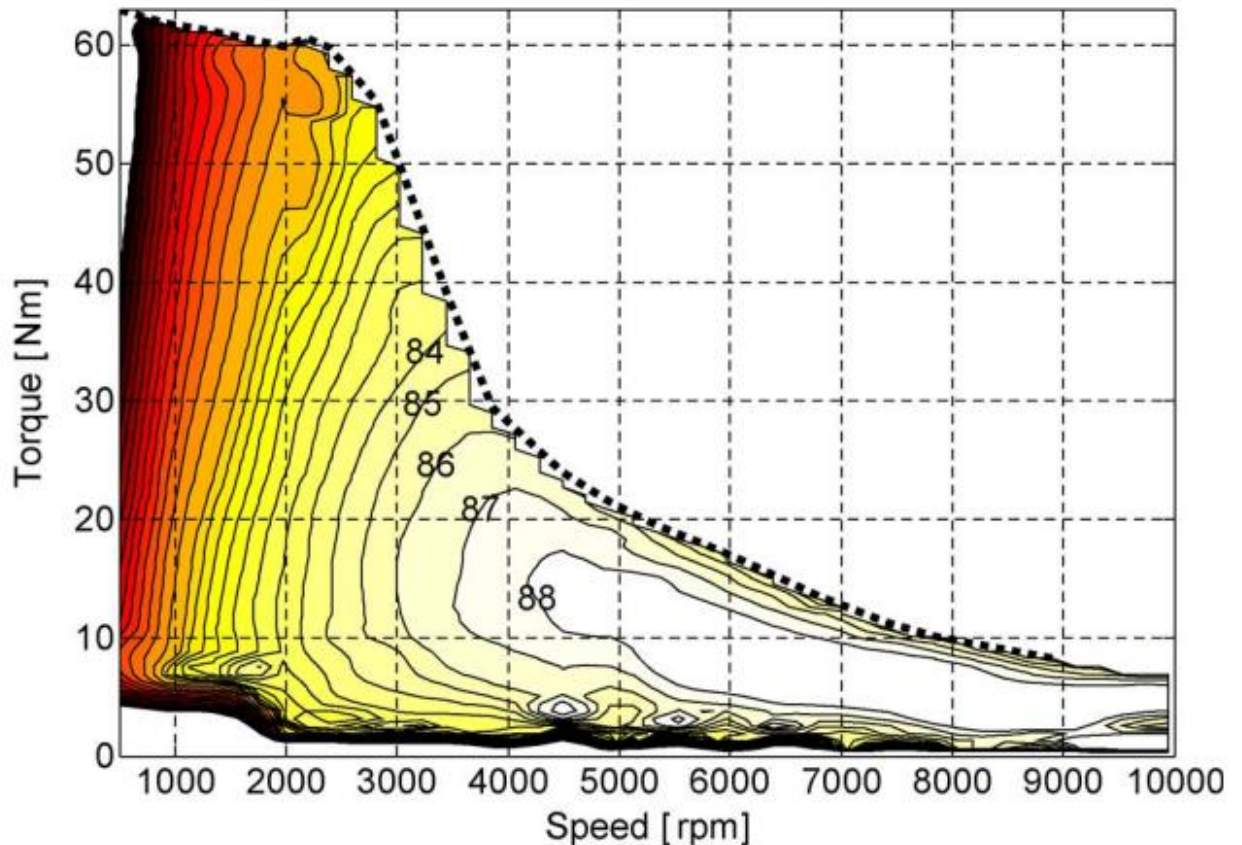


**Figure 4-17: General Motors eAssist induction motor efficiency map [18]**

This efficiency map is used, as it exists as a benchmark for mild hybrid induction motor. In order to adapt this motor map to various motor/battery size combinations, it is resized based on the rated speed equation found in section 3. Furthermore, the maximum torque curve used in the simulation is derived from the same eAssist source [18].

### 4.2.3 Inverter Model

The inverter model works in a similar fashion to the induction motor, without the use of a transfer function to filter the torque demand. As information on inverter efficiency for the eAssist technology was not available, data was taken from the 2010 Toyota Prius breakdown. Specifically, [43] demonstrates the Prius' inverter efficiency map when operating at low voltage levels. As with the motor, the inverter is scaled to reflect the variation in motor and battery size between each run of the sizing algorithm.

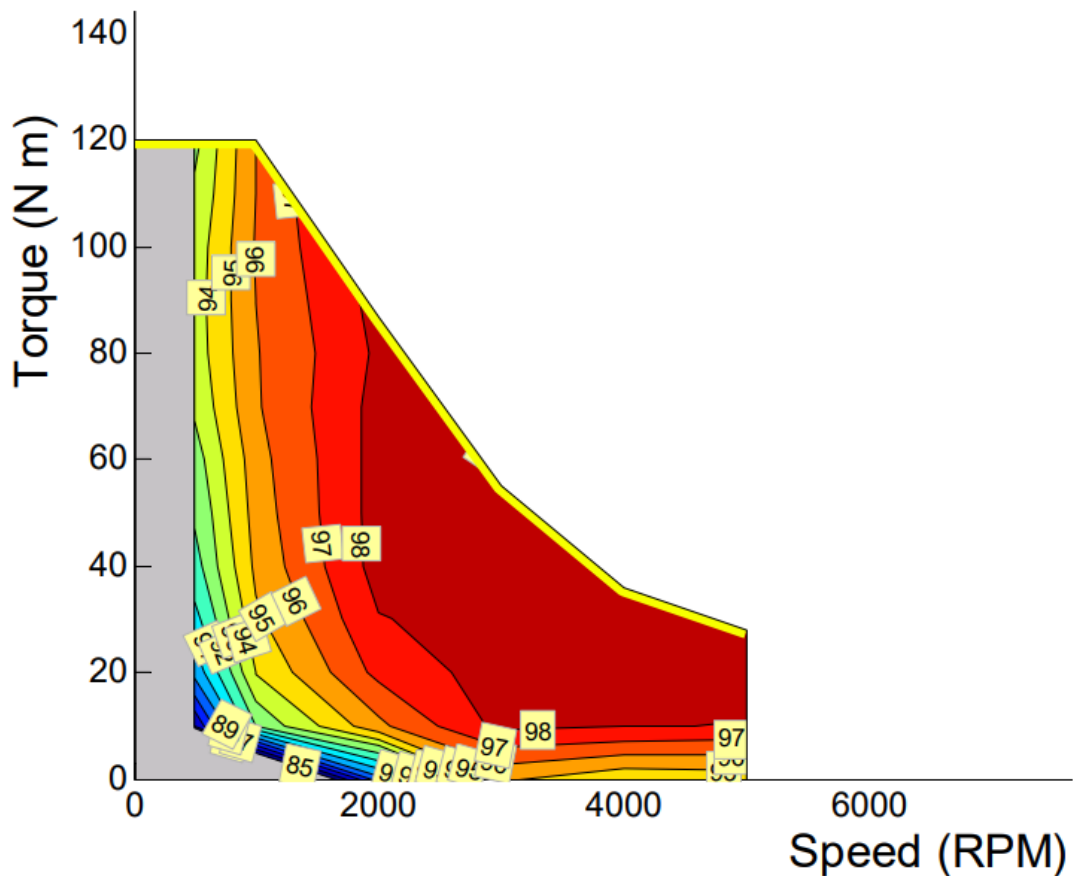
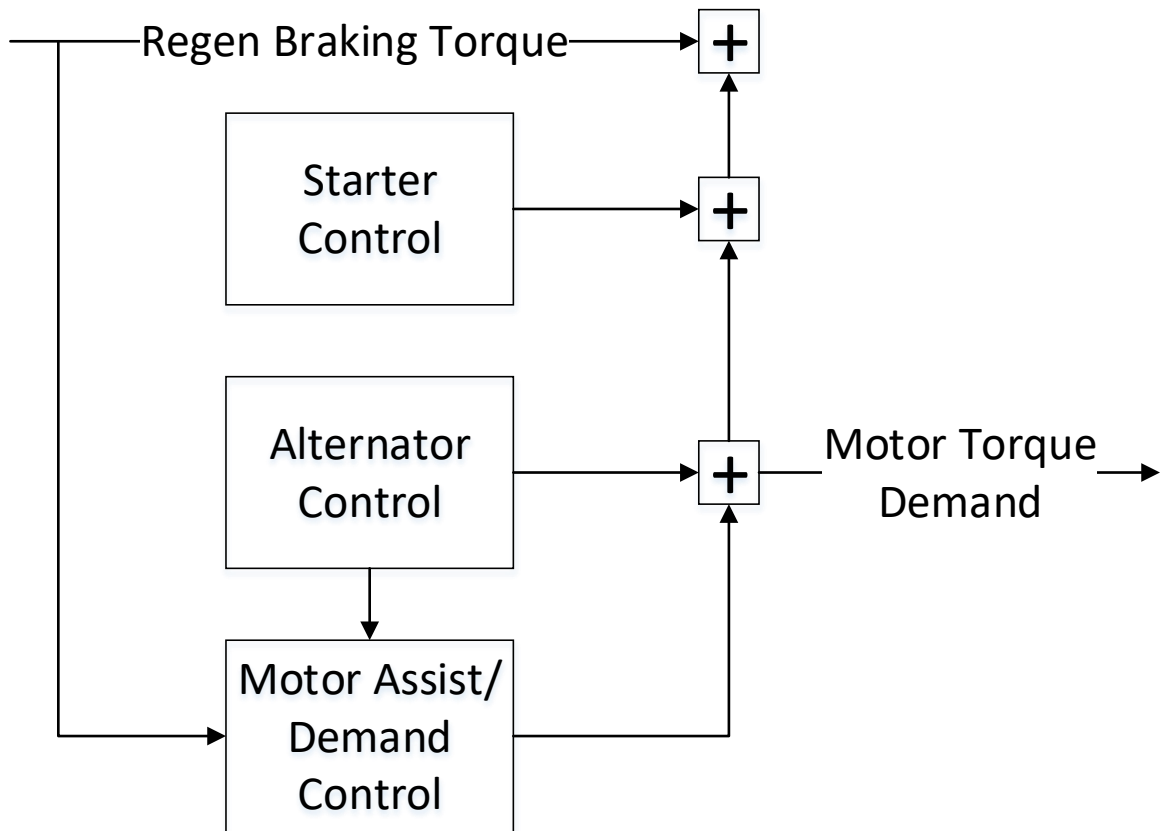


Figure 4-18: Toyota Prius inverter efficiency map [43]

#### **4.2.4 Motor Control**

In order to properly demonstrate the effects of the sizing algorithm, a motor controller was implemented into the mild hybrid vehicle model. The focus of this section is the implementation and adaption of the rule based controller found in Chapter 3, into the mild HEV model. As shown in Figure 4-19, the controller determines the torque signal sent to the motor model. The controller has three sub controllers, the alternator, starter, and motor supply/demand. The alternator controller functions to replace the conventional alternator control found in the ICE model. The function of the alternator controller in the mild hybrid model is to manage the torque request to regenerate the power drawn from the 12V electrical accessories, which are powered through the 12V battery, which is recharged through a DCDC bus. The starter motor works to replicate the starter found in the ICE model, and simply supplies a small torque demand from the motor when the demanded vehicle's speed is increased, and the engine is currently off. In addition, the torque from regenerative braking is determined in the brake controller, and used in subsequent calculations.



**Figure 4-19: Motor Controller**

The motor supply/demand controller is the main control strategy found in the mild hybrid model. Specifically, the rule-based control demonstrated in Chapter 3 was implemented into the mild HEV model through a set of mathematical equations. Table 4-7 demonstrating the parameter definitions and values for the rule based controller.

The motor control strategy is broken down into two main components, torque supply and torque demand. As discussed in the algorithm, torque supply works to help propel the vehicle during acceleration and low speeds, with the controller itself being based upon that found in the Honda Insight [39]. The first step in the supply calculation is to determine if the vehicle speed is below the speed limit set in the controller. Next, the current

SOC is checked against the minimum SOC, and a torque calculation is performed as long as the SOC is above its minimum limit. The total torque supplied will be the lower of the maximum torque the motor can produce at the current speed, and the demanded engine torque, as shown in (4-15).

$$\tau_{mot_{sup}} = \begin{cases} \min(\tau_{eng}, \tau_{mot_{lim}}), & SOC \geq SOC_{min}, a > 0 \\ 0, & otherwise \end{cases} \quad (4-15)$$

In contrast, the torque demand controllers determines the appropriate load to add to the engine to increase efficiency, and regenerate the battery at appropriate times, allowing the motor to further supply the engine at low speeds. The first step in determining the additional torque is to determine the torque required to reach maximum efficiency. As shown in (4-16) the torque is a function of the current engine speed, where the maximum efficiency point is found through the fuel map of the engine, and a reverse lookup function determines the torque difference required to reach that point. Next, the maximum additional torque that can be demanded from the engine is calculated. Demonstrated in (4-17), the controller checks to see if the SOC is below its maximum capacity limit. If the SOC is below the limit, the maximum torque possible is determined by adding the alternator controller and regenerative braking controller torque demand, and subtracting that from the motor's torque limit at the current speed. Next, the controller determines if the motor can support the additional torque required to reach maximum efficiency, if it cannot, the torque demanded is capped at the adjusted motor torque limit.

$$\tau_{eng_{max_{eff}}} = f(\omega_{eng}) \quad (4-16)$$

$$\tau_{eng_{add}} = \begin{cases} \min\left((\tau_{mot_{lim}} - \tau_{reg} - \tau_{alt}), \tau_{eng_{max_{eff}}}\right), & SOC < SOC_{max} \\ 0, & otherwise \end{cases} \quad (4-17)$$

After the maximum additional engine torque is determined, the next step is to determine the combined efficiency of the mild hybrid powertrain. Equation (4-18) demonstrates that components used to determine the new efficiency. Specifically, the additional engine torque along with the regenerative torque and the alternator torque are fed into the efficiency lookup tables of the motor and inverter. Next, the efficiency of the motor is determined through the total power draw from the system. Finally, the new engine efficiency is calculated based on the increased engine torque, and the fuel map.

The final stage of the motor demand controller is demonstrated in (4-19). The new powertrain efficiency is compared to the previous engine efficiency to determine if it is more efficient to charge the vehicle at an increased engine efficiency or to simply run the engine at the original torque. If the new efficiency is higher, and the vehicle is not stopped, the motor will demand the additional torque load from the engine.

$$\eta_{tot_{new}} = \eta_{mot} \cdot \eta_{inv} \cdot \eta_{eng_{new}} \cdot \eta_{batt} \quad (4-18)$$

$$\tau_{mot_{dmd}} = \begin{cases} \min\left((\tau_{eng_{add}} + \tau_{reg} + \tau_{alt}), \tau_{mot_{lim}}\right), & \eta_{tot_{new}} > \eta_{eng} \\ 0, & otherwise \end{cases} \quad (4-19)$$

Finally, the controller compares the vehicle's acceleration to the acceleration set point to determine if the vehicle is operating at a steady state condition, as shown in (4-20).

If the vehicle is slower than the speed limit, then the motor supply controller is active, otherwise, the motor demand controller will be active. Finally, as shown in (4-21), the total motor torque is calculated by added the regenerative braking, alternator, and starter torque requests. The engine torque is sent only the motor supply/demand and alternator torque requests.

$$\tau_{mot_{sup/dmd}} = \begin{cases} \tau_{mot_{sup}}, & v \leq v_{lim} \\ -(\tau_{mot_{dmd}}), & otherwise \end{cases} \quad (4-20)$$

$$\tau_{mot_{tot}} = \tau_{mot_{sup/dmd}} - \tau_{reg} - \tau_{alt} + \tau_{str} \quad (4-21)$$

**Table 4-7: Motor controller parameters and values**

<b>Term</b>	<b>Description</b>	<b>Value</b>
$v$	Vehicle speed (m/s)	
$v_{lim}$	Speed limit (m/s)	(Dependent on algorithm)
$\eta_{scale}$	Engine efficiency limit scaling factor (%)	4
$\tau_{mot_{sup}}$	Motor supply torque demand (Nm)	
$\tau_{eng}$	Engine torque demand (Nm)	
$\tau_{mot_{lim}}$	Maximum motor torque (Nm)	(Dependent on motor speed)
$SOC$	State of charge (%)	
$SOC_{min}SOC_{max}$	Maximum and minimum SOC (%)	70 and 40
$\eta_{eng}\eta_{mot}\eta_{inv}\eta_{batt}$	Component efficiencies (%)	
$\tau_{eng_{max_{eff}}}$	Maximum possible engine efficiency (%)	(Dependent on engine speed)
$\omega_{eng}$	Engine speed (rad/s)	
$\tau_{eng_{add}}$	Adjusted additional engine torque (Nm)	
$\tau_{reg}\tau_{alt}\tau_{str}$	Regen, alternator, starter (Nm)	
$\tau_{eng_{max_{eff}}}$	Max efficiency torque difference (Nm)	
$\eta_{tot_{new}}$	New total powertrain efficiency (%)	
$\eta_{eng_{new}}$	New theoretical engine efficiency (%)	
$\tau_{mot_{dmd}}$	Motor demand torque demand (Nm)	
$\tau_{mot_{sup/dmd}}$	Supply/demand motor torque (Nm)	
$a$	Vehicle acceleration (m/s <sup>2</sup> )	
$\tau_{mot_{tot}}$	Total motor controller torque (Nm)	

#### 4.2.5 Comparison to Existing Designs

There are no results for an existing mild HEV F-150, as the 2019 production vehicle has yet to release solid fuel improvement data. However, the vehicle can still be compared to similar technologies on the market today in the 2017 Chevy Silverado eAssist model. The eAssist model provides a 5% overall fuel economy improvement, when compared to the non-hybrid vehicle model [4]. In comparison, the savings for the created mild HEV F-

150 model run are found in Table 4-8. The mild hybrid implementation leads to an average of 3.6% improvement in fuel consumption when run on standard drive cycles, which is in a similar range.

**Table 4-8: Mild HEV fuel savings**

<b>Cycle</b>	<b>ICE Fuel Consumption (kg)</b>	<b>Mild HEV Fuel Consumption (kg)</b>	<b>Improvement (%)</b>
UDDS	0.885	0.829	6.33
HWY	0.988	0.976	1.21
US06	1.085	1.050	3.23

### 4.3 Algorithm Validation

Similar to the model validation, the algorithm script used to optimize the component sizing and controller must be accurate to the mild hybrid model. The main difference between the algorithm and the model will be in the motor control, and its implementation into the vehicle model. After the torque request is sent from the controller to the vehicle model, it is fed back through the plant and eventually reaches the battery, where it will directly affect the state of charge. As such, the main variable used to validate the algorithm is the Li-Ion battery SOC. In addition to the figures discussed below, the MAE of the battery SOC can be found in Table 4-9.

Shown in Figure 4-20, are the validation results for the UDDS cycle. This cycle was run on a 1.1kWh battery with a speed limit of 7m/s. Overall; the algorithm follows the model very well, with an MAE 0.54%, and a final error of approximately 1.1%. In addition, Figure 4-21 demonstrates the results on the HWY cycle on a 1.1kWh battery with a speed limit of 13m/s. Similar to the UDDS validation, the HWY cycle has a very low MAE of



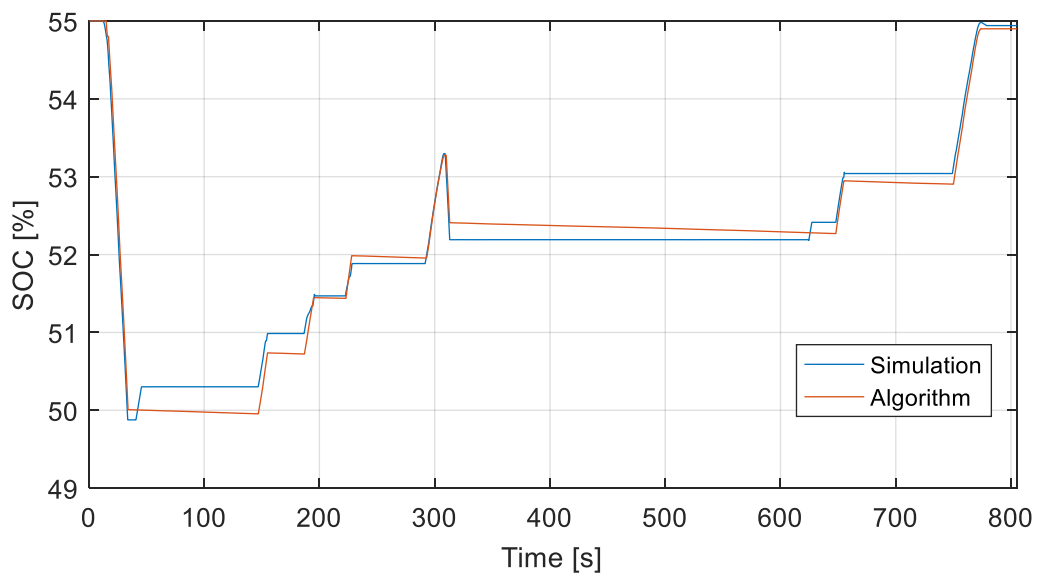


**Figure 4-21: HWY Li-Ion SOC validation**

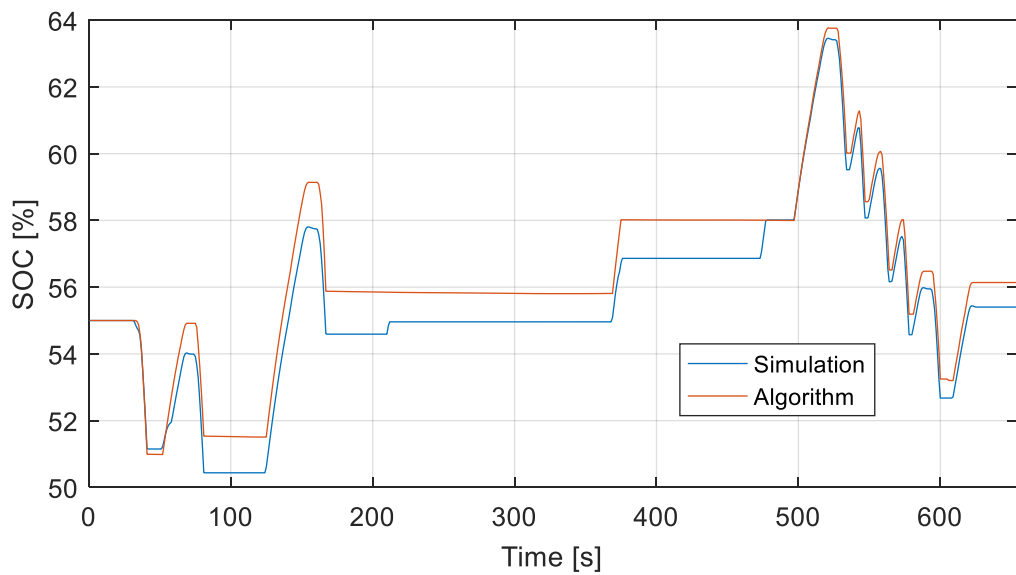


**Figure 4-22: US06 Li-Ion SOC validation**

**Table 4-9: Algorithm MAE validation results**

<b>Cycle</b>	<b>Battery Capacity (kWh)</b>	<b>Max Motor Torque (Nm)</b>	<b>Speed Limit (m/s)</b>	<b>Battery SOC MAE (%)</b>
UDDS	1.1	44.2	7	0.54
HWY	1.1	44.2	13	0.15
US06	0.6	82.8	10	0.80

Total fuel consumption is compared between the algorithm and the mild HEV simulation a final measure of the algorithm’s performance. All three cycles performed well, with UDDS having the largest fuel consumption difference at 1.82%, and HWY at the lowest with 0.1%. All cycles demonstrate a strong fit between the algorithm and model.

**Table 4-10: Algorithm fuel consumption validation results**

<b>Cycle</b>	<b>Algorithm Fuel Consumption (kg)</b>	<b>Simulated Fuel Consumption (kg)</b>	<b>Difference (%)</b>
UDDS	0.814	0.829	1.82
HWY	0.975	0.976	0.10
US06	1.045	1.050	0.48

## **5 Hybrid Powertrain Design Results**

The results below demonstrate the advantage of using real-world driving data over the use of standard drive cycles in the design of a mild hybrid truck, the 2017 Ford F-150. The truck is first designed using a combination of standard drive cycles to obtain an optimal component size/ control pairing. Next, real world data is used to determine an optimal pairing reflecting the driving habits of the average driver. Finally, all pairings are compared, and the difference in fuel savings are examined.

### **5.1 Component Performance**

In order to demonstrate the effectiveness of the additional power electronic components introduced in the mild HEV powertrain, the individual components are examined, along with their physical outputs. The figures below demonstrate the low-level performance during the simulation of the mild HEV model on the US06 cycle, running on the 0.6kWh battery pack, at a speed limit of 10m/s, as described in the validation section. The US06 cycle demonstrates a combination of high steady speeds, along with its rapid accelerations, representative of a mixture of city and highway driving.

Shown in Figure 5-1 is the output from the motor in the simulation. The motor supplies torque during low vehicle speeds, and regenerates torque during high speed-low efficiency periods, and during regenerative braking. In addition, the motor is constantly demanding a low torque signal, less than 5Nm during high-speed operation. This low torque signal can be found to be compensated by the engine torque found in Figure 5-2, as it acts to supply the DCDC link with power to maintain a constantly high SOC on the 12V battery.

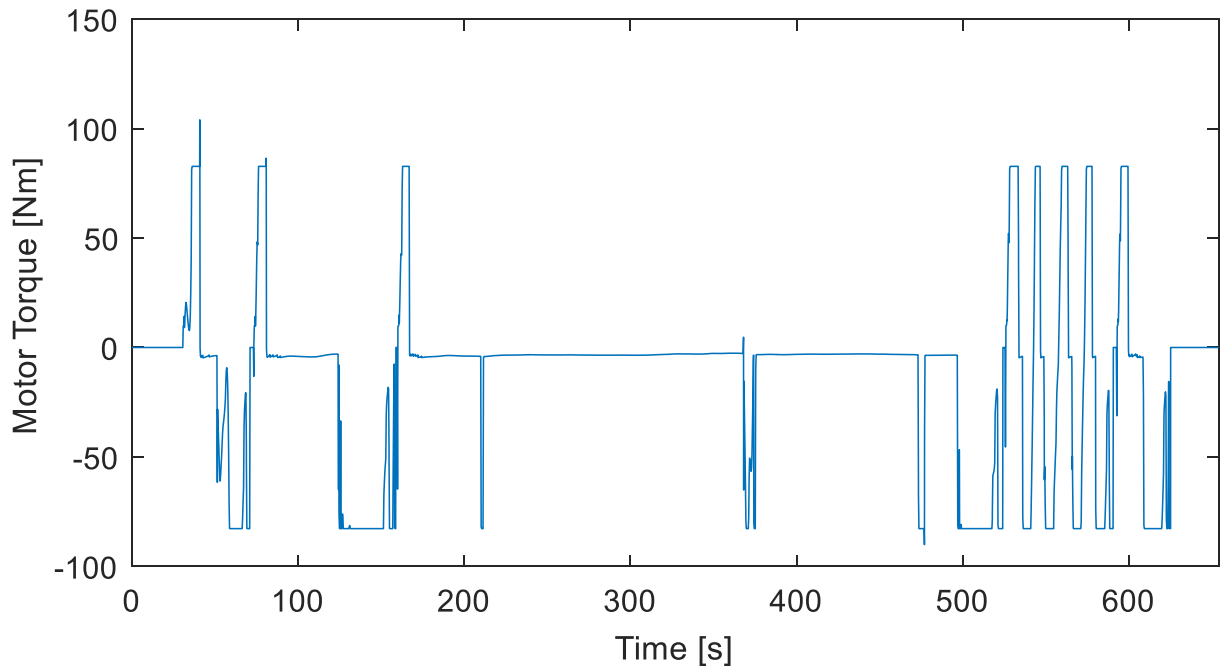


**Figure 5-1: Simulated US06 motor torque**

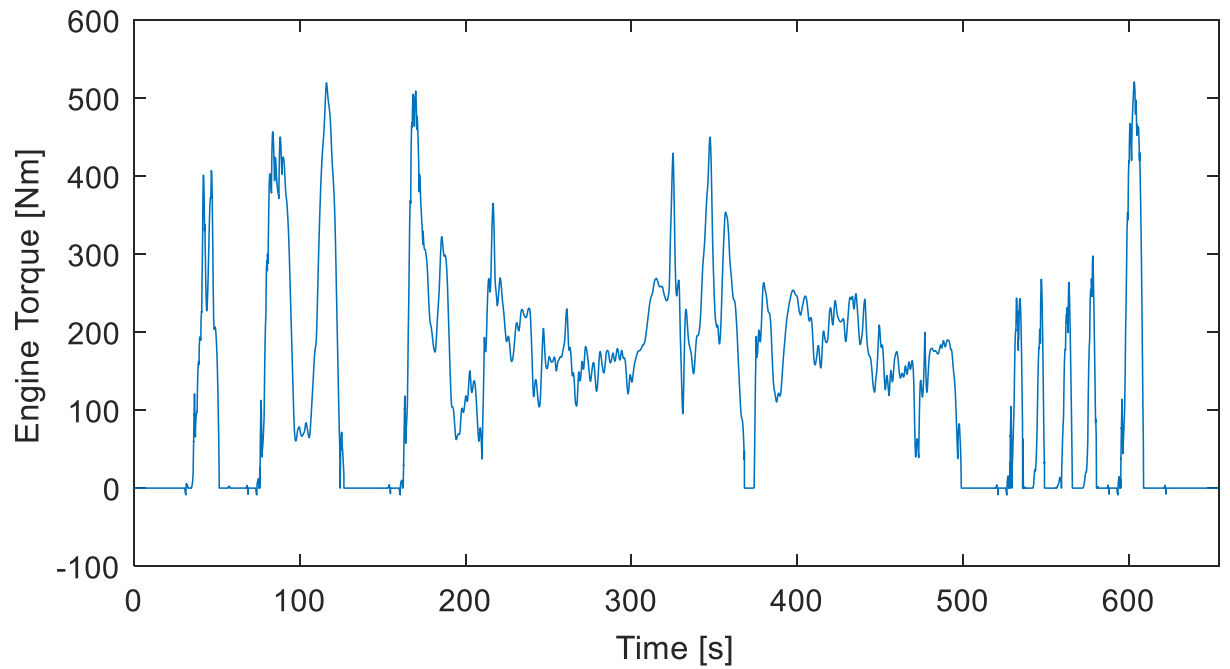


**Figure 5-2: Simulated US06 engine torque**

In addition to the motor and engine mechanical outputs, the electrical outputs of the battery are examined. Figure 5-3 demonstrates the current from the li-ion battery pack. The current is representative of the load taken from the DCDC converter as well as the motor described prior. The high positive value current spikes occur during propulsion assist, particularly when the vehicle is accelerating from a stopped position. Furthermore, the smaller magnitude negative current represent the amount of regenerative energy sent to the battery. To note in this instance, the alternator controller is compensating for the small current required by the DCDC converter, and the results is a net zero current draw from the battery. In addition, Figure 5-4 demonstrates the terminal voltage of the li-ion battery found in the model. Overall, the battery voltage changes with respect to the charging and discharging resistances associated the battery SOC and the current drawn. The li-ion battery voltage varies from approximately 86V to 110V depending on the demand from the battery, with steady state voltage of approximately 99V, representative of the OCV curve at the ~55% SOC demonstrated in Figure 5-5. Overall, the resulting battery SOC varies from 50-63%, well within the control limits of the battery (40-70%). The changes in SOC reflect the current demand from the battery described in Figure 5-3, and the net SOC change is less than 1%.

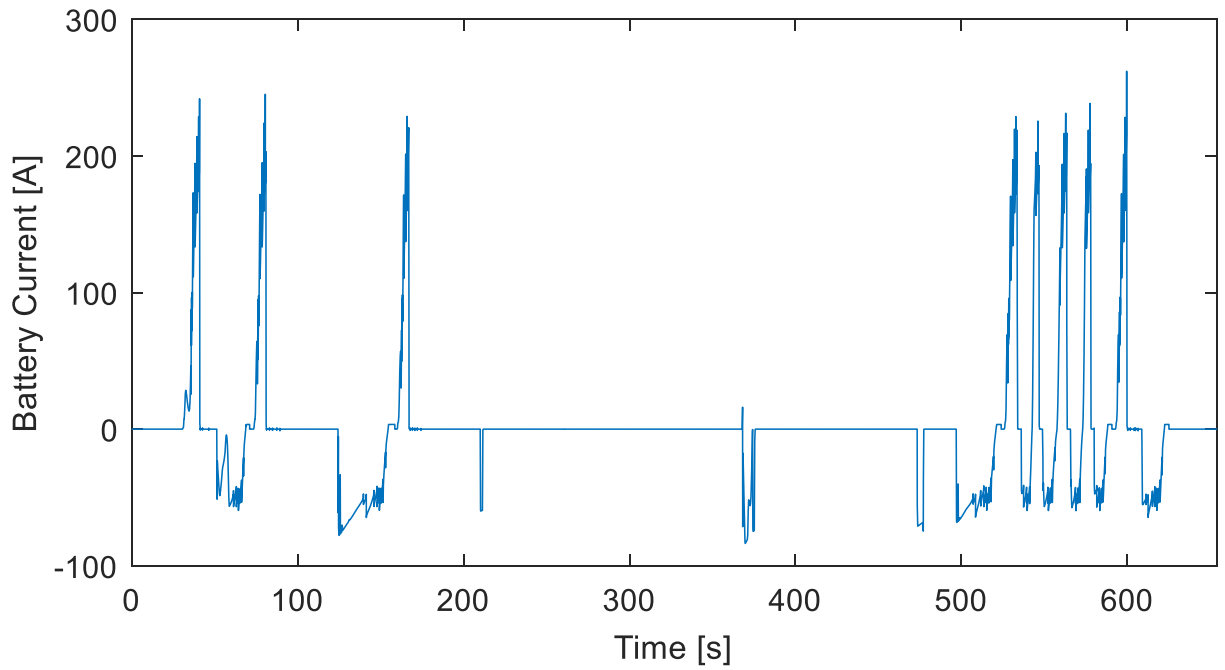


**Figure 5-3: Simulated US06 li-ion battery current**

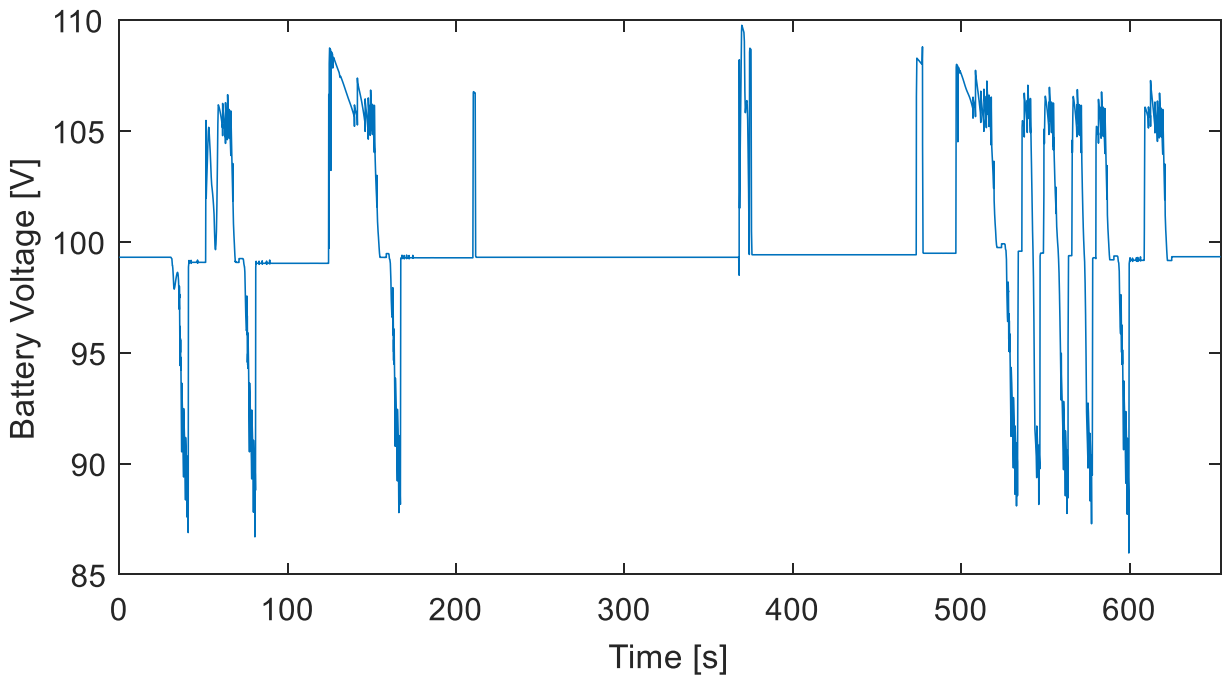


**Figure 5-4: Simulated US06 li-ion battery terminal voltage**

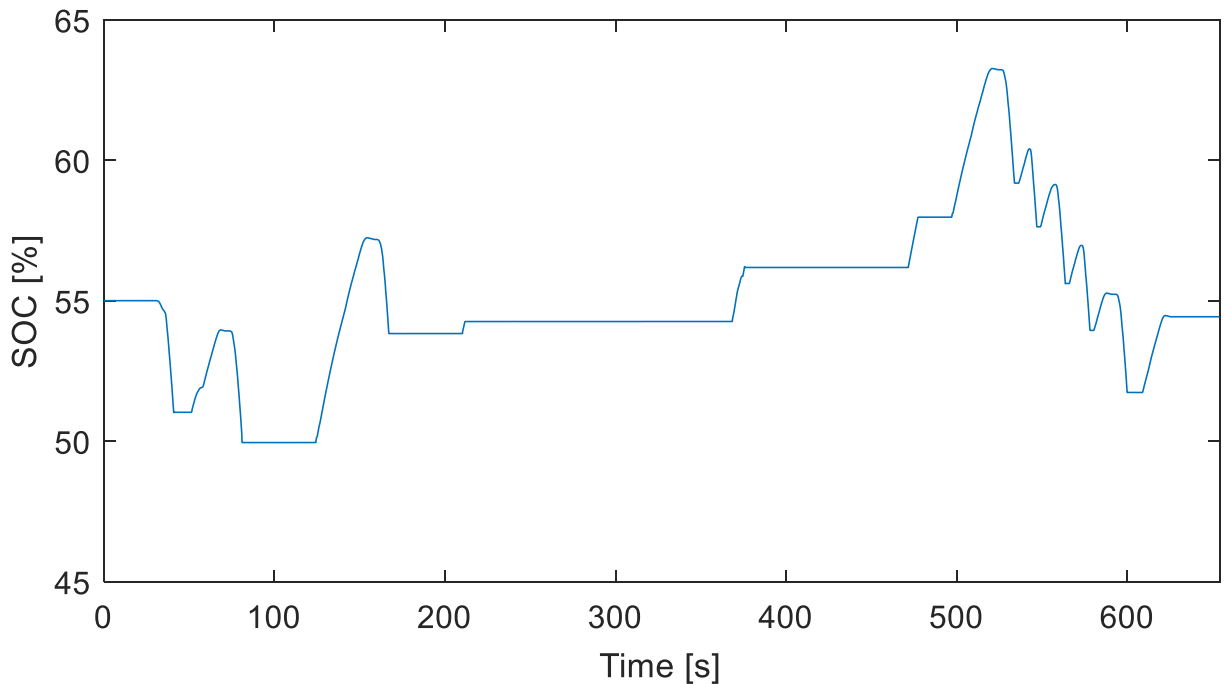


**Figure 5-5: US06 li-ion battery SOC**

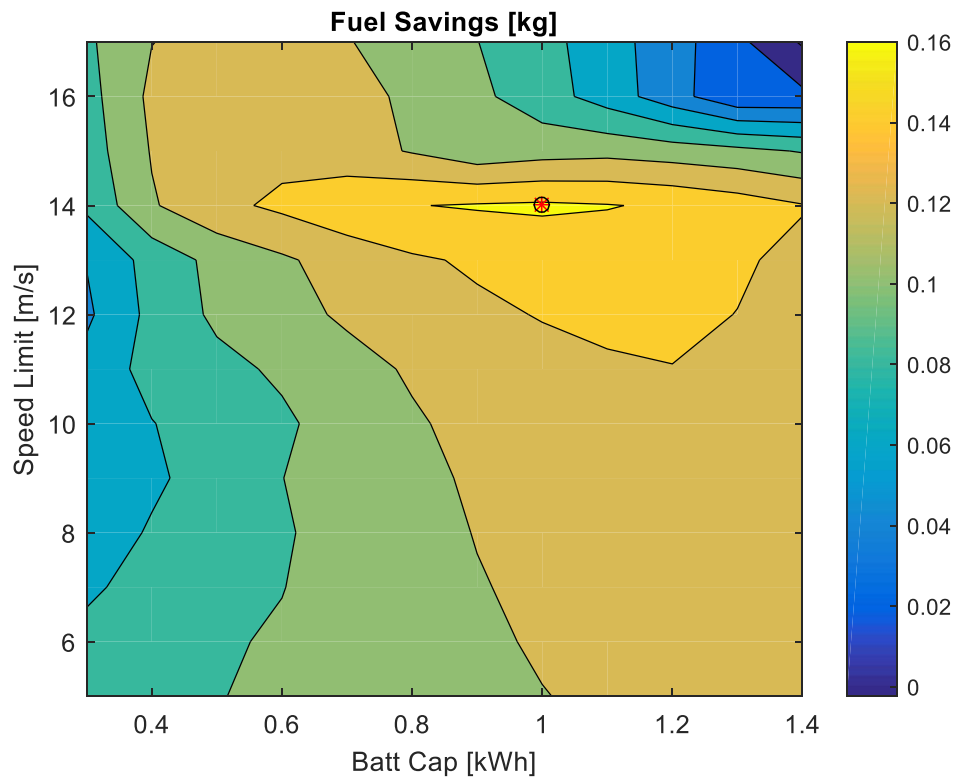
## 5.2 Standard Drive Cycle Algorithm Results

In order to determine an optimal component sizing and controller design, the algorithm described in section 3 was utilized across four separate drive cycles. The drive cycles included the three prior drive cycles, US06, UDDS, and HWY. However, the fourth drive cycle was a combination of all three cycles, and is referred to as the SEW cycle. The SEW cycle consist of 2xUDDS follow by 1xUS06 and 1xHWY. This cycle is meant to demonstrate a mixture of highway and city driving, mimicking what a real world drive may examine. In order to minimize the effect of the difference between battery starting and ending SOC during these cycles, the standard three drive cycle (HWY,UDDS,US06) were run back to back ten times, whereas the longer SEW cycle was run three times back to back. However, all four cycles had their final fuel savings adjusted using SOC correction, where

the difference in battery energy is assumed to have used the average efficiency of the battery, inverter, motor, and engine. The difference in energy for the battery was converted into an equivalent fuel difference using the efficiencies listed above. The results from the algorithm were then set in the mild HEV model to determine the final fuel savings, and compared to the simulated ICE model results, which are summarized in Table 5-1.

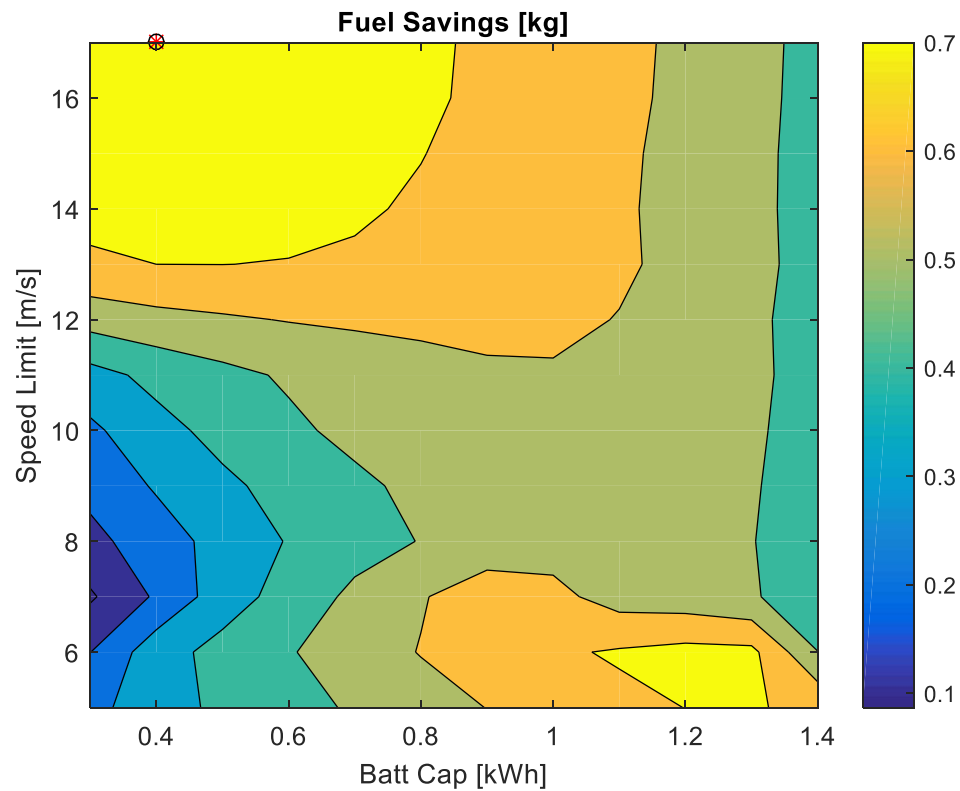
The algorithm iterated through a SOC range from 0.3kWh to 1.4kWh, at a 0.1kWh step size, at a fixed cost limit of \$350 between the motor and battery, with the motor size directly determined through this cost limit and the battery size, as shown in (3-3)-(3-6). In addition, the algorithm iterated through the speed limit control variables. The speed limit ranged from 5m/s to 17m/s at a step size of 1m/s. The hard limit of 17m/s was chosen as this tends to be the higher end of city driving, and it was considered unnecessary for the motor to help assist when the engine was operating at higher speeds and efficiencies.

Shown in Figure 5-6 are the fuel savings results for the HWY cycle. Overall, the HWY cycle has little to no acceleration and only crossed into the motor torque supply mode when initially accelerating. As such, the motor required for such a low demand cycle is small, but large enough to regenerate some energy from the end of the cycle. As such, a large battery size of 1.0kWh was used, with a speed limit of 14m/s. The HWY cycle offers little use from the motor, and as such, gives little fuel improvement from the ICE to the mild HEV model, with a total fuel improvement of 1.21%.



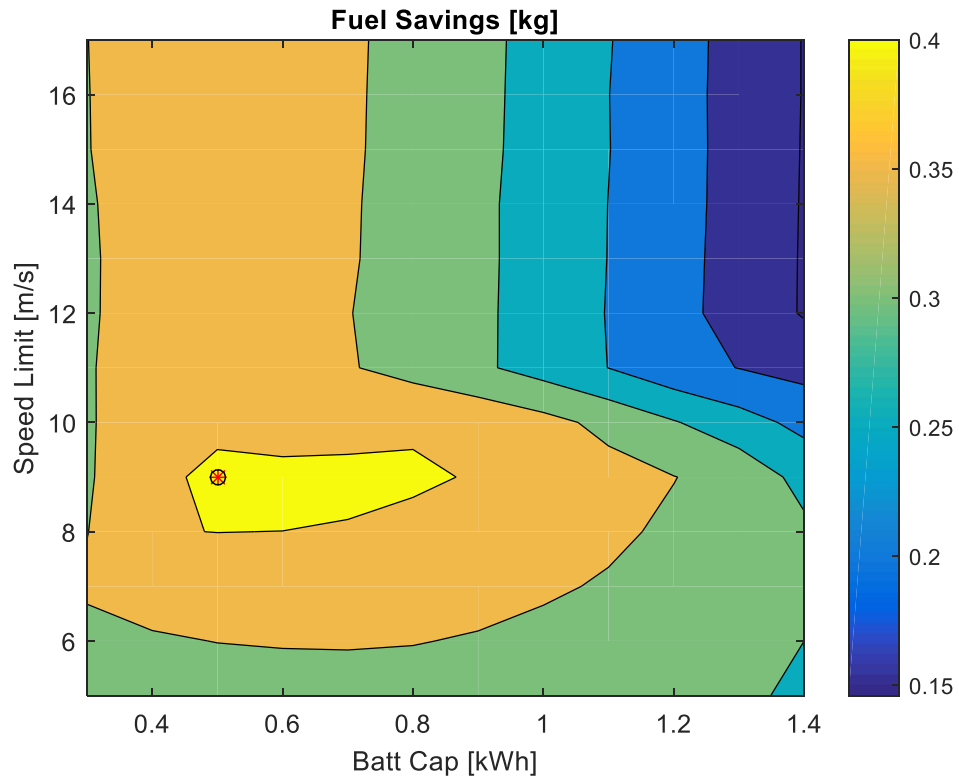
**Figure 5-6: HWY fuel savings comparison**

Figure 5-6 demonstrates the fuel savings results for the UDDS cycle. The UDDS cycle is representative of city driving and has several sections of accelerations while maintaining low speeds. The large amount of accelerations requires the motor to be large enough to provide a decent amount of torque. As such, a small battery size of 0.4kWh was found, with a speed limit of 17m/s, allowing the motor to operate often during its city driving, and making full use of the motor during regenerative braking. The UDDS cycle offers a total fuel improvement of 8.25%. Another point of high fuel savings is in the lower speed, higher capacity area, where the single UDDS run on the algorithm determined the maximum savings would occur.



**Figure 5-7: UDDS fuel savings comparison**

In the last of the standard drive cycles, Figure 5-8 demonstrates the fuel saving results during the US06 cycle. The US06 cycle is a mixture of city and highway driving with rapid accelerations and high vehicle speeds. As such, the algorithm determined that the vehicle requires a larger motor, and smaller battery size at 0.5kWh. However, the large shifts in the cycle caused the algorithm to have a total speed limit of 9m/s. The total fuel savings for the US06 cycle are 3.04%.



**Figure 5-8: US06 fuel savings comparison**

Last, the SEW cycle demonstrated similar results to the UDDS cycle, as shown in Figure 5-9. The SEW cycle gave a final battery capacity of 0.5kWh, and a speed limit of 16m/s. The total fuel savings found on the SEW cycle were 5.56%. The SEW cycle is understandably highly influenced by the UDDS cycle it includes, but its battery capacity and speed limit is likely lowered due to the inclusion of the HWY and US06 cycle.

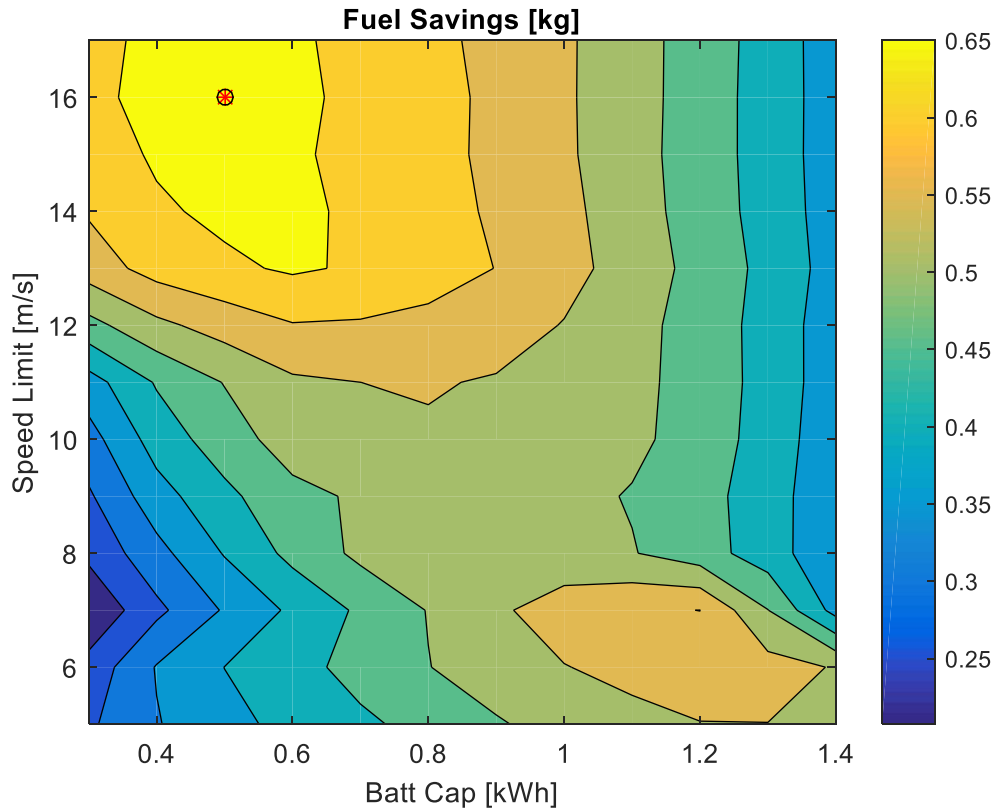


**Figure 5-9: SEW fuel savings comparison**

**Table 5-1: Standard cycle fuel savings summary**

Cycle	Best Battery Capacity (kWh)	Max Motor Torque (Nm)	Best Speed Limit (m/s)	ICE Fuel (kg)	Mild HEV Fuel (kg)	Improvement (%)
UDDSx10	0.4	98.2	17	8.85	8.12	8.25
HWYx10	1.0	52.0	14	9.88	9.76	1.21
US06x10	0.5	90.5	9	10.85	10.52	3.04
SEWx3	0.5	90.5	16	11.56	10.92	5.56

### 5.3 Real World Optimization results

In a similar fashion to the standard cycles, the real world dataset was used in the optimization algorithm. The trips were cycled through by driver, and the final fuel savings

were totaled to determine the optimal battery size and speed limit pairing. The lower limit for the battery size range was changed to 0.4kWh; otherwise, the exhaustive search was performed identically. In total, the script totaled a run time of 3:28 hours, whereas the runtime for the equivalent number of optimization runs on the mild HEV model took approximately 15:59 hours. The difference in computational time results in a 78% reduction in total computational time.

Figure 5-10 demonstrates the script's results for total fuel savings. The optimization algorithm determined that the best pairing was at 1.0kWh battery size, with a speed limit of 17m/s. This is an interesting set point, as the algorithm demonstrates the same battery sizing as the HWY cycle, but the large speed limit found in the UDDS cycle.

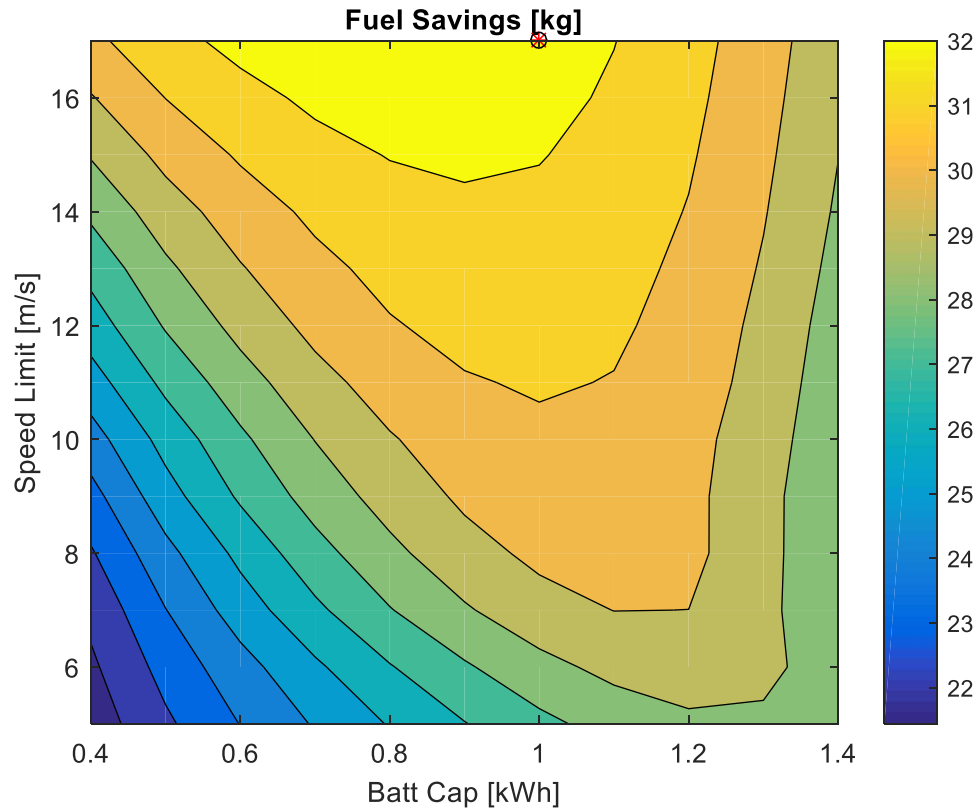


**Figure 5-10: Real world dataset fuel savings**

In order to compare the effect of using real world data in the optimization to the use of standard cycles, the real world data set was run on each of the optimal battery size/ speed limit pairings found for each standard drive cycle, as well as the optimal pairing found in the script. In addition to the initial 4 cycles used, a 5<sup>th</sup> pairing was selected as the total average between the HWY, UDDS, and US06 optimal pairing. The resulting average pairing was a 0.63kWh battery size, along with an 11.3m/s speed limit.

Table 5-2 demonstrates a summary of the results found between sizing/control pairing. Examining the results of the standard certification cycles, the US06 performed the worst at a 4.12% decrease in fuel consumption, whereas the HWY cycle was the best at 6.86%. These results are logical, as the only difference between the optimization, pairing from HWY to real world was an increased speed limit, whereas the US06 cycle had both a lower speed limit and battery size. In addition, the SEW and average pairings produced similar results, with the SEW cycle demonstrating a 5.58% improvement, and the average resulting in a 5.45% improvement when compared to the ICE model. Finally, the use of the real world data gave the best results with a decrease in fuel consumption of 7.10%. As expected, the use of real world data in the optimization process gave the best results when compared to standard drive cycles. However, it should be noted that the US06 cycle which contains a mixture of highway and city driving performed significantly worse.

**Table 5-2: Real world dataset fuel consumption comparison**

<b>Cycle</b>	<b>Best Battery Capacity (kWh)</b>	<b>Max Motor Torque (Nm)</b>	<b>Best Speed Limit (m/s)</b>	<b>Fuel Used (kg)</b>	<b>Improvement (%)</b>
ICE model	-		-	433.7	-
UDDSx10	0.40	98.2	17.0	409.5	5.59
HWYx10	1.00	52.0	14.0	403.9	6.86
US06x10	0.50	90.5	9.0	415.8	4.12
SEWx3	0.50	90.5	16.0	409.5	5.58
Cycle Avg	0.63	80.4	11.3	410.1	5.45
Real Best	1.00	52.0	17.0	402.9	7.10

One of the main differences between the real world driving data and the standard cycle data is the amount of time spent at very low speeds; the real world data more often shows idling or slow driving, likely due to traffic constraints. This difference is a likely reason why the real world optimum battery size is larger (1kWh) than most of the standard cycle optimums in Table 5-2. The larger battery allows the vehicle to idle or drive slowing in traffic in all-electric mode, meaning the engine can stay off for longer time periods. In addition, abrupt shifts in speed between city and highway can be found within most trips in the real world driving data, where the standard cycles demonstrate a full stop before shifting to different speed classifications – this may impact the results as well. Overall, the use of real world data captures the average driver better than a standard drive cycle alone, due to the differences in driving styles and traffic constraints.

## **6 Conclusion and Future Works**

### **6.1 Summary of Contributions**

Mild hybridization is a low cost, low footprint technology that can be implemented into an existing vehicle's design with ease. In order to optimize the benefits in fuel savings that a mild hybrid electric vehicle can provide, care must be taken in the sizing of components and control design. The use of real world data in the design process of a vehicle can help optimize the vehicle when compared to the use of standard drive cycles, and reduce real world fuel use and emissions. This thesis demonstrates a data driven approach to the mild hybridization of an internal combustion engine vehicle, with a focus on the design process used to convert an F-150 to a mild HEV. The following discussion summarizes the contributions of this thesis.

In Chapter 2, a review was performed on the various hybrid electric vehicle topologies along with the optimization methods used in hybrid vehicles. Through this review, the use of real world dataset to optimize powertrain performance was found to provide benefits when compared to the use of standard cycles. This chapter also proposed a novel approach to the design process of a mild hybrid electric vehicle, using exhaustive search optimization using rule based control on a real world dataset of over 5000km of data. The proposed design process consists of three main stages, vehicle modelling in Simulink, optimization through an algorithm in MATLAB script, and a comparison of results on real world driving data using a Simulink model of a mild HEV.

Chapter 3 further explains the optimization algorithm present in the MATLAB script. A script was used due to the decreased computational time over the use of a full

vehicle model, so that thousands of kilometers of real-world data can reasonably be used in the design process. The algorithm uses a nested optimization method, where the component sizing and control are optimized together. The use of a rule based controller is further expanded on, and the heuristic technique behind the rule based control is further expanded upon, with the motor torque supply control being based upon the Honda Insight [39], while the motor torque demand controller being based upon maximizing the engine efficiency during recharging. The algorithm also expands upon the use of a cost function to determine motor size from the iterative battery size, and uses a speed constant to switch between motor supply and demand.

Chapter 4 provides a detailed breakdown of the vehicle modelling process. The modelling process is based upon a physical representation of a vehicle's powertrain, with the torque flowing towards the wheels and the speed fed backwards to the propulsion device. This chapter further breaks down the control strategies used in the internal combustion engine and mild hybrid vehicle. In addition, this chapter focuses on the validation between the real world vehicle and model, mild hybrid performance, and the script performance compared to the mild hybrid model.

Chapter 5 demonstrates the results from the design process detailed in Chapter 2. The chapter expands upon the low-level component performance during mild hybrid operation. In addition, the optimal motor size/ speed limit pairing is determined for standard drive cycles. The optimization algorithm is then run using a real world driver dataset, and it was determined that the optimal component size/ speed limit pairing within the exhaustive search was 1.0kWh, with a motor producing 90Nm maximum torque, and a

speed limit of 17m/s. The pairing from the drive cycles and real world data were run on a mild hybrid model utilizing the same rule based control found in the algorithm. The end result was a 7.2% decrease in fuel consumption using the real world dataset pairing, with an average cycle result demonstrating a 5.58% decrease in fuel consumption when compared to the ICE model.

The design process in this thesis demonstrated the importance in the selection of data used to optimize powertrain plant design and control. Standard drive cycles while used in vehicle certifications, performed worse in the real world than using a real world data-driven approach. The difference in results is particularly evident when comparing the US06 cycle that only decreased fuel consumption by 4.12%.

## **6.2 Suggestions for Future Work**

In regards to the future work on a data driven design process on mild hybrid vehicles, the following directions are proposed:

- The vehicle model can be improved by using a more in-depth engine model.

The engine model demonstrated in this thesis assumes a static temperature throughout the cycle, and does not account for the difference in fuel consumption during cold starts.

- The optimization algorithm uses nested plant/control optimization with exhaustive search and rule based control to determine the optimal battery size/speed limit pairing. The exhaustive search method is only as accurate as the size of the steps, and limits used in the optimization. The limits and sizing of the exhaustive search algorithm can be altered to create a more fine mesh.

- Finally, the configuration of the mild hybrid used was a belt driven ISG. Other configurations of mild hybrids could produce more optimal results, and should be pursued and compared with the current configuration.

## References

- [1] Trading Economics, "Canadian Gasoline Prices," Trading Economics, 2018.
- [2] Environmental Protection Agency, "History of Reducing Air Pollution from Transportation in the United States," Environmental Protection Agency, 2018.
- [3] Toyota, "2018 Camry & Camry Hybrid," Toyota, 2018.
- [4] T. Appel, "2017 Silverado with eAssist: Meet Chevy's "Secret" Hybrid Pickup," Consumer Guide, 2016. [Online]. Available: <http://blog.consumerguide.com/2017-silverado-hybrid-meet-chevys-secret-thrifty-pickup/>.
- [5] E. Silvas, T. Hofman, N. Murgovski, L. Pascal Etman and M. Stienbuch, "Review of Optimization Strategies for System-Level Design in Hybrid Electric Vehicles," *IEEE Transactions on Vehicular Technology*, vol. 66, no. 1, pp. 57-70, 2017.
- [6] T. Szalai, T. Heidrich, U. Schwalbe, F. Endert and S. D. Ivanov, "Dimensioning of ultra capacitors used for range extension in electric vehicles," *2013 15th European Conference on Power Electronics and Applications (EPE)*, pp. 1-9, 2013.
- [7] M. Zhou, H. Zhang and Z. Gao, "Parameters optimization and performance simulation for parallel hybrid electric vehicle," *Proceedings of 2011 6th International Forum on Strategic Technology*, pp. 242-245, 2011.
- [8] M. Pourabdollah, B. Egardt, N. Murgovski and A. Grauers, "Convex Optimization Methods for Powertrain Sizing of Electrified Vehicles by Using Different Levels of Modeling Details," *IEEE Transactions on Vehicular Technology*, vol. 67, no. 3, pp. 1881-1893, 2018.
- [9] C. Thompson, "The 20 best-selling cars and trucks in America," Business Insider, January 2018. [Online]. Available: <https://www.businessinsider.com/best-selling-cars-and-trucks-in-us-2017-2018-1>.
- [10] D. Greene, A. J. Khattak, J. Liu, X. Wang, J. Hopson and R. Goeltz, "What is the Evidence Concerning the Gap between On-Road and Environmental Protection Agency Fuel Economy Ratings?," *Transport Policy*, vol. 53, pp. 146-160, 2017.
- [11] A. Moawad and A. Rousseau, "Effect of Electric Drive Vehicle Technologies on Fuel Efficiency -Final Report," Argonne National Laboratory, Argonne, IL, 2012.
- [12] H. Tataria, O. Gross, C. Bae, B. Cunningham, J. A. Barnes, J. Deppe and J. Neubauer, "USABC Development of 12 Volt Battery for Start-Stop Application," *EVS27 International Battery, Hybrid and Fuel Cell Electric Vehicle Symposium*, 2013.
- [13] K. van Berkel, T. Hofman, B. Vroemen and M. Steinbuch, "Optimal Control of a Mechanical Hybrid Powertrain," *IEEE Transactions on Vehicular Technology*, vol. 61, no. 2, pp. 485-497, 2012.
- [14] K. v. Berkel, S. Rullens, T. Hofman, B. Vroemen and M. Steinbuch, "Topology and Flywheel Size Optimization for Mechanical Hybrid Powertrains," *IEEE Transactions on Vehicular Technology*, vol. 63, no. 9, pp. 4192-4205, 2014.

- [15] R. Bojoi, A. Cavagnino, M. Cossale and A. Tenconi, "Multiphase Starter Generator for a 48-V Mini-Hybrid Powertrain: Design and Testing," *IEEE Transactions on Industry Applications*, vol. 52, no. 2, pp. 1750-1758, 2015.
- [16] A. Emadi, Y. J. Lee and K. Rajashekara, "Power Electronics and Motor Drives in Electric, Hybrid Electric, and Plug-In Hybrid Electric Vehicles," *IEEE Transactions on Industrial Electronics*, vol. 55, no. 6, pp. 2237-2245, 2008.
- [17] Autoweek, "Here's why a hybrid Ford F-150 pickup could be the perfect camping truck," Autoweek, 2018. [Online]. Available: <https://autoweek.com/article/trucks/hereshow-ford-hopes-make-buyers-want-hybrid-pickups>.
- [18] S. Jurkovic, K. M. Rahman, J. C. Morgante and P. J. Savagian, "Induction Machine Design and Analysis for General Motors e-Assist Electrification Technology," *IEEE Transactions on Industry Applications*, vol. 51, no. 1, pp. 631-639, 2015.
- [19] S. Abuelsamid, "2019 Ram 1500 Gets 48V Mild Hybrid On All Gas Engines," Forbes, 2018. [Online]. Available: <https://www.forbes.com/sites/samabuelsamid/2018/01/15/2019-ram-1500-gets-standard-48v-mild-hybrid-on-all-gas-engines/#771a99aa7e9e>.
- [20] B. Bilgin et al., "Making the Case for Electrified Transportation," *IEEE Transactions on Transportation Electrification*, vol. 1, no. 1, pp. 4-17, 2015.
- [21] S. Tosserams, L. Etman, and J. Rooda, "A classification of methods for distributed system optimization based on formulation structure," *Struct. Multidisciplin. Optim.*, vol. 39, no. 5, pp. 503-517, 2009.
- [22] B. Egardt, N. Murgovski, M. Pourabdollah, and L. Johannesson Mardh, "Electromobility studies based on convex optimization: Design and control issues regarding vehicle electrification," *IEEE Control Syst*, vol. 34, no. 2, pp. 32-49, 2014.
- [23] Gregory Rousseau, Delphine Sinoquet, Antonio Sciarretta, Yohan Milhau, "Design Optimisation and Optimal Control for Hybrid Vehicles," *EngOpt 2008 - International Conference on Engineering Optimization*, 2008.
- [24] E. Vinot, R. Trigui, B. Jeanneret, J. Scordia, and F. Badin, "HEVs comparison and components sizing using dynamic programming," *Proc. IEEE Veh. Power Propulsion Conf*, pp. 314-321, 2007.
- [25] X. Zhang, H. Peng, J. Sun, and S. Li, "Automated modeling and mode screening for exhaustive search of double-planetary-gear power split hybrid powertrain," *n Proc. ASME Dyn. Syst. Control Conf.*, pp. 1-8, 2014.
- [26] T. H. Cormen, C. E. Leiserson, R. L. Rivest, and C. Stein, *Introduction to Algorithms*, 3rd ed., Cambridge, U.K.: MIT Press, 2009.
- [27] R. Trigui, E. Vinot and M. Boujelben, "Offline optimization for components sizing and analysis of a plug-in hybrid urban microbus," *2009 IEEE Vehicle Power and Propulsion Conference*, pp. 382-387, 2009.
- [28] K. Çağatay Bayındır, M. A. Gözüküçük, and A. Teke, "A comprehensive overview of hybrid electric vehicle: Powertrain configurations, powertrain control techniques

- and electronic control units," *Energy Conversion and Management*, vol. 52, pp. 1305-1313, 2011.
- [29] F. R. Salmasi, "Control Strategies for Hybrid Electric Vehicles: Evolution, Classification, Comparison, and Future Trends," *IEEE Transactions on Vehicular Technology*, vol. 56, pp. 2393-2404, 2007.
- [30] C.-C. Lin, H. Peng and J. W. Grizzle, "Power Management Strategy for a Parallel Hybrid Electric Truck," *IEEE Transactions on Control Systems Technology*, vol. 11, no. 6, pp. 839-849, 2003.
- [31] Z. Song, H. Hofmann, J. Li, X. Han, and M. Ouyang, "Optimization for a hybrid energy storage system in electric vehicles using dynamic programming approach," *Appl. Energy*, vol. 139, pp. 151-162, 2015.
- [32] M. Shams-Zahraei, A. Kouzani, S. Kutter, and B. Bäker, "Integrated thermal and energy management of plug-in hybrid electric vehicles," *J. Power Sources*, vol. 216, pp. 237-248, 2012.
- [33] Environmental Protection Agency, "Vehicle Fuel Economy Labeling and the Effect of Cold Temperature, Air-Conditioning Usage and Aggressive Driving on Fuel Economy," Environmental Protection Agency, U.S., 2005.
- [34] Environmental Protection Agency, "40 CFR Parts 86 and 600 Fuel Economy Labeling of Motor Vehicles: Revisions To Improve Calculation of Fuel Economy Estimates; Final Rule," Environmental Protection Agency, 2006.
- [35] Environmental Protection Agency, "40 CFR § 600.114-12 - Vehicle-Specific 5-cycle Fuel Economy and Carbon-Related Exhaust Emission Calculations.," Environmental Protection Agency, 2016.
- [36] P. Nyberg, E. Frisk and L. Nielsen, "Driving Cycle Equivalence and Transformation," *IEEE Transactions on Vehicular Technology*, vol. 66, no. 3, pp. 1963-1974, 2017.
- [37] H. K. Roy, A. McGordon and P. A. Jennings, "A Generalized Powertrain Design Optimization Methodology to Reduce Fuel Economy Variability in Hybrid Electric Vehicles," *IEEE Transactions on Vehicular Technology*, vol. 63, no. 3, pp. 1055-1070, 2014.
- [38] E. Silvas, K. Hereijgers, H. Peng, T. Hofman and M. Steinbuch;, "Synthesis of Realistic Driving Cycles With High Accuracy and Computational Speed, Including Slope Information," *IEEE Transactions on Vehicular Technology*, vol. 65, no. 6, pp. 4118-4128, 2016.
- [39] National Renewable Energy Laboratory, "Test Results and Modeling of the Honda Insight Using Advisor," *SAE Future Transportation Technologies Conference*, 2001.
- [40] Energy Systems Division, "Energy Systems D3 2017 Ford F150," Argonne National Laboratory, 2018.
- [41] B. N. E. Finance, "2018 Sustainable Energy in America Factbook," Bloomberg New Energy Finance, 2018.
- [42] T. N. A. Press, *Transitions to Alternative Vehicles and Fuels*, Washington, D.C.: The National Academies Press, 2013.

- [43] R. H. Staunton, C. W. Ayers and L. D. Marlino, "Evaluation of 2004 Toyota Prius Hybrid Electric Drive System," *Oak Ridge National Laboratory*, 2006.
- [44] T. Read and T. Kuhnen, "Holy Shift! A Look inside GM's new 10-Speed Automatic," General Motors Corporate Newsroom, Detroit, MI, 2016.
- [45] Ford, *2017 F-150 Brochure*, Ford, 2016.
- [46] E. D. Sexton and J. B. Olson, "Coulombic efficiency of a sealed, thin plate, spiral lead-acid battery," *Thirteenth Annual Battery Conference on Applications and Advances. Proceedings of the Conference*, pp. 297-301, 1998.
- [47] C. Y. Wu, C. H. Ke, C. L. Chang and Z. Y. Chiou, "Useful life characteristics of a LiFePO<sub>4</sub> battery for estimating state of battery health," *2018 IEEE International Conference on Applied System Invention (ICASI)*, pp. 1338-1341, 2018.
- [48] R. Ahmed, "Modelling and State of Charge Estimation of Electric Vehicle Batteries," *McMaster Univeristy*, 2014.
- [49] S. Piller, M. Perrin and A. Jossen, "Methods for state-of-charge determination and their applications," *Journal of Power Sources*, vol. 96, no. 1, pp. 113-120, 2001.
- [50] E. A. Sanchez, "Ram Still Officially Most Aerodynamic Fullsize Truck," *Truck Trend*, 2014. [Online]. Available: <http://www.trucktrend.com/news/1408-ram-still-officially-most-aerodynamic-fullsize-truck/>.